REGENERATION AND THERMAL STRESS MODIFICATION IN FIBER BRAGG GRATING USING CO_2 LASER ANNEALING TECHNIQUE

LAI MAN HONG

INSTITUTE OF GRADUATE STUDIES
UNIVERSITY OF MALAYA
KUALA LUMPUR

2017

REGENERATION AND THERMAL STRESS MODIFICATION IN FIBER BRAGG GRATING USING CO_2 LASER ANNEALING TECHNIQUE

LAI MAN HONG

THESIS SUBMITTED IN FULFILMENT OF THE REQUIREMENTS FOR THE DEGREE OF DOCTOR OF PHILOSOPHY

INSTITUTE OF GRADUATE STUDIES
UNIVERSITY OF MALAYA
KUALA LUMPUR

2017

UNIVERSITY OF MALAYA

ORIGINAL LITERARY WORK DECLARATION

Name of Candidate: Lai Man Hong

Matric No: HHE130005

Name of Degree: Doctor of Philosophy (Photonics)

Title of Thesis ("this Work"): Regeneration and Thermal Stress Modification in Fiber Bragg Grating using CO_2 Laser Annealing Technique

Field of Study: Physics (Photonics Engineering)

I do solemnly and sincerely declare that:

(1) I am the sole author/writer of this Work;
(2) This Work is original;
(3) Any use of any work in which copyright exists was done by way of fair dealing and for permitted purposes and any excerpt or extract from, or reference to or reproduction of any copyright work has been disclosed expressly and sufficiently and the title of the Work and its authorship have been acknowledged in this Work;
(4) I do not have any actual knowledge nor do I ought reasonably to know that the making of this work constitutes an infringement of any copyright work;
(5) I hereby assign all and every rights in the copyright to this Work to the University of Malaya ("UM"), who henceforth shall be owner of the copyright in this Work and that any reproduction or use in any form or by any means whatsoever is prohibited without the written consent of UM having been first had and obtained;
(6) I am fully aware that if in the course of making this Work I have infringed any copyright whether intentionally or otherwise, I may be subject to legal action or any other action as may be determined by UM.

Candidate's Signature Date:

Subscribed and solemnly declared before,

Witness's Signature Date:

Name:

Designation:

ABSTRACT

Regenerated fiber Bragg grating (RFBG) is a temperature-resistant grating fabricated from a standard fiber Bragg grating using high temperature annealing treatment. It is well known for its economic production and high temperature sustainability in which the operating temperature of the developed RFBG can be as high as the maximum annealing temperature. It is believed that stress relaxation is one of the contributing factors to the thermal regeneration process. Exploiting the benefits of CO_2 laser in terms of dynamic temperature control and focused heating zone, thermal regeneration of RFBG based on CO_2 laser annealing has been successfully demonstrated for the first time. The ensuing cooling process after the post-fabrication annealing treatment is the controlling parameter for the modification of thermal stress in the fiber. After an isothermal annealing treatment followed by a slow cooling process, the Bragg wavelength of the RFBG was red-shifted. This modification is reversible by repeating the annealing treatment followed by a rapid cooling process. It is repeatable with different cooling processes in the subsequent annealing treatments. This phenomenon can be attributed to the thermal stress modification in the fiber core by means of manipulation of glass transition temperature with different cooling rates. This finding is important for accurate temperature measurement of RFBG in dynamic environment. Furthermore, the thermal stress relaxation study was extended to birefringence modification in regenerated grating in polarisation maintaining fiber (RGPMF) by using a CO_2 laser annealing technique. After conducting a post-fabrication isothermal annealing procedure followed by a slow cooling process, the birefringence of the RGPMF has been increased. This phenomenon can be explained by the changes in the thermal expansion coefficient and glass transition temperature of the stress applying part at different cooling rates. The birefringence modification is reversible by re-annealing with a subsequent rapid cooling process. This finding is useful for the study

of the birefringence modification, operation range, sensitivity, and accuracy of PMF or PMF-related fiber components. The finding of this thesis has opened up a new avenue of research on the application of CO_2 laser annealing in thermal regeneration, stress relaxation and birefringence modification in FBG components.

ABSTRAK

Parutan gentian Bragg terpulih (RFBG) merupakan parutan tahan panas difabrikkan dengan parutan gentian Bragg standard menggunakan rawatan penyepuhlindapan suhu tinggi. Ia terkenal dengan pengeluaran yang ekonomi dan kemampanan suhu yang tinggi di mana suhu operasi RFBG terhasil adalah setinggi suhu penyepuhlindapan maksimum. Kesantaian tegasan dipercayai merupakan salah satu faktor menyumbang kepada proses pemulihan RFBG. Mengeksploitasi manfaat CO_2 laser dari segi kawalan suhu yang dinamik dan zon pemanasan yang fokus, pemulihan haba RFBG berdasarkan penyepuhlindapan CO_2 laser telah berjaya didemonstrasikan untuk kali pertama. Proses penyejukan selepas rawatan penyepuhlindapan lepas fabrikasi adalah parameter kawalan bagi pengubahsuaian tegasan terma dalam gentian. Selepas penyepuhlindapan isoterma disusuli dengan proses penyejukkan yang perlahan, panjang gelombang Bragg RFBG telah beralih merah. Pengubahsuaian ini boleh diterbalikkan dengan mengulangi rawatan penyepuhlindapan diikuti dengan proses penyejukan yang pesat. Process ini adalah terulangkan dengan menggunakan proses penyejukan yang berbeza dalam rawatan penyepuhlindapan berikutnya. Fenomena ini boleh dikaitkan dengan pengubahsuaian tegasan terma dalam teras gentian optik melalui manipulasi suhu peralihan kaca dengan kadar penyejukan yang berbeza. Penemuan ini adalah penting untuk pengukuran suhu yang tepat daripada RFBG dalam persekitaran yang dinamik. Di samping itu, kajian kesantaian tegasan haba telah dilanjutkan kepada pengubahsuaian dwibiasan dalam parutan Bragg gentian terpulih kekal pengutuban (RGPMF) dengan menggunakan teknik penyepuhlindapan CO_2 laser. Selepas menjalankan prosedur penyepuhlindapan isoterma lepas fabrikasi diikuti dengan proses penyejukkan yang perlahan, dwibiasan RGPMF telah meningkat. Fenomena ini boleh dijelaskan oleh perubahan dalam pekali pengembangan terma dan suhu peralihan kaca di bahagian mengenakan tegasan pada kadar penyejukan yang berbeza. Pengubahsuaian dwibiasan

boleh berbalik dengan penyepuhlindapan semula serta proses penyejukan yang pantas berikutnya. Penemuan ini adalah berguna untuk kajian pengubahsuaian dwibiasan, julat operasi, kepekaan, dan ketepatan dalam gentian optik kekal pengutuban (PMF) atau komponen PMF yang berkaitan. Hasil tesis ini telah membuka ruang baru bagi penyelidikan dalam penggunaan penyepuhlindapan CO_2 laser dalam pemulihan haba, kesantaian tegasan dan pengubahsuaian dwibiasan dalam komponen FBG.

ACKNOWLEDGEMENTS

Firstly, I would like to express my sincerest gratitude to my supervisors, Distinguished Prof. Datuk Dr. Harith Ahmad, Dr Lim Kok Sing and Prof. Dr. Hang-Zhou Yang for the continuous support of my Ph.D study and related research, for their patience, motivation, and immense knowledge. Their guidance helped me in all the time of research and writing of this thesis.

Furthermore, I would like to thank all the departments, units, and staffs in University of Malaya which supported and helped me in administrative work. In addition, I would like to extend my sincerest gratitude to MyBrain15, Ministry of Higher Education Malaysia for providing me scholarship throughout my PhD study.

My sincere gratitude to Dr. Chong Wu Yi and his lab members who have granted me access to their laboratory and research facilities so that I could complete part of my study. I am grateful to my fellow labmates, Dr. Muhammad Mahmood Ali, Dr. Dinusha Serandi Gunawardena, Mr. Rajibul Islam, and Lee Yen Sian. Thanks for the fruitful discussions, advice, information, handful of help, and for all the fun we have had in the last three years. Last but not the least, I would like to thank my family and friends for supporting me spiritually throughout my PhD study and my life in general.

Lai Man Hong

June 2017

TABLE OF CONTENTS

LIST OF FIGURES

LIST OF TABLES

LIST OF SYMBOLS AND ABBREVIATIONS

$\mu\varepsilon$	:	Micro strain
1-D	:	One-dimensional
AC	:	Alternating current
Al	:	Aluminium
Ar	:	Argon
ArF	:	Argon fluoride
ASE	:	Amplified spontaneous emission
B	:	Boron
BTD	:	Bragg transmission depth
CCG	:	Chemical composition grating
CH_4	:	Methane
CO	:	Carbon monoxide
CO_2	:	Carbon dioxide
CW	:	Continuous wave
dB	:	Decibel
dBm	:	Decibel with reference power as 1 milli Watt (mW)
DC	:	Direct current
EDF	:	Erbium doped fiber
ESM-PCF	:	Endless single mode photonic crystal fiber
F_2	:	Fluorine
FAF	:	Fast axial flow
FBG	:	Fiber Bragg grating
FC	:	Fiber coupler
Fig.	:	Figure

FMG	:	Few mode grating
Ga	:	Gallium
Ga $(NO_3)_3.xH_2O$	:	Gallium (III) nitrate hydrate solution
Ge	:	Germanium
GeO_2	:	Germanium dioxide/germania
GODC	:	Germanium-oxygen deficient centre
GPIB	:	General purpose interface bus
H_2	:	Hydrogen
H_2O	:	Water
He	:	Helium
HV	:	High voltage
IR	:	Infrared
Kr	:	Krypton
KrF	:	Krypton fluoride
LP	:	Linearly polarised
LPG	:	Long period grating
MCVD	:	Modified chemical vapour deposition
MFD	:	Mode field diameter
N_2	:	Nitrogen
NA	:	Numerical aperture
Nb_2O_5	:	Niobium pentoxide
Ne	:	Neon
O_2	:	Oxygen
OH	:	Hydroxyl
OSA	:	Optical spectrum analyser
PBF	:	Photonic Bandgap fiber

PCF	:	Photonic crystal fiber
PM	:	Polarisation maintaining
PMF	:	Polarisation maintaining fiber
ppm	:	Part per million
RF	:	Radio frequency
RFBG	:	Regenerated fiber Bragg grating
RGPMF	:	Regenerated grating in polarisation maintaining fiber
RI	:	Refractive index
SAF	:	Slow axial flow
SAP	:	Stress applying part
SEM	:	Scanning electron microscope
Si	:	Silicon
Si_3N_4,	:	Silicon nitride
$SiCl_4$	:	Silicon tetrachloride
SiO_2	:	Silicon dioxide/Silica
SMF	:	Single mode fiber
T_a	:	Annealing temperature
Ta_2O_5	:	Tantalum pentoxide
TEA	:	Transversely excited atmospheric pressure
TEC	:	Thermal expansion coefficient
TEM_{00}	:	Fundamental transverse electromagnetic mode
TF	:	Transverse flow
T_g	:	Glass transition temperature
UV	:	Ultraviolet
WGM	:	Whispering-gallery modes
ZnSe	:	Zinc selenide

LIST OF APPENDICES

CHAPTER 1: INTRODUCTION

The invention of optical fiber has transformed the telecommunication industry by enabling voice, data and video communications to meet the ever increasing demands of various network applications. The advantages of optical fiber such as low transmission loss, low optical nonlinearity, good immunity to electromagnetic interference and high optical damage threshold has enabled the realization of long-distance communication. These cylindrical dielectric waveguides made from silica glass have low transmission loss, high optical damage threshold, and good immunity to electromagnetic interference making them indispensable components in various applications such as telecommunication, structural health monitoring, biomedical, military and industrial sensing applications. In the fabrication process, several different processing techniques can be performed on fiber before turning them into final products. The most common fabrication technique is via the use of laser ranging from ultraviolet (UV) to mid infrared (IR) to inscribe grating along the optical fiber. The grating produced called fiber Bragg grating (FBG) is useful in telecommunication and sensing application. A brief overview of the historical development and introduction of FBG is presented in this chapter.

1.1 Introduction and Background

Hill *et al.* (1978) discovered the photosensitivity of germanosilicate fiber with Argon ion laser (488 nm). The periodic refractive index modulation along the fiber core produces the reflection of propagating light in the fiber core. This discovery has introduced FBG into the field of fiber optic research and industry. However, the progress in the research of FBG was slow due to the limitation in fabrication technique and lack of demand in the obtained reflection wavelength (visible range) at that time. This situation changed with the invention of holographic writing technique of FBG using single-photon absorption at 244 nm as reported by Meltz *et al.* (1989). The holographic writing technique is based on two interfering beams irradiated on the optical fiber to create periodic refractive index modulation. The grating period can be designed by adjusting the angle of irradiation through this technique. This technique enables the grating reflection wavelength to be extended to the regime of 1550 nm (suitable for telecommunications) and the demonstration of first fiber laser based on reflection photosensitive FBG (Kashyap *et al.*, 1990) to take place. On a similar note, in order to further increase the refractive index modulation, Lemaire *et al.* (1993) has reported the photosensitisation technique based on hydrogen gas loading.

Generally, photosensitivity of optical fiber depends on the transformation of defect in the glass structure (fiber core) during light irradiation. One of the examples is the transformation of GeO to GeE' centre during UV irradiation. This transformation is responsible for the changes in density and refractive index of the silica glass. Different defects result in different absorption band which decides the photosensitive wavelength of the material.

The photosensitivity of optical fiber can be enhanced by increasing the concentration of defects in silica glass structure. The most common technique is adding different dopants into the fiber core during the manufacturing process. The addition of germanium (Ge) into silica glass introduces GeO defect into the glass structure which has absorption at 240 nm (Cohen and Smith, 1958). Boron (B) can be used as co-dopant together with germanium to reduce refractive index. This enables more doping of germanium into optical fiber to achieve larger photosensitivity. Tin is another type of co-dopant with germanium that helps in enhancing the thermal sustainability of grating and reducing the absorption of germanium dopant in the 1500 nm window. Furthermore, the photosensitivity of optical fiber can be enhanced with postmanufacture techniques such as hydrogen loading at different temperature and pressure condition. Generally, hydrogen loading can be applied on all types of germanosilicate fiber. The hydrogen molecules react with oxygen in the silica structure to form hydroxyl ions (OH^-). The germanium ion also reacts with hydrogen molecules to form GeH, which changes the absorption band structure in the UV region. Besides germanosilicate fiber, fiber photosensitisation based on hydrogen loading can be applied on fibers with other dopants. The hydroxyl ions are formed inside the fiber core during UV irradiation on low temperature and high pressure hydrogenated optical fiber. The rate of diffusion of hydrogen into the optical fiber increases with temperature. Therefore, heating the optical fiber using flame in a hydrogen-rich atmosphere is an alternative method of hydrogenation. It is believed that the refractive index change in the optical fiber is due to the stress change and densification effect in the optical fiber (Douay *et al.* 1995, Riant *et al.* 1995, Douay *et al.* 1997, Fonjallaz *et al.* 1995).

The grating structure can be inscribed into the optical fiber by means of bulk interferometer, Lloyd mirror and prism interferometer, phase mask, or point-by-point irradiation method. Bulk interferometer method uses two UV beams from the same source to form an interference pattern on the optical fiber (Figure 1.1). The grating period depends on the wavelength and incident angle of the UV beams. A phase plate can be added to one of the arms in the setup to compensate the path length difference between two UV beams. The second method uses phase mask to form interference pattern on the optical fiber. Phase mask is a relief grating etched in a silica plate (Kashyap, 1999). The interference between different diffraction orders of UV beams form interference pattern behind the phase mask (Figure 1.2).

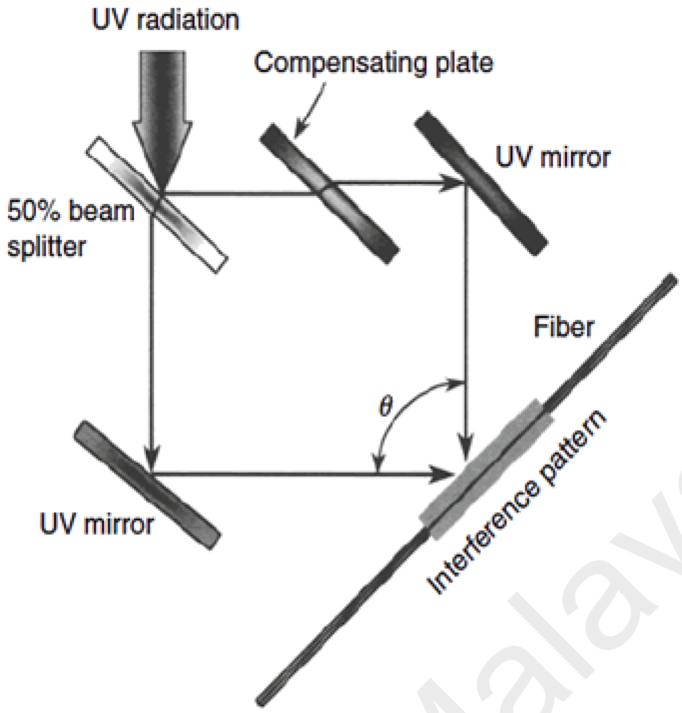

Figure 1.1 UV interferometer for FBG inscription. (Kashyap, 1999)

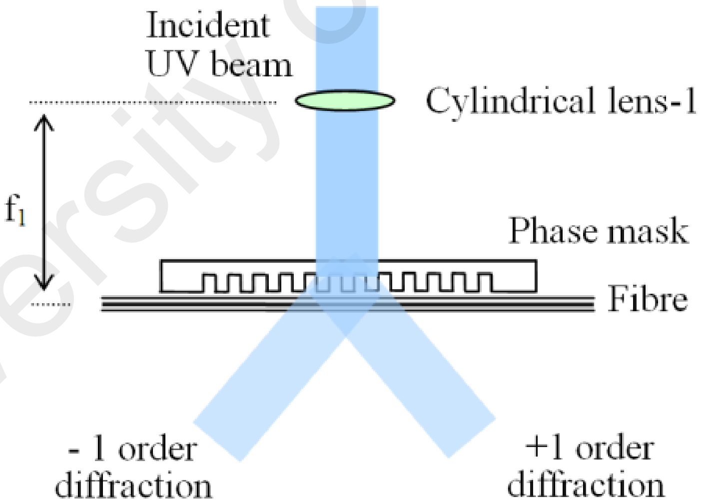

Figure 1.2 The schematic diagram of the beam diffraction from a phase mask. (Chen, 2013)

The phase mask can be in idle position or scanned along the optical fiber during UV irradiation. Phase mask can also be used as a beam splitter in an interferometer for FBG inscription (Figure 1.3). Instead of using beam splitter and mirrors to form interference,

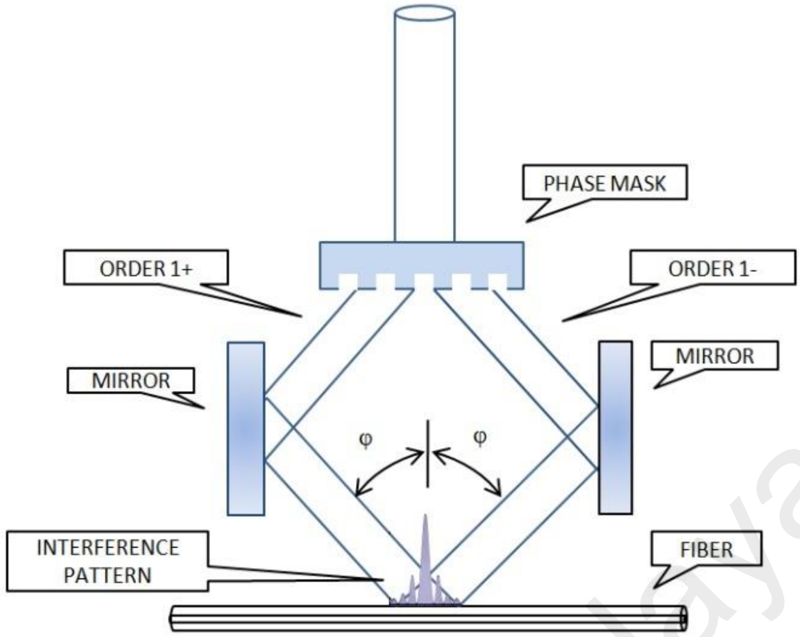

Figure 1.3 The phase mask interferometer for the inscription of FBG. (Werneck *et al.*, 2013)

Lloyd mirror method uses a fold-mirror to induce interference between two halves of the incident beam (Figure 1.4). This method is simple but results in low grating quality.

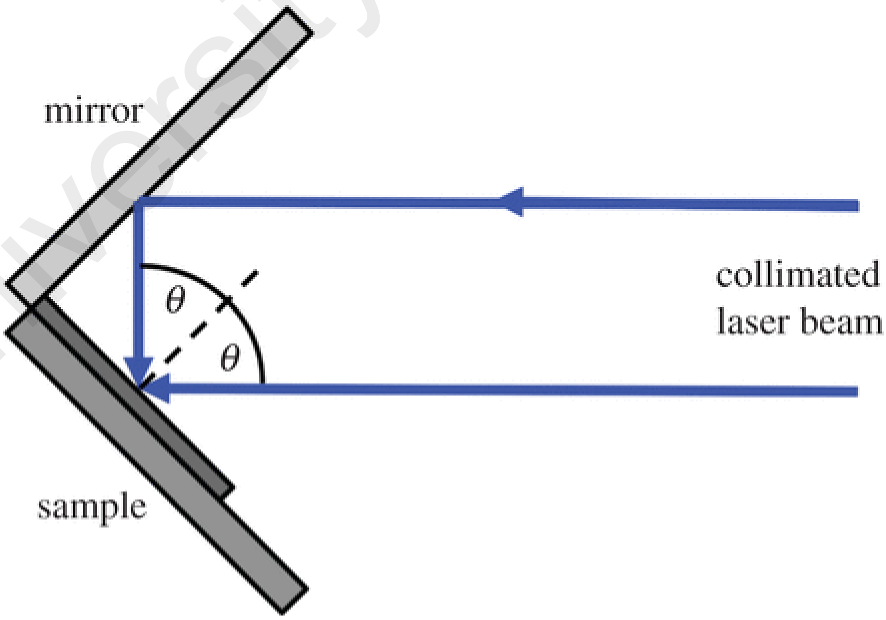

Figure 1.4 Schematic diagram of Lloyd mirror configuration. (Patole *et al.*, 2015)

Alternatively, the mirror can be replaced by a prism to achieve a much more stable interferometer. Technically, the grating structure can be inscribed into the optical fiber using point-by-point inscription scheme (Figure 1.5). However, this method is suitable for short grating due to the difficulties in controlling the accuracy of translation stage. This method is commonly used in long period grating writing.

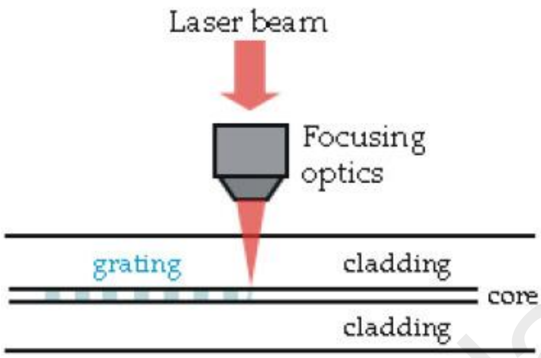

Figure 1.5 Point-by point writing technique of grating in optical fiber. (Coelho *et al.*, 2013)

1.2 Recent Development in Regenerated Fiber Bragg Grating and CO_2 laser

Since the introduction of FBG as temperature sensors, numerous efforts have been put into improving the performance of FBG in terms of maximum operation temperature. Among the important efforts include the study on different dopant composition, (Shen at al., 2007; Butov *et al.*, 2006) type-I*n* and type-II gratings (Xie *et al.*, 1993; Dong *et al.*, 1996; Groothoff & Canning, 2004; Archambault *et al.*, 1993; Hill *et al.*, 1995), femtosecond IR laser inscribed grating (Grobnic *et al.*, 2006), radiation pre-treatment (Åslund & Canning, 2000; Canning *et al.*, 2001) for high temperature sensing. Regenerated fiber Bragg grating (RFBG) is one of the emerging candidates for high temperature detection. A recent work has reported an RFBG with maximum operation temperature of 1400 °C based on multi-material optical fiber (Yang *et al.*, 2014). In the earlier development of RFBG, a similar thermal-resistant grating known as chemical composition grating (CCG) was reported by Fokine (2002). The CCG was demonstrated in hydrogen-loaded type-I grating in germanosilicate fiber. The regeneration behaviour of the grating was thought to be due to the diffusion of hydrogen fluoride in the grating at high temperature. However, this assumption has been denied by Trpkovski *et al.* (2005). A new theory based on stress relaxation due to glass structural transformation at high temperature was proposed (Bandyopadhyay *et al.*, 2008; Canning *et al.*, 2008). The grating regeneration without hydrogen loading has been demonstrated by Linder *et al.* (2009). In addition, Cook *et al.* (2012) successfully demonstrated grating regeneration in helium loaded germanosilicate fiber, which further strengthens the earlier hypothesis which states that hydrogen loading is not essential for grating regeneration. Bueno *et al.* (2013) has reported fast thermal regeneration in four different types of optical fibers: hydrogenated standard germanosilicate fiber, hydrogenated highly germanium-doped fiber, hydrogenated photosensitive germanium/boron co-doped fiber, and non-hydrogenated photosensitive germanium/boron co-doped fiber. The time required for thermal regeneration has been reduced drastically to less than 1 minute. In another work, Yang *et al.* (2013) has demonstrated thermal regeneration on etched-core FBG. The result obtained not only shows improvement in temperature sustainability of etched-core FBG sensors, it was an important finding on the relationship between thermal regeneration and stress in optical fiber.

The application of CO_2 laser annealing in material processing and manufacturing is still being studied intensively. Several new reports have been put together in the field of laser cutting (Madić *et al.*, 2014; Prajapati *et al.*, 2013; Ermolaev & Yudin, 2014), welding (Khorram *et al.*, 2011), drilling (Apostolos *et al.*, 2012; Benghalem & Allag, 2015; Subramonian *et al.*, 2015), marking (Deprez, *et al.*, 2012; Abloud *et al.*, 2007), and medicine (Rao, 2013; Jung, 2008). In the field of fiber optic research, CO_2 laser is well known for its use in long period grating (LPG) fabrication. Different types of LPG have been fabricated using CO_2 laser annealing, such as LPG in optical microfiber

(Xuan *et al.*, 2009), LPG under tension (Liu & Chiang, 2008), LPG in erbium doped fiber (Slavik & Kulisohov, 2007), periodic grooves induced LPG (Wang *et al.*, 2006a), LPG in air-core photonic bandgap fiber (Wang *et al.*, 2008b), Azimuthally symmetric LPG (Kritzinger *et al.*, 2009), and etc. Besides that, the heat generated by CO_2 laser beam can raise temperature at the irradiated spot sufficiently high to soften the glass and evaporate the surface contaminant. Therefore, it can be used for surface polishing of silica glass (Cormont *et al.*, 2013; Cormont *et al.*, 2015; Palmier *et al.*, 2009; Cormont *et al.*, 2010). The heating effect of CO_2 laser was also proven to be applicable in fiber drawing (Ward *et al.*, 2006), tapering (Özcan *et al.*, 2007) and splicing (Matsusaka *et al.*, 2008).

1.3 Motivation

The development of optical fiber-based temperature sensors with good sensitivity, robustness, high temperature sustainability and durability still remains a challenge. Several types of existing fiber optic temperature sensors have been reported, for example CCG (Fokine, 2002), sapphire fiber gratings (Grobnic *et al.*, 2004; Busch *et al.*, 2009), laser micro-machined cavity-based sensors (Rao & Ran, 2013), chemically etched sensors (Yang *et al.*, 2015) and RFBG (Inaudi & Glisic, 2006). Among all these fiber optic temperature sensors, there is an increasing interest in the study of RFBG as high temperature sensor as it has many advantages, especially the excellent temperature detection performance (Laffont *et al.*, 2013a; Laffont *et al.*, 2013b) and economic production. The operating temperature of the developed RFBGs can be as high as the maximum thermal annealing temperature. To date, RFBGs with an operating temperature up to 1400 °C has been reported (Yang *et al.*, 2014). A lot of effort has been exerted in understanding the physics and improving the performance of RFBGs. However, the real mechanism of FBG regeneration still lacks a comprehensive explanation. Several different theories have been proposed to explain this phenomenon.

However, none of them is completely valid in all cases. For example, Canning *et al.* (2008) proposed a model based on thermal and internal stress induced glass crystallization in B/Ge co-doped fibers to explain the phenomenon of grating regeneration. High temperature annealing of the FBGs induces periodic variation in the stress of fiber which leads to crystallization at the interface of periodic index modulation region. Moreover, the conventional RFBG fabrication technique utilising high temperature furnace requires further improvement in terms of productivity, flexibility and efficiency. Although RFBG have many superior characteristics, it has not been commercialized yet. In order to encourage the wide-spread application of RFBGs, the cost-effectiveness and productivity need to be further improved to at least be on par with the conventional devices. This can be achieved by developing an alternative fabrication technique that has lower fabrication cost and higher productivity. The improvement in operating accuracy, operation limit and lifespan of RFBG component are important criteria that need to be validated prior its commercialization. In addition, studies in the aspect of the thermal stress and thermal-dependent birefringence in RFBGs are limited. These factors have a great influence to the performance of RFBG, especially those that are inscribed in high birefringence fibers.

External perturbation causes the Bragg wavelength of FBG to change according to the intensity of perturbation. Therefore, the external perturbations such as temperature, stress, refractive index change can be quantified by measuring the change in Bragg wavelength of the FBG. However, the Bragg wavelength of the FBG also depends on thermal stress, thermal expansion mismatch between the fiber core and cladding (Lim *et al.*, 2013). The change in Bragg wavelength due to thermal stress variation will affect the performance of FBG components. Therefore, the study of thermal stress in FBG is crucial to its operating accuracy. Similar issue happens in polarisation maintaining fiber (PMF). The stochastic behaviour of birefringence in PMF due to different thermal history has been reported in Ourmazd *et al.* (1983). The birefringence change due to this stochastic behaviour is indistinguishable from the spectral change caused by the sensing parameter (Pavlath & Shaw, 1982). Furthermore, lower birefringence limits the operation range of the high birefringent fiber sensor. For example, the two reflection peaks that correspond to the two orthogonal modes overlap with each other when the applied strain induces more wavelength shift than the Bragg wavelength spacing (Ye *et al.*, 2002). Besides high-birefringent grating sensors, the performance of interferometric sensors based on PMF also strongly relies on the fiber birefringence (Ourmazd *et al.*, 1983; Lim *et al.*, 2010; Barlow, 1985). Therefore, studying and analysing the stochastic behaviour of PMF make an appealing approach for controlling and improving the performance of high birefringent fiber sensor in terms of operation range and sensitivity.

1.4 Objectives

The advantages of RFBG in high temperature fiber components such as high operating temperature, electromagnetic immunity, light weight, and low cost renders it a good candidate for sensing application in extreme temperature environment. Therefore, the research for developing and improving the current RFBG is essentially important in the commercialization of RFBG components. This research aims to propose an alternative fabrication method and to understand the mechanism of thermal regeneration on FBG. In addition, the carbon dioxide (CO_2) laser annealing is proposed to demonstrate the possibility of thermal regeneration, thermal stress and birefringence modification in FBG. The objectives of this research are as follow:

- To explore the mechanism of RFBG in relationship with stress relaxation in germanosilicate glass fiber.

- To develop a new fabrication technique of RFBG component using CO_2 laser annealing technique.
- To demonstrate the thermal regeneration in polarisation maintaining fiber, few-mode fiber and gallium doped fiber.
- To investigate the thermal stress and birefringence characteristic in RFBGs using CO_2 laser annealing technique and PMF.

The work starts with the demonstration of thermal regeneration of different types of fibers. The thermal response of each type of fiber was analysed and characterised using optical spectrum analyser. Subsequently, the CO_2 laser annealing was used to demonstrate the thermal regeneration and thermal stability enhancement of FBGs. The thermal stability of the CO_2 laser treated FBG was studied in terms of photosensitivity and accelerated aging of grating reflectivity at different temperatures. Furthermore, the CO_2 laser annealing was used to study the effect of cooling rate towards the thermal stress and birefringence of RFBG.

1.5 Thesis Outline

This thesis presents the study about thermal regeneration and thermal stress characteristic of FBG. This work covers the fabrication of RFBG using conventional method (hot furnace) and CO_2 annealing technique, as well as the thermal stress and birefringence modification in RFBG. The thesis outline is presented as follows.

Chapter 2 presents the theoretical and literature review of CO_2 laser and RFBG. The classification and application of CO_2 laser have been summarized. The modelling of heat transfer and temporal thermal response of optical fiber during CO_2 laser annealing and previous studies in thermal regeneration of FBG are reported and discussed. Apart from that, the effect of CO_2 laser on thermal stress and birefringence of FBG is also discussed in this chapter.

Chapter 3 presents the fabrication process of RFBG from photosensitisation to thermal sensitivity characterisation. The details of FBG inscription process is provided in this chapter. Furthermore, the results of thermal regeneration on different types of fibers are presented.

Chapter 4 introduces the CO_2 laser annealing treatment on optical fiber. The experimental setup of CO_2 laser annealing was demonstrated and characterised by studying the thermal response of FBG to CO_2 laser beam. The demonstration of thermal regeneration using CO_2 laser annealing is reported in this chapter. Furthermore, the enhancement of thermal stability of FBG using CO_2 laser is also reported in this chapter.

Chapter 5 further discusses the application of CO_2 laser annealing treatment in terms of thermal stress and birefringence modification in RFBG. The thermal stress in RFBG was proven to be related to the cooling rate after annealing. The same method has been used to modify the birefringence in regenerated grating in polarisation maintaining fiber (RGPMF).

Last but not least, all works in this thesis are concluded in Chapter 6. The future exploration of this research is also discussed in the second part of this chapter.

CHAPTER 2: LITERATURE REVIEW

This chapter presents the literature review and theories related to carbon dioxide (CO_2) laser whereby the mechanism and classification of CO_2 laser are discussed, followed by a brief review of the CO_2 laser application in optical fiber components. The modelling of fiber annealing using CO_2 laser is also presented and explained. The studies in thermal response of optical fiber are presented as well. Subsequently, a short summary of the research in thermal regeneration of fiber Bragg grating (FBG); the residual stress and birefringence in optical fiber; the relationship between birefringence of the stress-applied polarisation maintaining fiber (PMF) and the thermal properties of the optical fiber are also presented. The importance of the study of stochastic behaviour in thermal properties of the optical fiber components is discussed.

2.1 CO_2 Laser

CO_2 laser was introduced more than half a century ago (Patel, 1964). Ever since then, the CO_2 laser has found tremendous amount of applications in various fields due to its unique characteristics. Several reports on the principles and industrial application of CO_2 laser were established (Ion, 2005; Duley, 1976; Adams, 1993; Crafer *et al.*, 1998; Evans, 1990; Witteman, 1987). Typically, the active medium of a commercial CO_2 laser comprises of CO_2, helium (He), nitrogen (N_2) and a small amount of other gases. The exact composition of gas mixture needed for optimal laser performance depends on the gas flow rate, the output coupler being used and the design of the optical cavity. The addition of a small amount of water vapour and xenon gas to the active medium can improve the lifetime of active medium and output efficiency of the laser. The mixture of laser gas comprises large amount of He gas for the purpose of maintaining continuous excitation and heat conduction in the laser system.

By using different isotopes of CO_2 in laser's gas mixture of CO_2:N_2:He, numerous discrete output wavelengths in infrared (IR) range (at least 400 individual vibration lines in between 8.7-11.8 μm) (Duley, 1976) can be designed (DeMaria & Hennessey, 2010). Typically, the active medium of a commercial CO_2 laser comprises of 1-9 % of CO_2 gas, 60-85 % of He, 13-35 % of N_2 and a small amount of other gases. The gases used in the active medium must be highly purified. Among the gases in active medium, the N_2 is used to improve the efficiency of the excitation of CO_2 molecules to the upper laser level. The CO_2 molecules would be excited to the upper laser level by colliding with excited N_2 which has the similar excitation energy to the CO_2 upper laser level. The excited N_2 is metastable, which increases the efficiency of energy transfer between N_2 and CO_2. On the other hand, the He gas in the active medium has the function of improving cooling of the system. During the operation of CO_2 laser, pollutants are generated in the gas chamber. For example, the hydrogen ions (from the decomposition of water vapour), carbon (from the decomposition of hydrocarbon) and nitrogen oxide (the byproduct of reaction between N_2 and oxygen (O_2)). All these pollutants can be harmful to the laser system and degrade its performance. The addition of a small amount of water vapour and xenon gas to the active medium can improve the lifetime of the active medium and output efficiency of the laser.

CO_2 molecule has three vibrational modes: bending, symmetric stretching and asymmetric stretching corresponding to 2.0×10^{13}, 4.2×10^{13}, and 7.0×10^{13} Hz respectively as shown in Figure 2.1.

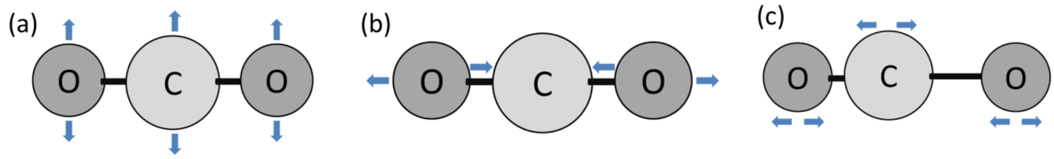

Figure 2.1 Modes of vibration of CO_2 molecules. (a) bending, (b) symmetric stretching, (c) asymmetric stretching. (Ion, 2005)

The vibrational states of the CO_2 molecule can be represented by three vibrational quanta in the order of symmetric stretching, bending, asymmetric stretching. The number of quanta of the rotational mode is denoted by the superscript on bending mode. The electronic transition during the photon generation in CO_2 laser is a four-level system, which consists of ground state, lower laser level, upper laser level and absorption level (see Figure 2.2).

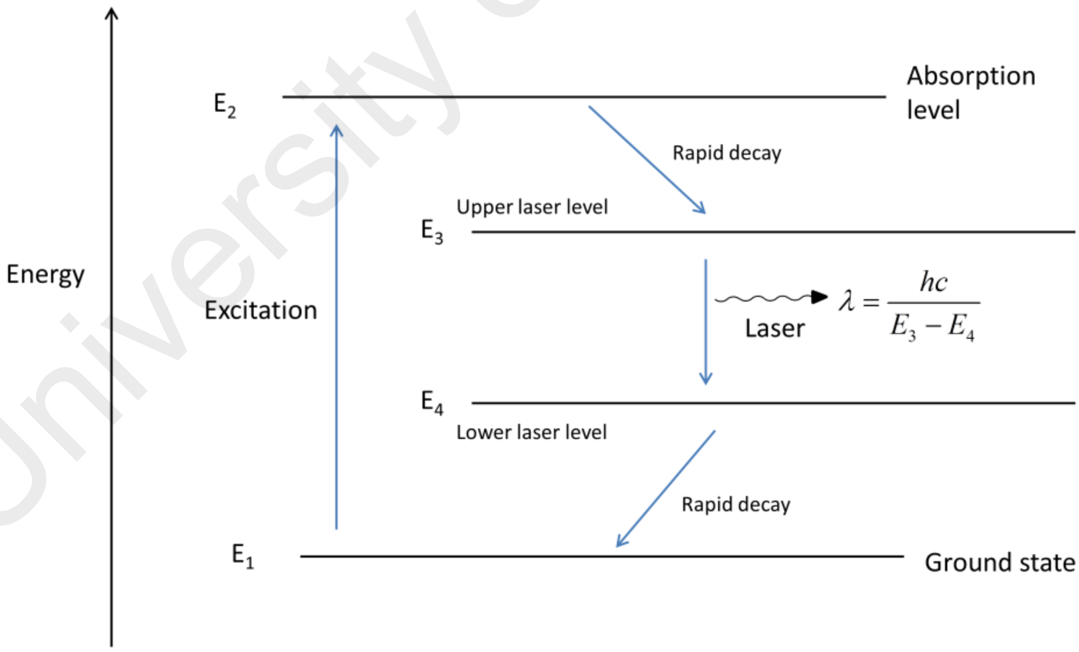

Figure 2.2 A brief presentation of electronic transitions during the photon generation in CO_2 laser (four-level laser system).

The CO_2 molecules are excited from ground state to upper laser level via inelastic collision with low energy electron or vibrationally excited N_2 molecules. The vibrational state of the CO_2 molecules is excited from ground state (00^00) to asymmetric stretching state (00^01). The generation of infrared emission at 10.6 μm can be attributed to the transition from asymmetric stretching mode to symmetric stretching mode (10^00), which corresponds to the transition from upper laser level to lower laser level. The resonator cavity is designed in such a way that the 10.6 μm emission is more favourable as compared to the others. The transition from lower laser level to ground state is important for the continuous excitation process. This process can be achieved by energy redistribution through the transfer of resonant energy to other CO_2 molecules in (02^00), (01^10), or (00^00) state. In addition, the energy of CO_2 molecules in lower laser level can be transferred to the cavity wall, other CO_2 molecules or other gas molecules by inelastic collision. This process converts the energy of the CO_2 molecules into heat that needs to be removed from the system. Therefore, a large amount of He gas is added into the laser gas mixtures for the purpose of maintaining continuous excitation and heat conduction in the laser system.

Electrical excitation is the most commonly used approach in industrial grade CO_2 laser. It can be achieved by applying direct current (DC) or alternating current (AC) to the laser system. The AC excitation can be further divided according to the frequency into radio frequency (2-100 MHz), high (20-50 kHz) and medium frequency.

2.1.1 Classification of CO_2 laser

CO_2 laser can be classified according to its cooling system. There are two basic cooling techniques being used in CO_2 laser: convection cooling and diffusion cooling. In convection cooling, the heat is carried away by flowing the laser gas mixture in sub-atmospheric pressure within the laser tube. Convectively-cooled CO_2 laser has a higher average output power as compared to diffusively-cooled CO_2 laser due to larger discharge volume allowed by this technique. On the other hand, diffusion cooling uses the cooled walls containing the gas discharge, to cool down the molecules within the laser discharge by collisions. In order to shorten the duration taken for the hot CO_2 molecules to reach the electrodes that had cooled down, electrodes need to be separated by a small distance. This results in a smaller discharge volume of diffusively-cooled CO_2 laser, making its average output power smaller than the convectively-cooled CO_2 laser (DeMaria & Hennessey, 2010). In general, CO_2 laser suffers the overheat problem due to its lower energy conversion. Therefore, cooling is the primary concern in CO_2 laser designing. Since CO_2 laser beam quality is very sensitive to the alignment stability of the resonator's mirrors, symmetric and uniform cooling of laser discharge is very important to avoid bending and twisting of mechanical structure holding the resonator's mirrors.

On the other hand, it is possible to categorize the commercially available CO_2 laser based on the geometry of laser gas flow in the optical cavity. There are five types of commonly used geometries namely, sealed, transversely excited atmospheric pressure (TEA), slow axial flow (SAF), fast axial flow (FAF) and transverse flow (Ion, 2005). Each of these geometries will be discussed in detail in the following sections.

2.1.1.1 Sealed

The sealed CO_2 laser has an optical cavity made up of large bore glass tube or square metal/dielectric tube, a fully reflecting focusing mirror and a partially transmitting output coupler that bounds the cavity. The optical cavity is excited using radio frequency (RF) applied transversely to the resonator axis. This type of CO_2 laser can produce higher power by expanding the size of the optical cavity with low contamination in the optical cavity (replenishment of laser gas to the cavity can be avoided). H_2 or water and heated nicker cathode may be added into the optical cavity to resolve CO_2 dissociation issue. The cooling of gas mixture in the optical cavity is carried out by conduction through the cavity walls and natural convection via external fins. However, forced air or liquid cooling can be applied to the laser cooling in high duty cycle application. The narrow design of the optical cavity in a sealed CO_2 laser has advantages and disadvantages. This type of cavity design produces stable output laser and mode quality. It is easy to be transported or integrated with other system, but has limited output power. Sealed CO_2 laser can be used without complex optical trains to deliver the laser beam and it can operate for a few thousands hours without needing the gas mixture to be changed.

Sealed laser can be used for various purposes such as laser marking, fusing, scribing, surface engraving, cutting, trimming, welding and drilling. This type of laser is widely used in desktop manufacturing and surgical application. To achieve a higher output power in sealed CO_2 laser, a pseudo-sealed CO_2 laser design is available. A relatively higher power density is achieved by using two parallel copper electrodes for RF excitation in a larger surface area. The water cooled electrodes are closer to each other. Hence, the heat generated in the gas can be dissipated via diffusion through the electrodes, which improves the cooling of the cavity. When compared to other types of gas flow CO_2 laser with same output power, the gas consumption and size of sealed CO_2 laser is smaller.

2.1.1.2 Transversely Excited Atmospheric Pressure (TEA)

In TEA CO_2 laser, a higher power level can be achieved due to higher gas pressure (several atmospheric pressures) in the cavity. The active medium is excited by a large voltage electrical discharge that is applied transversely along the optical axis. The output of the TEA CO_2 laser is a pulsed laser beam. The reason behind this limitation is the discharge instabilities which occur due to high gas pressure in the cavity, resulting in a degradation of the output power. The output laser beam of TEA CO_2 laser is typically large (few cm^2 in cross-sectional area). Low energy (in joules) and short pulse (in nano to microseconds) can be achieved by using very short discharge times. A short duration but high power pulse can be achieved by using mode locking technique. TEA CO_2 laser is commonly used in marking on aluminium cans and plastic packages due to its low output power and light weight.

2.1.1.3 Slow Axial Flow (SAF)

The SAF CO_2 laser has the similar gas pressure as in sealed CO_2 laser. However, the He content in the gas mixture is relatively higher for cooling purpose. The optical cavity is made up of glass tube several centimetres in diameter. The generated output power is proportional to the cavity length. The two ends of the optical cavity consist of a fully reflecting spherical mirror and a partially transmitting output coupler situated opposite to each other. The focal point of the spherical mirror is located in the plane of the output coupler. In SAF CO_2 laser, the gas flows in the direction parallel to the optical axis of the cavity at a relatively slower rate to remove the contamination in the cavity. The laser gas is excited by a tens of thousands of volts. When the temperature is below the threshold temperature, the output laser power increases with the discharge current. The optimum discharge current depends on the cavity diameter and laser gas pressure. Due to slower gas flow rate, the gas mixture in the cavity can easily be overheated. Therefore, the wall of the discharge tube is cooled by water, oil, or air to increase the out diffusion of excessive heat from the hot laser gas. The discharge tube of SAF CO_2 laser is designed to be narrow to increase the cooling efficiency.

A high quality and stable TEM_{00} mode laser beam can be generated by SAF CO_2 laser, due to the stable mirror alignment, limited cavity length and average gain along the laser beam path in cavity. The gas flow in SAF CO_2 laser solves the problem found in sealed CO_2 laser, such as contamination and size. The running and maintenance cost of SAF CO_2 laser is low. This laser is ideal for fine cutting, scribing, precision drilling and pulsed welding application.

2.1.1.4 Fast Axial Flow (FAF)

In FAF CO_2 laser, the output power is increased by increasing the laser gas flow rate and the diameter of optical cavity. The laser gas in the cavity is circulated by turbine blowers at a high flow rate. A little amount of make-up gas is continuously added into the laser gas mixture in order to maintain the laser gas mixture composition. The cooling of laser gas is achieved by passing the gas through a deionised water heat exchanger. In FAF CO_2 laser, both RF and DC excitation are used to excite the active medium. In RF excitation design, the electrodes are located outside of the discharge tube. On the other hand, the anode and cathode in DC excitation design are positioned inside the discharge tube in a coaxial manner and located downstream at the end of the discharge region, respectively as shown in Figure 2.3.

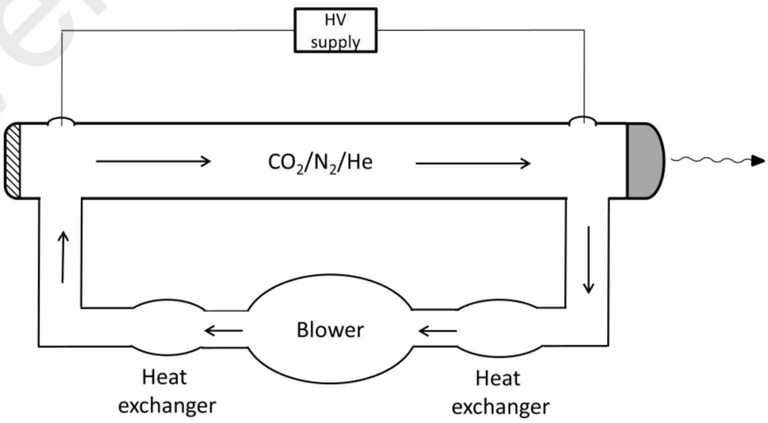

Figure 2.3 Schematic diagram of FAF CO_2 laser. HV: High voltage.

The high density electron clusters in the discharge tube is removed by shockwaves generated by orifices in order to stabilise the discharge of laser. The orifice also provides cooling effect to the system by rapid expansion of gas downstream of it. Due to the gain-smoothing effect of the turbulent gas flow, FAF CO_2 laser can generate stable output laser beam in low order mode. Pulsed laser can be mechanically and electrically triggered in DC and RF excitation systems, respectively.

The maximum tube diameter of the resonator tube is restricted by mechanical, thermal distortions and high order modes generation. Larger tube diameter provides higher output power, but lower stability and non-single mode output. By using mirrors, the resonator tubes of the can be folded in different geometries. For example, superimposed vertical squares, vertical zig-zag, inclined triangle and octagon. The excitation and gas flow is applied to each section of these folded geometries. Aperture and hemispherical cavity design can improve the output laser beam modes at the expense of lower output power. For output power above 10 kW, an aerodynamic window is required, otherwise solid-coated zinc selenide (ZnSe) output coupler is used. The polarisation of output laser beam is affected by the folding geometry of laser cavity. The material processing characteristic of laser beam travelling in different direction is affected by the state of polarisation. For example, different polarisation of light has different level of absorption by metal at different grazing angles of incidence. The kerf produced is narrower and faster when the laser beam is polarised in the direction of incident. Otherwise, the kerf produced is wider when the polarisation is at an angle to the cut. FAF CO_2 laser is used in various material processing applications, like cutting, welding, drilling and surface treatment. Due to the difficulties in maintaining glow discharge under high gas pressure and blower technology, the maximum throughput power of commercial FAF CO_2 laser is limited to ~20 kW.

2.1.1.5 Transverse Flow (TF)

In transverse flow CO_2 laser, the laser gas is circulated across the laser cavity with a large cross-sectional area. When compared to FAF type CO_2 laser, TF CO_2 laser has a lower gas flow rate (10 % of FAF flow rate) which reduces the need of a blower for the system. The effect of gas flow rate on temperature, population inversion and beam power can be reduced in TF CO_2 laser. A shorter cavity can be constructed in this laser by making use of the high power generated per unit cavity length. The active medium of TF CO_2 laser can be excited by DC or RF excitation. The axis of excitation and the direction of gas flow and optical axis are perpendicular to each other, allowing a lower working voltage to be used as compared to the FAF design. The two electrodes used in RF excitation are located outside the discharge region. A turbulence generator or a high energy electron beam can be accommodated when stabilising the discharge. Pre-ionization is required if the main discharge is to fill the laser volume. The excess heat in the laser gas is carried away with the aid of a heat exchanger containing deionized water. In DC excitation, the electrode used consists of a complex segmented configuration in order to maintain a homogeneous discharge over the large resonator section and also to avoid arcing. The cathode is usually water-cooled.

The output coupler is an annular curved scraper mirror. The homogeneity of the power of laser beam is affected by the optical cavity geometry and extraction technique. An asymmetric and higher divergence laser beam is generated when the transverse discharge is inhomogeneous. A multimode laser beam (mixture of low order transverse modes) is produced by a stable cavity. Whereas, a laser beam with annular intensity distribution is generated from an unstable cavity due to the annular scraper mirror. The advantages of TF CO_2 laser include high throughout power, economical, compact design, low gas usage and low operating voltage (DC excitation). However, the low mode quality of laser beam and difficulty in producing pulse output are the drawbacks of the design. This type of CO_2 laser is used for thick section welding and large area surface treatment.

2.1.1.6 Gas Dynamic

Apart from the five types of CO_2 laser mentioned above, there is another type of CO_2 laser which is not commercially available. It is the gas dynamic CO_2 laser. The population inversion of this type of laser is achieved by thermodynamic excitation. The CO_2 gas is produced by the combustion between carbon monoxide (CO) and methane (CH_4). The CO_2 molecules are excited through the collision with excited N_2 molecules at high temperature. Energy transferred from N_2 molecules excites the CO_2 molecules to the upper laser level when the gas is expanded through a supersonic nozzle. The non-equilibrium condition created by momentarily frozen higher energy state facilitates the population inversion. Continuous output power, as high as 100 kW, has been produced by this type of laser which is useful for material processing.

2.1.2 Applications

Due to the high absorptance of various materials to mid-infrared radiation (Dobrovinskaya *et al.*, 2009), CO_2 laser has gained attractiveness in the field of manufacturing, particularly in the material treatment applications such as cutting (Madić *et al.*, 2014; Prajapati *et al.*, 2013; Ermolaev & Yudin, 2014; Vergeest, 2001), machining (Markillie *et al.*, 2002; Presby *et al.*, 1990; Forrest *et al.*, 1996), welding (Khorram *et al.*, 2011), drilling (Apostolos *et al.*, 2012; Benghalem & Allag, 2015; Subramonian *et al.*, 2015; Yeo *et al.*, 1994) and marking (Deprez *et al.*, 2012; Abloud *et al.*, 2007). In nanoscale material fabrication, nanoparticles can be produced by irradiating liquid solution with CO_2 laser (Ion, 2005). In furniture, different colours and textures are obtained in laser engraving on wood using CO_2 laser using different pulse length and gas for shielding. In automobile and display industry, CO_2 laser is very useful due to lower operational cost and waste, as well as higher productivity. Besides that, it is also found to be useful in a broad range of applications in the field of medicine (Rao, 2013; Ascher & Heppner, 1984; Baker *et al.*, 1984; Beck, 1980) and military industry (Harney, 1989). In medical application, CO_2 laser is used for skin resurface, dermatology (Jung, 2008), neurosurgery (Ascher & Heppner, 1984; Beck, 1980), plastic surgery (Baker *et al.*, 1984; Mittelman & Apfelberg, 1990) and otorhinolaryngology (Ossoff *et al.*, 1994). Multi-kilowatt CO_2 laser systems are now common in the production lines of automotive industry. They can be used for re-melting and hardening cam lobes as well as cutting and welding of bodywork, power train assemblies and accessories. In the field of arts, CO_2 laser is used for cutting and welding complex structure of artwork. In the aerospace industry, CO_2 laser is commonly used in wielding aircraft skin stringers. It is also used in drilling holes on the combustor of jet engine (Ion, 2005). In military application, CO_2 laser can be used in range finder, beamrider, radar, covert/secure communication link and active infrared countermeasures (Harney, 1989).

CO_2 laser annealing has proven to be an invaluable tool for the manipulation of fiber properties in order to enhance the functionality of optical fiber. In general, this is achieved via the controlled deposition of heat from the CO_2 laser operating in infrared regime into the fiber. This enables the CO_2 laser to be used as a heat source for fiber annealing, which is an important process in the manipulation of fiber properties. The advantages of CO_2 laser annealing include near-instantaneous heating rates, minimum contamination and controllable temperatures with varying laser intensity (Holmberg & Fokine, 2013). For example, fiber annealing is needed for long period grating (LPG) fabrication (Benda & Parasco, 2011) and stress relaxation (Kim *et al.*, 2001; Kim *et al.*, 2002; Kim *et al.*, 2000). Meanwhile, the high annealing temperature is sufficiently high for softening fiber glass. It is one of the vital enabling condition for (i) the manipulation of cross sectional shape of fiber (Kewitsch *et al.*, 2001), (ii) the fabrication of fused taper coupler (Yokota *et al.*, 1997; Dimmick *et al.*, 1999; McAtamney *et al.*, 2005), micro-resonator (Kakarantzas *et al.*, 2001), tapered fiber (Xuan *et al.*, 2009) and microfiber (Williamson & Miles, 1996; Fairbanks, 1991; Ward *et al.*, 2006; Özcan *et al.*, 2007), (iii) fiber drawing (Paek, 1974) and splicing (Fujita *et al.* 1976), (iv) healing of scratches and damaged site on silica surface (Temple *et al.*, 1982; Cormont, *et al.*, 2013; Cormont *et al.*, 2015) and (v) enhancing the surface smoothness and ultraviolet (UV)-laser damage resistance of silica glass (Cormont *et al.*, 2013; Brusasco *et al.*, 2002; Palmier, 2009, Cormont *et al.*, 2010). Several patents on the application of CO_2 laser for stripping, splicing, tapering and heating of optical fiber have been filed (Cale *et al.*, 2011; Zheng *et al.*, 2015; Danley *et al.*, 2015). Other than that, CO_2 laser was used for fiber end-shaping (Forrest *et al.*, 1996; Danley, *et al.*, 2007; Vaidya & Harrington, 1992) that can enhance the light coupling from diode source (Presby *et al.*, 1990). Fiber end being shaped into a hemisphere using CO_2 laser will act as a micro-lens that is useful for high efficiency coupling between optical fibers (Paek & Weaver, 1975). In the meantime, a patent of CO_2 laser polishing technique that applies on fiber optics connector has been reported by Szentesi & McMahon (1993). Imen *et al.* (1990) reported a technique to fabricate fiber optical taps for interconnector and optical data processing device using continuous wave (CW) CO_2 laser. Pre-treatment with CO_2 laser has proven to be useful for photosensitivity enhancement in optical fiber when exposed to UV radiation. LPG fabricated by point-to-point irradiation method using focused CO_2 laser pulses has appeared to exhibit high thermal stability characteristics up to a temperature level of 1200 °C (Davis *et al.*, 1999).

2.1.2.1 Long Period Grating (LPG)

During LPG fabrication using CO_2 laser, thermal relaxation in fiber glass matrix is the main constituent that contributes to the refractive index perturbation along the fiber.

Pulsed CO_2 laser is often used in LPG fabrication, whereas CW CO_2 laser requires a modulator or a shutter to achieve point-to-point irradiation during fabrication process (Kakarantzas *et al.*, 2002). LPG was successfully inscribed on different fibers using CO_2 laser, like conventional single mode fiber (SMF), boron-doped SMF, erbium doped fiber (EDF) (Slavik & Kulisohov, 2007), photonic crystal fiber (PCF), PMF, photonic bandgap fiber (PBF) and etc.

LPG can be manufactured based on several techniques such as tapering (Xuan *et al.*, 2009), carving (Wang *et al.*, 2006a), through mechanical stress relaxation or air-hole collapsing (for PCF and PBF) (Wang *et al.*, 2008b) using CO_2 laser. Another investigation has demonstrated the fabrication of an asymmetric LPG with a high attenuation of −47.39 dB and a low insertion loss of 0.34 dB using a focused CO_2 laser beam and carving periodic grooves on one side of the optical fiber (see Figure 2.4).

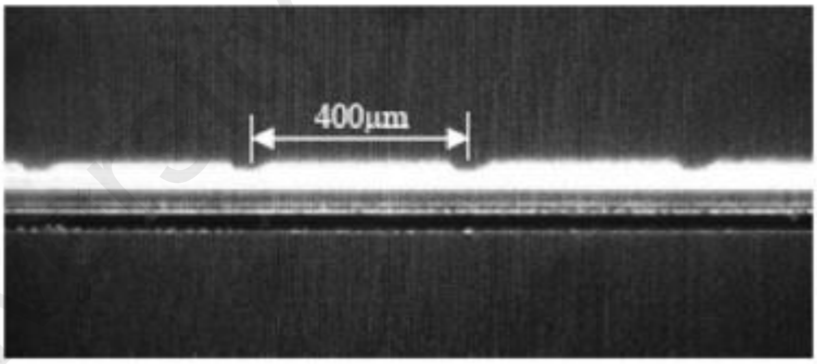

Figure 2.4 Micrograph of the CO_2-laser-carved LPG with a grating period of 400 μm. (Wang *et al.*, 2006a)

The refractive index modulation and average strain sensitivity of the LPG can be enhanced by these CO_2-laser-induced periodic grooves and stretch-induced periodic microbends (Wang *et al.*, 2006a). The resonant wavelength of LPG was blue-shifted when the number of grooves on the fiber was increased. This results in simultaneous increase in the attenuation peak and a decrease in the 3 dB bandwidth of LPG. When the fiber with periodic grooves is stretched longitudinally, microbends can be induced on the grooved section of the fiber. The refractive index perturbation Δn in the fiber can be expressed as

$$\Delta n = \Delta n_{residual} + \Delta n_{groove} + \Delta n_{strain} + \Delta n_{microbend} \tag{5}$$

where $\Delta n_{\text{residual}}$ is the initial refractive index perturbation due to residual stress relaxation in the fiber caused by high temperature, Δn_{groove} initial refractive index perturbation due to periodic grooves on the fiber, Δn_{strain} refractive index perturbation due to difference in stretch-induced strains between grooved and ungrooved region in the fiber and $\Delta n_{\text{microbend}}$ refractive index perturbation due to stretch-induced microbend. As a result, the efficiency of refractive index modulation of the grooved LPG is higher than the ungrooved LPG. This in turn leads to a larger attenuation peak and a lower insertion loss. Although the resonant wavelength of LPG shifts to a shorter wavelength when tensile stress is applied on the LPG, the resonant wavelength starts to shift towards a longer wavelength if the tensile strain exceeds the critical level (~100 με). This is due to over-coupling between the fundamental core modes and cladding mode when a large refractive index perturbation in the LPG gives rise to the maximum coupling efficiency. By periodically carving grooves on the optical fiber using CO_2 laser, the strain sensitivity of the resonant wavelength of LPGs in the same type of optical fiber can be increased by 229 times. However, the polarisation dependence of LPG is not enhanced by asymmetric periodic grooves of the fiber. This is because the refractive index perturbation on fiber is limited to the outer cladding. This method of grooved LPG fabrication using CO_2 laser had been patented (Wang *et al.*, 2008a).

On the other hand, the azimuthally asymmetry in LPG introduces additional birefringence which causes polarisation losses. A fabrication method for azimuthally symmetric LPGs based on a TEM_{01}-mode CO_2 laser was reported by Kritzinger *et al.* (2009). The mode quality of laser beam was improved by inserting an aperture into the laser cavity. The original laser beam of TEM_{01} mode is shown in Figure 2.5(a). After the insertion of aperture into the laser cavity, the output laser beam's shape had been transformed into the shape as shown in Figure 2.5(b). The method and design of fabricating anti-symmetric LPG by microbending has been patented by Samsung Electronics Co., Ltd (Paek *et al.*, 2002).

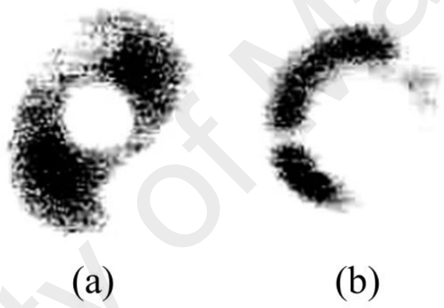

Figure 2.5 (a) Original TEM_{01} mode of the CW CO_2 laser. (b) Improved TEM_{01} mode after insertion of aperture into the laser cavity. (Kritzinger *et al.*, 2009)

The efficiency of writing a LPG in a SMF using CO_2 laser pulses increases significantly with respect to the axial stress applied along the fiber. The threshold of energy density of CO_2 laser radiation required to inscribe the grating on the optical fiber decreases greatly with an increase in the applied tension. The micrograph of LPGs fabricated under unstressed and stressed conditions is presented in Figure 2.6.

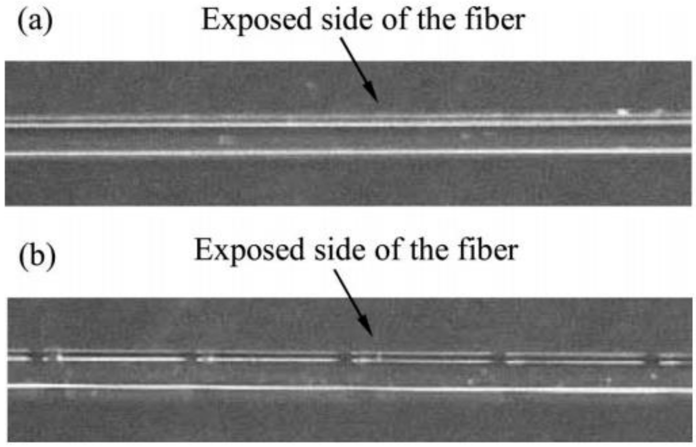

Figure 2.6 Micrograph of the SMF-130 V LPG inscribed using three scanning cycles of CO_2 laser exposure at an intensity of 6.0 J/mm^2 (a) No visible deformation is observed. (b) Deformation is formed on the exposed side of the fiber under stressed (250 g) condition. (Liu & Chiang, 2008)

The inelastic frozen-in strains induced by CO_2 laser irradiation under tension contributes to the enhancement in the efficiency of LPG inscription. Therefore, the control of axial stress distribution along a fiber during the CO_2 laser writing process provides an additional degree of freedom for the control of resultant grating characteristics (Liu & Chiang, 2008). Exposing one side of the fiber to a high energy density CO_2 laser induces additional, nonaxially symmetrical refractive index change across the cladding part. This causes the couplings of light between the axially and nonaxially symmetric cladding modes in the LPG. However, for the fiber under high tension, higher energy density was required to generate a significant nonaxially symmetrical refractive index distribution in the cladding through direct absorption (Liu *et al.*, 2007). Although the tension applied on fiber before grating inscription was axially symmetrical across the fiber, the axial temperature inhomogeneity across the fiber at the exposed side caused the frozen-in inelastic strain to be much stronger at irradiation side (Grellier *et al.*, 1998). This results in axially asymmetrical index distribution being induced on the fiber. In Slavík's (2006) work, the realization of a long-period fiber grating-based filter made in a standard telecom optical fiber with a resonant attenuation of more than 60 dB had been reported.

(a) ***Photonic Crystal Fiber (PCF)***

The first structural LPGs written in pure-silica solid core PCFs was reported by Kakarantzas *et al.* (2002). The gratings were inscribed on PCF by periodic collapse of air holes via annealing with a CO_2 laser. The resulting periodic hole-size perturbation produced core-to cladding-mode conversion, thus creating a novel LPG in the PCF. This technique, combining with periodic mechanical twisting, can be used to fabricate a rocking filter in a polarisation-maintaining (PM) PCF. Besides that, a LPG sensor with a high strain sensitivity (−7.6 pm/με) and a low temperature sensitivity (3.91 pm/°C) was fabricated using a focused CO_2 laser beam to carve periodic grooves on a large mode-area PCF. Such strain sensor can effectively reduce the cross-sensitivity between strain and temperature. And as a result, the temperature-induced strain error obtained was only 0.5 με/°C without using temperature compensation (Wang *et al.*, 2006b). Through the fabrication of LPG in endless single mode photonic crystal fiber (ESM-PCF) using pulsed CO_2 laser, the glass volume change and densification were revealed by the shift in the resonant wavelength (Rao *et al.*, 2010).

(b) ***High Birefringent Fiber / Polarisation maintaining Fiber (PMF)***

The first optical fiber rocking filter based on high birefringent PCF LPG was demonstrated by Kakarantzas *et al.* (2003). The permanent twist in the fiber's principal axes was produced by mechanically twisting the fiber and annealing with CO_2 laser one point at a time. The fiber was clamped and twisted from one end by the motorized clamps at a desired angle, speed and frequency. The twisted fiber was then annealed with a focused CO_2 laser beam at a particular point along the fiber. The complete LPG rocking filter has been formed by sweeping the CO_2 laser beam along the fiber to produce periodic twists. The CO_2 laser irradiation intensity and time have to be carefully controlled in order to deform the fiber and at the same time to avoid the collapse of air holes.

The grating inscription efficiency in PMF is greatly orientation dependent. When the CO_2 laser irradiation direction is parallel to the principal axis of the PMF, the grating inscription efficiency reaches the highest level. This effect is strongest in conventional PMF as compared to PM PCF. The high boron dopant concentration in stress applying part (SAP) induces a higher mechanical stress and lower fictive temperature into the SAP. Therefore, the heating effect induced by CO_2 laser irradiation causes the stress relaxation of SAP and indirectly affects the refractive index of the fiber core. The LPG formation in PMF is the combination of direct and indirect (by SAP) modification of stress distribution in the fiber core. As a result, when the CO_2 laser irradiation direction is perpendicular to the principal axis of the PMF, the stress relaxation in SAP is lower due to greater distance between the SAPs and laser source. This causes the LPG inscription efficiency to be lower in this particular scenario. Comparatively, the PM PCF requires a higher CO_2 laser intensity for grating inscription than that for conventional PMF. This is because the stress relaxation of fiber core is not responsible for grating formation in PM PCF. The cladding and the core of PM PCF are made up of pure silica, which limits the mechanical stress in the fiber core. The higher laser density required for grating inscription in PM PCF suggests that the glass densification and hole deformation are responsible for LPG formation (Lee *et al.*, 2008). Due to larger distance between fiber core and SAPs, the orientation dependence during grating inscription process is not as significant as in conventional PMF. The effect of stress relaxation in SAPs has limited effect on the fiber core. Besides that, the air hole cladding in PM PCF can reduce the thermal and mechanical stress on the fiber core which further decreases the influence of SAPs on fiber core (Lee *et al.*, 2008). It is shown that the temperature and strain response of the resonance peaks for fast and slow axes are different not only in terms of their magnitudes but also in the signs of slope. Furthermore, the characteristics for different polarisation modes are different, both in magnitudes and signs (Zhou *et al.*, 2003).

(c) ***Photonic Bandgap Fiber (PBF)***

A high quality LPG inscribed on an air-core PBF was first demonstrated by Wang *et al.* (2008b). A focused pulsed CO_2 laser beam was used to periodically deform/perturb air holes along the fiber axis. The CO_2 laser irradiation induced high temperature on the fiber and caused ablation on the fiber surface. This changed the air hole size or shape in the cladding. The deformation in the holey cladding structure only occurred on the side of the fiber irradiated by the CO_2 laser. The deformation in the core is very insignificant to be observed. Therefore, out of the two phenomena (stress relaxation and perturbation in geometric structure) that contribute to the formation of PCF LPG, periodic perturbation in the holey cladding structure is the main factor that causes the resonant mode coupling. The CO_2 laser induced asymmetric fiber cross section (see Figure 2.7 (b)) produces birefringence and asymmetrical mode field profile, which is responsible for larger polarisation dependent losses.

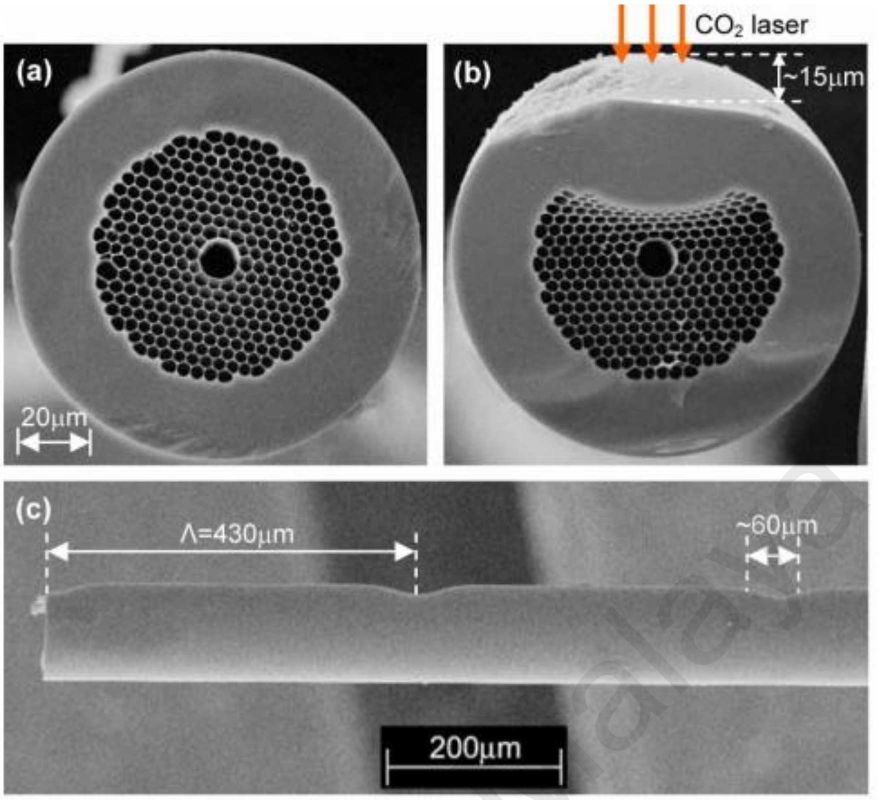

Figure 2.7 Scanning electron microscopic images of the cross-sections of PBF (a) before and (b) after CO_2 laser irradiation. (c) Periodic grooves on PBF after fifty scanning cycles. (Wang *et al.*, 2008b)

2.1.2.2 Fiber Components Fabrication

CO_2 laser has been proposed as a heat source for fiber drawing process by Paek (1974). A CO_2 laser with an ellipsoidal reflector system was used to produce clad and unclad fiber from a bulk-fused silica preform. The required laser power depends on the feeding speed of preform. Higher feeding speed requires higher laser power in order to draw the fiber from the preform. The fiber preform was first fed into the reflector (see Figure 2.8) and the CO_2 laser beam was focused on one end of the preform up to its softening point. The softened part was pulled down by a rotational take-up reel continuously to a thin fiber. In comparison with other heating techniques such as oxyhydrogen torch, induction heating, resistance heating and plasma heating, CO_2 laser heating offers the advantages of rapid temperature control because of the fast heat generation in silica glass and lesser amount of impurities required into the fiber (Paek, 1974).

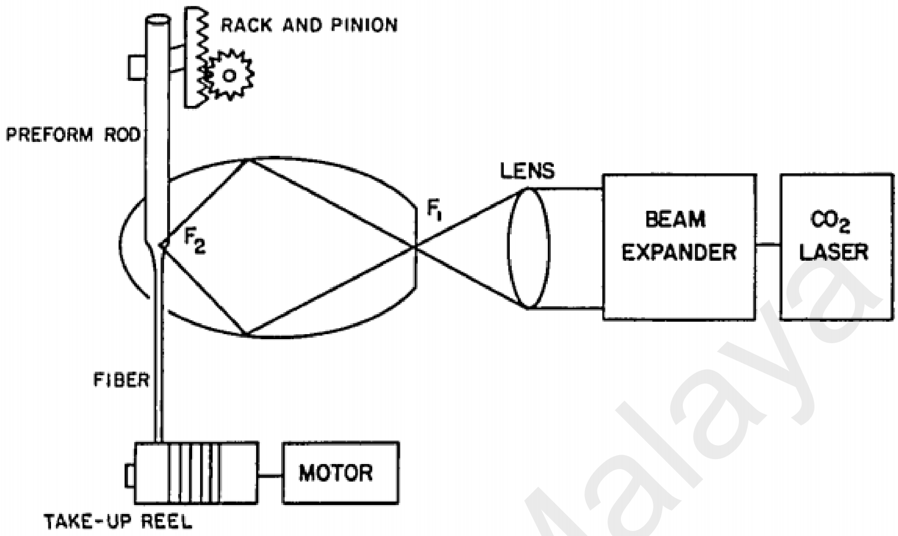

Figure 2.8 Schematic setup of fiber drawing using CO_2 laser. (Paek, 1974)

Laser processing on optical fiber is very useful in achieving miniaturization of compact active and passive all-fiber devices. The first example of CO_2 laser application in fiber optics device is the splicing of optical fiber. Instead of using electric arc fusion, CO_2 laser can also be used as the heat source for glass softening and fusion of two optical fibers. Low loss splicing in silica optical fibers using CO_2 laser was demonstrated by Fujita *et al.* (1976). Splicing losses of less than 0.5 dB per splice have been demonstrated in repeated experiments. The advantages of using CO_2 laser for splicing are the high precision in controlling the heating position and low contamination in splicing point. Following this, Egashira & Kobayashi (1977) had successfully demonstrated splicing of optical fiber using low power CO_2 laser. A minimum of 0.02 dB splicing loss was achieved by using 2.3 W and 1 mm diameter laser beam (Egashira & Kobayashi, 1977). Kinoshita & Kobayashi (1982) had demonstrated optical fiber splicing on a two dimensionally arrayed optical fiber bundle using CO_2 laser. In

Matsusaka *et al.* (2008) work, CO_2 laser has been used for the splicing of ribbon-shaped optical fibers. The control of CO_2 laser beam intensity is critical in achieving the softening point of silica fiber in order to splice the two fiber end.

Fabrication of taper fiber using CO_2 laser as the heat source had been reported by Yokota *et al.* (1997), Williamson & Miles (1996), and Fairbanks (1991). In comparison with other fabrication techniques, CO_2 laser heating technique offers many advantages in terms of low contamination, fast heating capabilities, stable and controllable beam conditions and less impact by the environmental factors. The taper profile of fiber can be precisely controlled by manipulating the heating zone. However, the minimum tapered fiber diameter fabricated using CO_2 laser is larger than the one fabricated using flame heating technique (Cale *et al.*, 2011). Ward *et al.* (2006) developed a new method to further reduce the minimum diameter of tapered fiber fabricated using CO_2 laser heating. A low loss tapered fiber with a diameter of 3-4 μm was fabricated using SMF and scanning beam technique. In the fabrication, a focused CO_2 beam was irradiating on a fiber translating in the perpendicular direction with the laser irradiating direction controlled by a motorised stage. At the same time, two ends of the fiber were elongated during the process to taper the fiber. This technique is useful in fabricating LPG, microresonator, fused tapered coupler and bottle resonator (Ward *et al.*, 2006).

Özcan *et al.* (2007) proposed a two-beam technique for the fabrication of tapered fiber using CO_2 laser. Two parallel and co-propagating CO_2 laser beams generated from the same source irradiate on the top and bottom part of an optical fiber during annealing process. In comparison with the single-beam technique, the fiber cross sectional symmetry was greatly maintained after annealing using the two-beam technique. The tapered fiber annealed with two-beam technique posed a uniform and low ellipticity of ~0.5 % along the fiber. This was due to the uniform heat distribution in the fiber when the fiber was irradiated by two CO_2 laser beam above and below the fiber axis simultaneously (Özcan *et al.*, 2007).

Generally, fused tapered fiber couplers are fabricated using the flame heating method and in-situ monitoring is carried out during the fabrication process to control the coupling ratio. The taper shape and waist radius can be precisely controlled by scanning the fiber with a point-like heat source in a controlled manner. This can be achieved using an oxybutane burner as the heat source. However, the disadvantages such as flame size, fluctuation in temperature due to environmental factors and insufficient dynamic control in the scanning direction limit the applicability of this technique. The slow heating rate in the resistive electrical heater makes it difficult to fully overcome the weakness of oxybutane burner. Comparatively, the use of CO_2 laser as the heat source provides the advantages of low contamination, fast thermal response and easy control of the heating temperature, location and scanning direction (Dimmick *et al.*, 1999). The fused tapered coupler fabrication using CO_2 laser annealing technique had been applied in both Yokota *et al.* (1997) and Dimmick *et al.* (1999) work. However, the study of Dimmick *et al.* (1999) deviated from that of Yokota *et al.* (1997), in which the CO_2 laser scans through the fiber to attain the precise fiber taper shape. Besides the conventional fused coupler, the fabrication of fused microcoupler using CO_2 laser as the heat source had also been reported. The fabricated fused microcoupler is shorter and resistant to bending loss compared to conventional fused coupler. Due to shorter length, the microcouplers can be constructed into integrated arrays without consuming much space. One of the examples would be the arrays of Mach–Zehnder interferometers (Kakarantzas *et al.* 2001).

McAtamney *et al.* (2005) reported the fabrication of fused biconic tapered coupler using CO_2 laser heating technique. In their work, the CO_2 laser was used as the heat source to fabricate fused biconic taper coupler based on two different approaches, namely scanning beam technique and diffractive optical element technique. The scanning beam technique is similar to that reported by Bayle & Meunier (2005). Two fibers were twisted around each other using a motorized rotational stage at the required tension. The fibers were pulled by the pulling stages while the CO_2 laser beam was irradiating and scanning along the fibers. The diffractive optical element technique was applied during fixed beam heating to solve the non-uniform heating caused by the Gaussian profile of CO_2 laser beam. Uniform heating zone was achieved by placing a diffractive optical element in between fiber target and beam expander. The lens structure of diffractive optical element has an adjusted Fresnel zone micro-relief pattern imparted on the plano side of a plano-concave lens to produce the required beam profile (Duparré *et al.*, 1995). The laser beam intensity was shaped into a rectangular top hat profile after passing through the diffractive optical element. The peaked regions at the edge were filtered by an aperture to produce a flat top beam profile. During laser heating process, the fiber was placed on the pulling stages with a specific tension. The fiber was then elongated by the pulling stages while being irradiated by the modified CO_2 laser beam (McAtamney *et al.*, 2005).

Xuan *et al.* (2009) reported a 20-period LPG with a 27 dB attenuation dip inscribed on microfiber with a diameter of ~6.3 µm. The conventional SMF was first tapered down to a microfiber with a few microns diameter using hydrogen flame heating technique. Then, the focused pulsed CO_2 laser irradiates periodically on the microfiber together with a small tension applied on both end of the fiber to introduce micro tapers along the fiber (see Figure 2.9). The scanning electron microscope (SEM) images of LPG fabricated in a microfiber are presented in Figure 2.10. The thermal characterisation result shows that the resonant wavelength of this micro-tapered LPG in

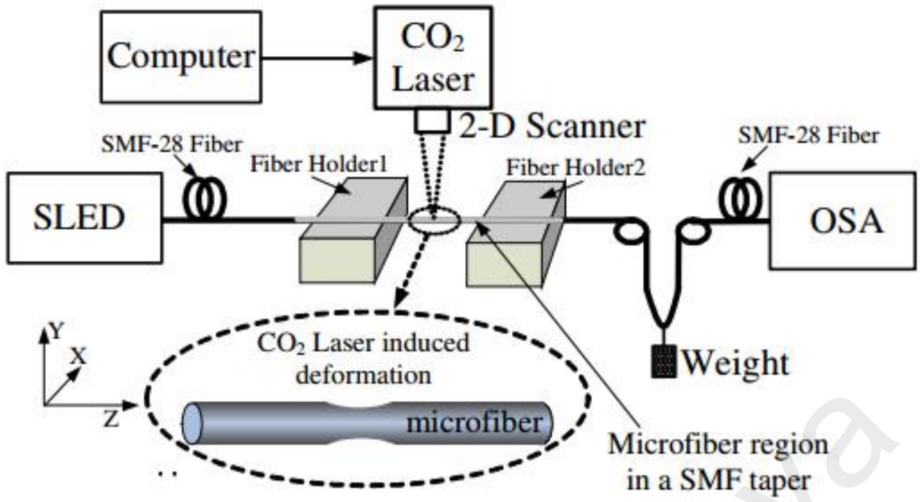

Figure 2.9 Schematic of the CO_2 laser system for fabricating LPGs in microfibers. (Xuan *et al.*, 2009)

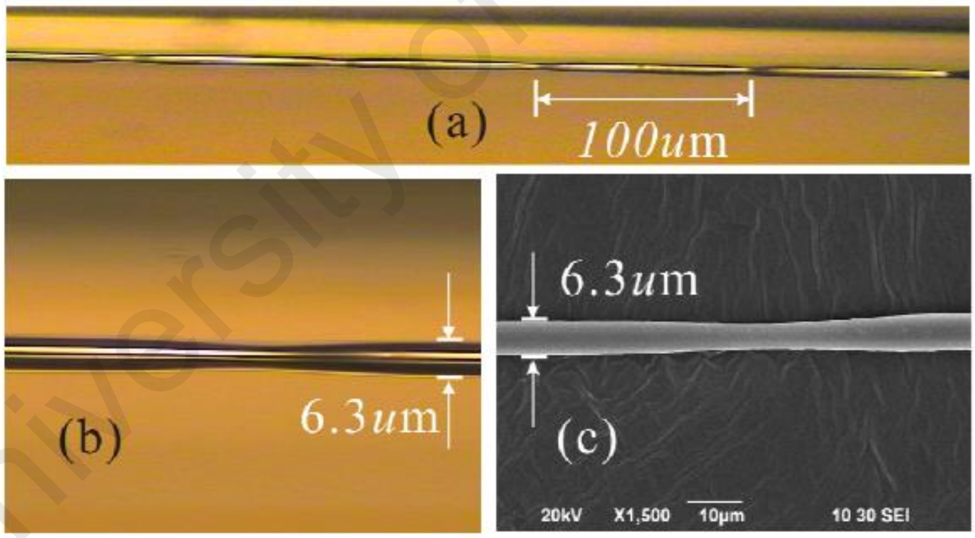

Figure 2.10 Microscopic images of a LPG fabricated in a microfiber. (a) The periodic microtapers along the LPG. (b) Microscope and (c) SEM images of two microtapers manufactured on a 6.3 μm diameter microfiber. (Xuan *et al.*, 2009).

microfiber has a negative coefficient and it is very sensitive to external refractive index change. The resonant wavelength is blue-shifted when the temperature increases at a slope of ~ -130 pm/°C. This behaviour deviates from that of the conventional LPG in which the resonant wavelength red-shifts with increasing temperature. The high sensitivity to external refractive index (RI) change (~1900 nm/RI) shows that it is a good candidate for refractive index sensing (Xuan *et al.*, 2009).

The fabrication of whispering-gallery modes (WGM) microresonator has been demonstrated using a CO_2 laser. WGM effect can be observed in microsphere, cylindrical fiber and in the bulge formed between the tapered sites of micro-tapered LPG. In the study of Kakarantzas *et al.* (2001), the narrowed fiber was micro-tapered using CO_2 laser to ~10 µm in diameter at two points (300 µm apart). The WGMs were excited in the micro-cavity formed in between two tapered sites. This type of microstructure is expected to have similar characteristics as the microsphere structure, such as add-drop filter and micro-laser. By controlling the micro-tapering, the dimension and aspect ratio of the micro-cavity can be manipulated (Kakarantzas *et al.* 2001).

2.1.2.3 Surface Processing

Studies have been carried out on optical polishing using CO_2 laser in the early 1980's (Temple *et al.*, 1982). The scratches and damaged sides on the silica surface can be melted and healed locally by the heat generated by CO_2 laser irradiation (Cormont *et al.*, 2013; Cormont *et al.*, 2015). In the work conducted by Temple *et al.* (1982), two different schemes of CO_2 laser heating were investigated, namely single-pass and multi-pass scheme. In the single-pass scheme, the fused silica surface is irradiated by an unfocused CO_2 laser beam at a near-normal incident angle. The laser beam scans across the fused silica glass surface from left-to-right motion and from the lower part to the upper part. In the multi-pass scheme, the unfocused CO_2 laser beam scans through the glass surface in a raster pattern (Temple *et al.*, 1982). The CO_2 laser-polished sample exhibits a better performance due to the healing of micro-cracks on the fused silica glass surface and evaporation of surface contamination. The large-spot laser-damage threshold of the glass surface was greatly increased after both single-pass and multi-pass scheme of CO_2 laser treatment. However, the fused silica sample treated with single-pass scheme was strained and partially devitrified. In multi-pass scheme, the residual stress had been built up in the fused silica sample that was treated with higher CO_2 laser intensity. Higher CO_2 laser intensity increases the damage threshold of fused silica and induces higher residual stress in it at the same time (Temple *et al.*, 1982).

Local processing of scratches on silica glass using CO_2 laser to enhance the nanosecond UV-laser damage resistance had been reported in several studies (Cormont *et al.*, 2013; Palmier *et al.*, 2009; Cormont *et al.*, 2010). In the study by Cormont *et al.* (2013), the scratches on silica surface had been healed by locally melting using CO_2 laser irradiation. CO_2 laser is suitable for fused silica surface processing because it is dynamic, localized to the area of defect and free of debris. Figure 2.11 shows the Nomarski microscopic image of scratch removal after a 10 W CO_2 laser irradiation within 1 s duration, with a beam diameter of 1.4 mm.

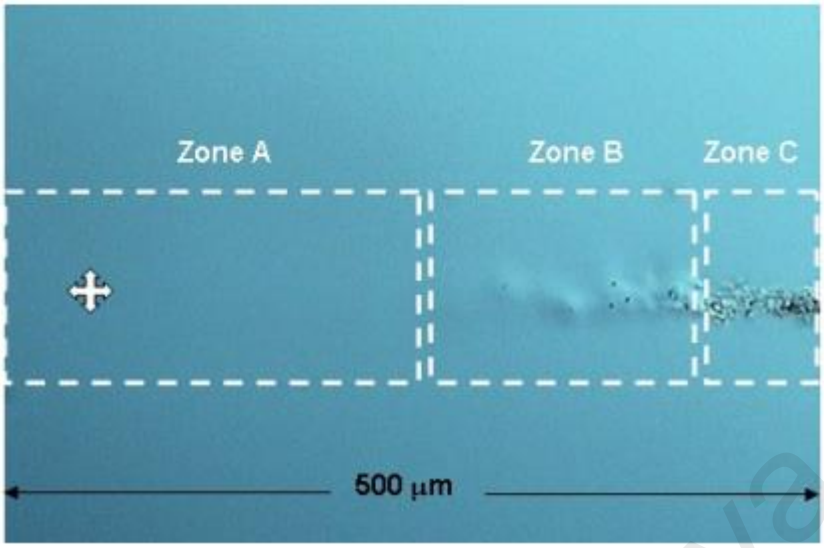

Figure 2.11 Nomarski microscopic image of a scratch on silica surface after irradiated by 1 s of 10 W CO_2 laser beam. Zone A is defined as a repaired area, whereas Zone B is a transition area and Zone C is an unaffected area. (Cormont *et al.*, 2013)

The white cross at the left hand side of the image is the centre of CO_2 laser beam. Due to the Gaussian beam profile of CO_2 laser, the removal of scratches is more effective at the zone nearer to the centre of laser beam. The appropriate temperature required for effective scratch removal using this technique was reported as 1650-1810 K (Cormont *et al.*, 2013).

As compared to the CW CO_2 laser, pulsed CO_2 laser has the advantage of avoiding the formation of raised rim around the mitigation site and consequent down-stream intensification. This is because the interval between each successive pulse provides substantial cooling which reduces the heat-affected zone and prevents thermos-capillary flow. Therefore, the size of the raised-rim and downstream intensification is reduced. Pulsed CO_2 laser offers the advantages of enhanced damage threshold of fused silica glass, reduced residual stress and re-deposited material on surface (Bass *et al.*, 2010). Dutta *et al.* (1982) has shown that the optical scattering losses of silicon nitride (Si_3N_4), niobium pentoxide (Nb_2O_5) and tantalum pentoxide (Ta_2O_5) waveguides fabricated on silica/silicon (SiO_2/Si) substrates can be reduced after CO_2 laser annealing. In particular, in Si_3N_4 waveguides, the attenuation was reduced from 6 dB/cm to 0.1 dB/cm (Dutta *et al.*, 1982). Besides that, the reduction in scattering loss for Corning 7059 glass thin-film optical waveguides was demonstrated by Dutta *et al.* (1980). The scattering loss was reduced from 17.4 dB/cm to 0.6 dB/cm. This shows that the surface defects and bulk inhomogeneity in the waveguides can be eliminated using CO_2 laser annealing.

2.1.2.4 Photosensitisation

Photosensitivity enhancement of hydrogenated optical fiber by thermal treatment using CO_2 laser was first proposed by Byron (1997). In 1999, Brambilla *et al.* proposed a post-fabrication technique to increase the photorefractivity of non-hydrogenated germanosilicate fibers by exposing them to an intense CO_2 laser radiation before grating inscription. The high photorefractive response of the treated fiber might be due to the higher concentration of Germanium-Oxygen deficient centre (GODC) after CO_2 laser exposure. According to Figure 2.12, the absorption of preform sample at 242 nm increases with respect to CO_2 laser exposed time duration.

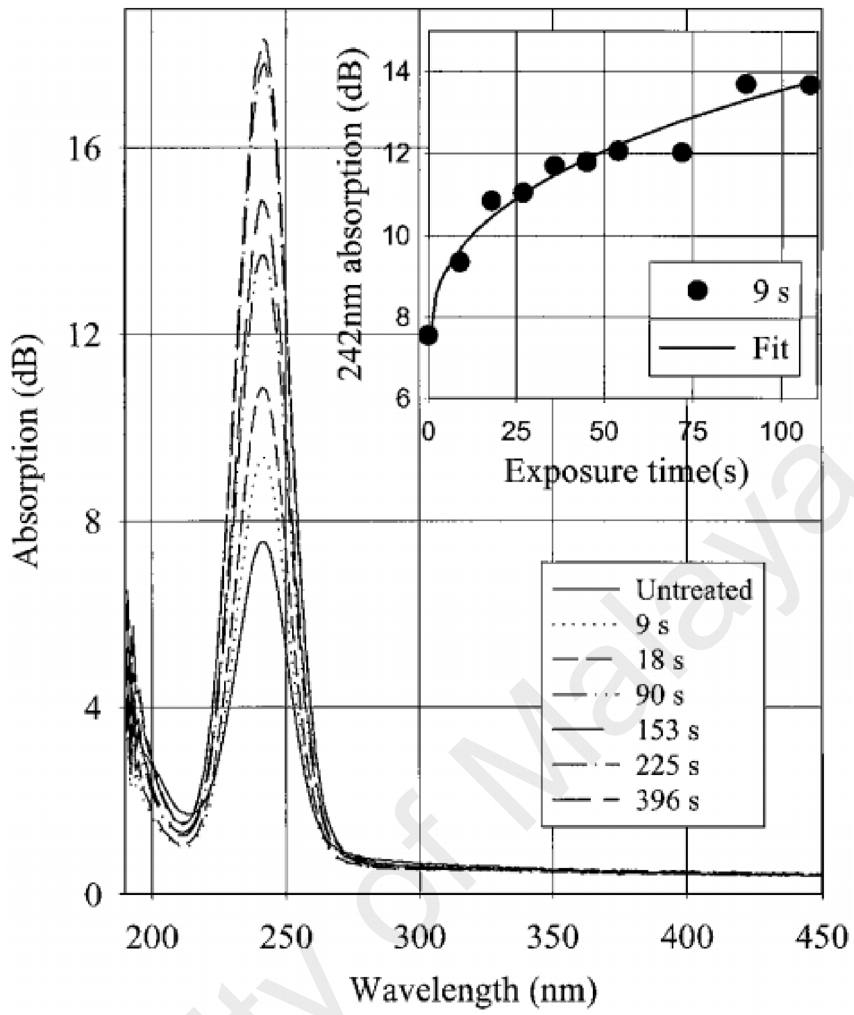

Figure 2.12 Absorption spectra of a 110 µm thick preform slide after exposed to different duration of CO_2 laser radiation (laser intensity, 210 W/cm^2). Inset: The increment of the absorption in 242 nm on cumulative CO_2 laser exposure time. (Brambilla *et al.*, 1999)

The observed dependence of photosensitivity enhancement on CO_2 laser intensity suggests that two types of defects contribute towards the existence of 242-248 nm absorption peaks. Based on the model reported by Brambilla *et al.* (1999), one type of the defects has a higher UV resistance compared to the other type of defects and its concentration increases after CO_2 laser irradiation. The high UV resistance of this defect might be attributed to multi-photon absorption.

2.2 Fiber Annealing

There are two existing models which describe the heat transfer in optical fiber during CO_2 laser irradiation, namely Mie theory model (Bohren & Huffman, 1983) and geometric model (Grellier *et al.*, 1997). Grellier *et al.* (1998) have modelled and examined the heat transfer in optical fiber during CO_2 radiation using both models. In the model proposed by Grellier, the optical fiber was treated as a one-dimensional (1-D) thin rod during CO_2 laser annealing where the laser beam was irradiated perpendicularly to the fiber axis. This approximation has been verified by thermal thinness condition (Myers, 1998). The equation below represents the minimum time required to achieve the desired temperature homogeneity in the optical fiber.

$$\frac{d^2 c\rho}{4Kt} \ll 1 \qquad \textbf{(2.1)}$$

where d is the fiber diameter, c is the specific heat of the fiber, ρ is the density of the fiber, K is the thermal conductivity of the fiber and t is the time. In this particular case where the fiber diameter is less than 125 μm, the temperature homogeneity across the fiber is less than 1 % for annealing time over 50 ms. This shows that the fiber can be considered as 1-D if the variation of laser irradiation is longer than 50 ms.

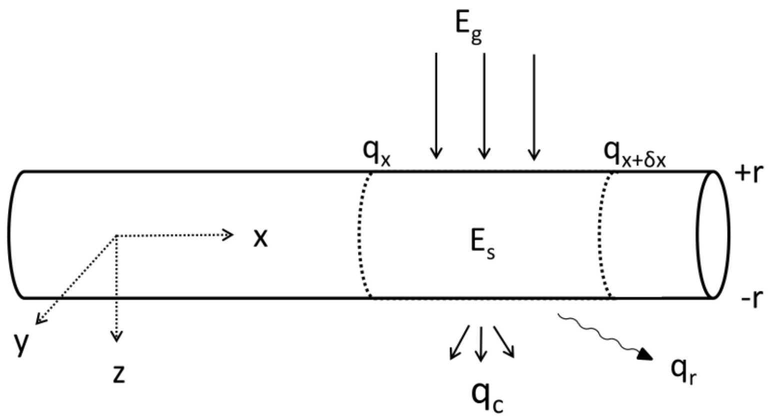

Figure 2.13 Schematic diagram of heat transfer in optical fiber. (Grellier *et al.*, 1998)

Based on Figure 2.13, the heat transfer relation can be expressed as

$$q_x + \dot{E}_g = q_c + \dot{E}_s + q_{x+\delta x} + q_r \tag{2.2}$$

where

rate of conduction, $q_x = -[KA(\delta t/\delta x)]_x$, $q_{x+\delta x} = -[KA(\delta t/\delta x)]_{x+\delta x}$

rate of convection, $q_c = Hp(T\text{-}T_{air})\delta x$

rate of energy store, $E_s = \rho cA(\delta T/\delta t)\delta x$

rate of heat generation, $E_g = Aq(x)\delta x$

rate of radiation, $q_r = \sigma\varepsilon p(T^4\text{-}T_{air}^{\ 4})\delta x$

Equation 2.2 can be expressed as

$$\frac{\partial^2 T}{\partial x^2} = \frac{4H}{dK}(T - T_{air}) + \frac{\rho c}{K}\frac{\partial T}{\partial t} + \frac{4\sigma\varepsilon}{dK}(T^4 - T_{air}{}^4) - \frac{q(x)}{K} \tag{2.3}$$

The rate of heat generation per unit volume in the fiber, is given by

$$q(x) = \frac{Q_{abs}\sqrt{2}P_{total}erf\left(d/\sqrt{2}w_y\right)}{w_x \pi^{3/2} r^2}\exp\left(\frac{-2x^2}{w_x{}^2}\right) \tag{2.4}$$

T represents the temperature, A the cross-sectional area of the fiber, H the surface conductance or convection heat-transfer coefficient, P the perimeter of the fiber, $q(x)$ the rate of heat generation from the laser on the fiber per unit volume, σ the Stefan-Boltzman constant, ε the emissivity, Q_{abs} the efficiency factor of absorption, w_x and w_y the beam waist in the x and y directions, respectively. Similar theoretical study was reported by Chryssou (1999) using Mie theory to analyses interaction of CO_2 laser with fused silica optical fibers during the tapering process (Chryssou, 1999).

The temporal thermal response of type II-IR FBG towards the CO_2 laser irradiation reported by Liao *et al.* (2009) is shown in Figure 2.14.

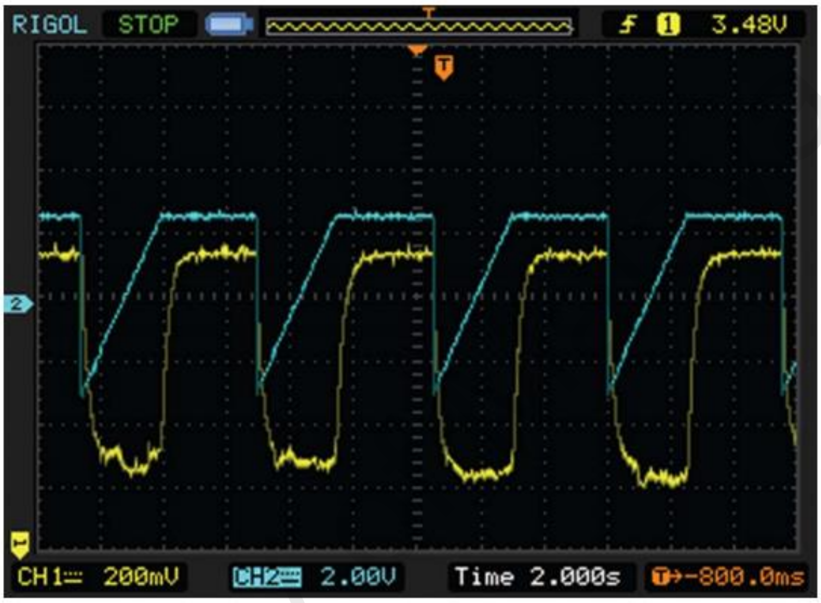

Figure 2.14 Temporal thermal response of the FBG (yellow) towards the CO_2 laser irradiation. The CO_2 Laser (blue) is ON at the rising edge and OFF at the constant high level. (Liao *et al.*, 2009)

Based on the exposure of the FBG to the CO_2 laser beam consisting of different intensities, the time constants of heating and cooling were calculated. The temporal thermal response of the FBG towards the CO_2 laser annealing appeared to be independent from the laser power and final annealing temperature. In their work, the reported time constants for heating and cooling were 230 ± 25 ms and 275 ± 25 ms, respectively. The direction of CO_2 laser irradiation also plays a vital role in fiber annealing. Asymmetric annealing will induce birefringence in the fiber due to non-uniform refractive index modification. The effect of axial asymmetry to the grating is studied by measuring the temporal thermal response to CO_2 laser irradiation while rotating the FBG in steps. The result obtained by Liao *et al.* (2009) is shown in Figure 2.15 (Liao *et al.*, 2009).

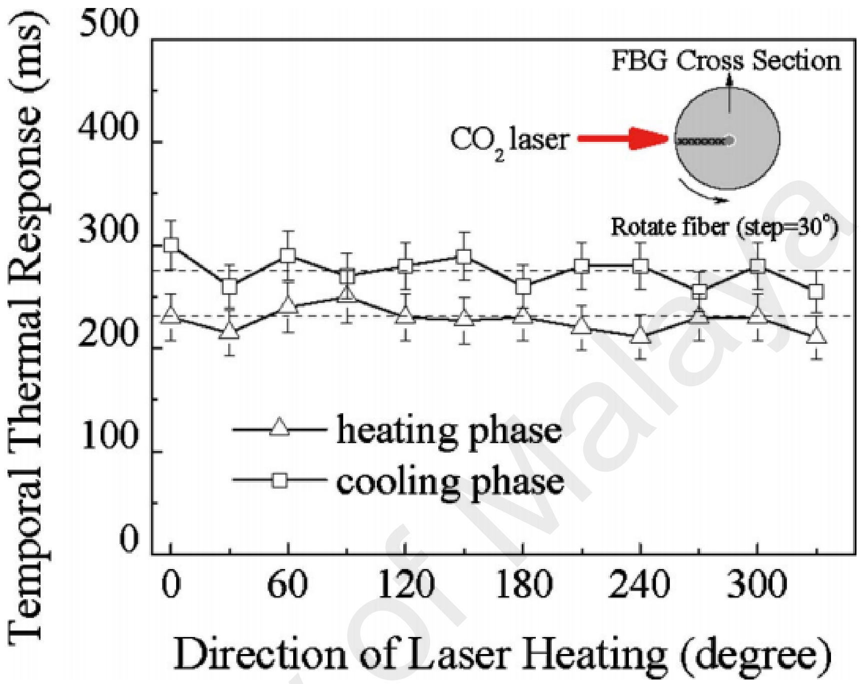

Figure 2.15 Temporal thermal response of a Type II–IR FBG at different laser irradiation direction. '∆' represents the heating phase, '□' represents the cooling phase. Inset shows the cross section of FBG with respect to CO_2 laser irradiation direction. (Liao *et al.*, 2009)

At the beginning, the grating groove is parallel to the incident CO_2 laser (Figure 2.15 inset). The time constants of heating and cooling represent the temporal thermal response of the FBG at different irradiation direction. By comparing the time constant during heating and cooling in Figure 2.15, the independent characteristic of temporal thermal response towards the irradiation direction is observed. The small fluctuation in the temporal thermal response can be attributed to the inconsistent irradiation condition during fiber rotation.

Yang *et al.* (2010) made a comparison between the performance of 4.6 µm mid-infrared laser and 10.6 µm far-infrared laser for silica glass annealing. Based on this study, it was found that silica glass has a higher absorptivity at far-infrared range as compared to the mid-infrared range. Thus, the absorption length of mid-infrared laser is longer than that of the far-infrared laser, which is better for deeper subsurface damage mitigation. For a depth below 500 µm, far-infrared laser at 10.6 µm is still considered to be a better choice for annealing purpose. Due to shallower penetration depth and steeper temperature gradient on the surface, 10.6 µm far-infrared requires shorter time to reach the steady temperature state as compared to 4.6 µm mid-infrared laser. Moreover, the relationship between temperature and laser power at 10.6 µm was found to be linear up to ~2800 K (Yang *et al.*, 2009).

In another study, Tian and Chiu (2004) simulated the annealing of a moving glass rod by CO_2 laser. They made improvements on the modelling of CO_2 laser heating on optical fiber as reported by Homsy and Walker (1979), Chryssou (1999) and Grellier *et al.* (1998). The spectral dependence of the glass to radiation has been included in their model. In Tian and Chiu's (2004) work, Rosseland diffusion approximation was used to study the radiation heat transfer in glass rod. Rosseland diffusion approximation is widely used in the modelling of radiative transport of heat in glass due to its simplicity (Homsy and Walker, 1979; Myers, 1989; Lee & Jaluria, 1997). Tian and Chiu (2004) have proven that Rosseland diffusion approximation is valid in modelling the radiative transport within the glass rod if the glass rod diameter is larger than ~5 mm. The result shows that the maximum surface temperature is located at the downstream of the laser focus centre. The high radial and axial diffusion, as well as radiative cooling that caused a rise in the surface temperature and a rapid drop in temperature was observed as the glass moved in and out from the heating zone (Tian and Chiu, 2004).

2.3 Thermal Regeneration in FBG

There is a growing interest in the study of high temperature sensor based on regenerated fiber Bragg grating (RFBG) due to its many advantages. Notably, the excellent temperature detection performance (Laffont *et al.*, 2013a; Laffont *et al.*, 2013b) and economical production. The operating temperature of the developed RFBG can be as high as the thermal regeneration temperature. To date, RFBG with an operating temperature up to 1400 °C had been reported (Yang *et al.*, 2014). For the manufacturing of RFBGs, hydrogen loading is an important pre-treatment for raw optical fibers before the UV-inscription is performed. During UV-inscription, hydroxyl is created and cumulated in the periodic grating structure, which is responsible for high grating reflectivity, increased transmission loss and grating regeneration (Bueno *et al.*, 2013; Fokine & Margulis, 2000; Friebele *et al.*, 1978; Messina *et al.*, 2005; Watanabe *et al.*, 1986). When the seed grating is heated up to a temperature between 600 °C and 1000 °C depending on the type of fiber used, grating strength gradually decreases until erasure followed by a progressive regeneration that leads to the formation of high-temperature-resistant grating (Bueno *et al.*, 2013). The thermal annealing process is considered complete when the reflected power reaches a stagnant condition.

A lot of effort has been put forth in understanding the physics and improving the performance of RFBGs. Investigations on different aspects such as the types of optical fibers, the wavelength of the laser source used for grating inscription (Barrera & Sales, 2013), fiber photosensitisation method (Eg. hydrogen / deuterium / helium gas loading) (Cook *et al.*, 2012), thermal annealing methods and procedures (control of temperature and time) (Bueno *et al.*, 2013) and etc. had been carried out. SEM analysis shows a transformation of silica and not germanosilicate, where the silicon (Si) concentration at the core-cladding interface is reduced while germanium (Ge) concentration remained unchanged after regeneration process (Canning *et al.*, 2010). Besides that, Type-IIa regenerated gratings are also realizable by thermal activation process at 600 °C from Type-I hydrogenated seed gratings. The thermal regeneration in the etched-core FBGs is another related research study which had been carried out and completed earlier. The sensitivity of the etched-core RFBG is higher than the unetched RFBG, which gives it an advantage in temperature sensing as compared to the conventional temperature sensor (Yang *et al.*, 2013). Typical thermal regeneration treatment can take up to an hour. However, with the usage of isothermal annealing technique for grating regeneration as presented in Bueno *et al.* (2013), the treatment time can be extensively reduced to several minutes or even seconds.

2.4 Residual Stress in Optical Fiber

Residual mechanical stress, also known as draw-induced residual stress, is built up in the fiber during fiber drawing process due to the viscosity differences between different parts of the fiber. High temperature annealing treatment can be used to relax the residual mechanical stress in the fiber. Residual mechanical stress relaxation by CO_2 laser annealing is the main element in LPG formation in optical fiber. The refractive index of the optical fiber is perturbed after residual mechanical stress relaxation. In addition, asymmetric mechanical stress relaxation over the fiber cross sectional area induces the birefringence of the fiber. A study on stress-induced birefringence was carried out by Ryu *et al.* (2003) using LPG and CO_2 laser annealing. It reveals that the asymmetric stress distribution in fiber cladding affects the polarisation dependent transmission characteristic, instead of stress distribution in fiber core. By measuring the wavelength shift of interference fringe formed by a LPG pair after the CO_2 laser annealing, refractive index change was measured. This mechanical stress relaxation induced refractive index reduction has been found to be linearly proportional to the fiber drawing force (Kim *et al.*, 2002). The mechanical stress can be fully relaxed using CO_2 laser annealing. Therefore, the remaining stress in the fiber core should be the thermal stress that is due to the thermal expansion coefficient mismatch between the fiber core and cladding (Kim *et al.*, 2001). Besides the optical fiber, stress relaxation also occurs in planar waveguide. Chiasera *et al.* (2013) reported that a refractive index increment of 0.04 was observed in germanium oxide (GeO_2) transparent glass ceramic planar waveguide at 1.5 μm after CO_2 laser annealing. The result of Raman spectroscopy analysis proved that CO_2 laser irradiation time affected the GeO_2 nanocrystal and its phase in the waveguide (Chiasera *et al.*, 2013).

Due to the high absorptivity of fused silica glass at 10.6 μm, the short absorption length induces a temperature gradient along the irradiation direction in the fused silica glass (Yang *et al.*, 2010). However, the low thermal expansion coefficient of silica (~0.55 ppm/K) limits the amount of thermal stress in the glass induced by laser-induced temperature gradient. When the laser-induced temperature increases above the glass transition temperature, the occurrence of plastic deformation will lead to stress relaxation at the heating zone (Bennett & Li, 2001). This is because silica behaves as a viscoelastic solid when the viscosity takes a value between 10^{12} to $10^{13.5}$ Pa·s (Hülsenberg *et al.*, 2008). The viscous flow in silica enables the stress relaxation. The viscous flow becomes even more significant when the viscosity of silica is lower than 10^{12} Pa·s, which enables the stress to be relaxed immediately. When the silica viscosity is in the range between 10^{12} to $10^{13.5}$ Pa·s, cooling rate is important for stress relaxation. The cooling rate threshold for stress relaxation to occur can be associated with stress relaxation time of silica (Daia *et al.*, 2011).

Other than the mechanical stress relaxation that contributes to LPG formation, thermal stress in fiber can also be relaxed by thermal treatment. The thermal stress in optical fiber is due to the difference in the dopant concentration between fiber core and cladding. In contrast to mechanical stress relaxation, thermal stress relaxation in optical fiber requires a sufficient cooling time to occur. Therefore, CO_2 laser has the advantage of achieving thermal stress relaxation in optical fiber due to its dynamic control and fast thermal response of optical fiber during CO_2 laser irradiation.

2.5 Birefringence in Optical Fiber

High birefringence fiber, which is also known as PMF, is widely used as polarisers, depolarisers, couplers, filters, isolators, polarisation controllers and sensors. Birefringence in PMF can be categorized into geometrical birefringence and stress induced birefringence. Generally, the geometrical birefringence is much smaller than the stress-induced birefringence (also known as material birefringence) exerted by the dopant concentration difference between each region in the fiber cross section (Chu & Sammut, 1984). Generally, SAPs that are positioned on both sides of the fiber core provide better precision in controlling the birefringence and fabrication of PMF. The birefringence of stress-applied PMF can be described using

$$B \cong K(\alpha_{clad} - \alpha_{SAP})\Delta T \quad \textbf{(2.5)}$$

$$\Delta T = T_{room} - T_{g(SAP)} \quad \textbf{(2.6)}$$

where α_{clad} and α_{SAP} represent the thermal expansion coefficients (TEC) of the cladding and SAPs, respectively; T_{room} and $T_{\text{g(SAP)}}$ represent the room temperature and glass transition temperature of SAP; and K is the fiber geometry constant which is defined by the fiber radius, dimension and position of SAPs in the fiber (Chu & Sammut, 1984).

During the drawing process of PMF, high mechanical stresses are induced in the fiber due to high drawing tensions and the stresses are permanently frozen in the fiber at room temperature. As a result, a compensating thermal stress is formed in the fiber core region, which leads to a lower stress-induced birefringence (Taccaa *et al.*, 2010).

Nonetheless, the thermal annealing treatment can serve as a solution to reduce frozen mechanical stresses and enhancing the birefringence in the fiber. The remaining stresses in fiber are purely thermal stress, which is usually observed in the tension free fiber preform (Just *et al.*, 2015). Besides the thermal relaxation of mechanical stress, the enhancement of birefringence can also be achieved by modifying the TEC of SAPs by means of thermal annealing treatment followed by a slow cooling process (Ourmazd *et al.*, 1983a; Ourmazd *et al.*, 1983b). The slow cooling process provides sufficient relaxation time for the molecular rearrangement at low-viscous state and eventually leads to the volume compaction of SAP. The T_g and TEC of the glass are affected by the cooling process after annealing at elevated temperature. Silica glass that is cooled at a slower rate has a lower T_g and a smaller volume (Moynihan *et al.*, 1974; Ojovan, 2008) but a higher TEC compared to that of rapidly cooled (Wang *et al.*, 2011). This can be attributed to the rearrangement of molecular structure of the glass matrix and the free volume model of amorphous material (Turnbull & Cohen, 1961). Slow cooling from the annealing temperature introduces lesser free volume in the molecular structure. In other words, higher compaction in volume is achieved at a slower cooling rate (Brückner, 1970). Therefore, higher stress-applied birefringence can be achieved. However, this process is reversible by repeating the annealing treatment and then, birefringence is induced in the fiber core due to smaller product of ΔT and TEC mismatch between SAPs and cladding after fast cooling.

FBGs inscribed on birefringent optical fibers have been reported in several studies using elliptical core (Meltzand & Morey, 1991), bow-tie (Hill *et al.*, 1995), Panda (Abe *et al.*, 2003a) and internal elliptical cladding (Abe *et al.*, 2003b). The spacing between the two Bragg wavelengths ($\Delta\lambda_B$) in birefringent optical fiber can be described by $\Delta\lambda_B = \delta n \cdot \Lambda_{pm}$ where $\Delta\lambda_B$ is the wavelength difference between the polarisation modes and Λ_{pm} is the phase mask period (Siekieraa *et al.*, 2010). Chehura et. al. (2004)

demonstrated FBGs inscribed on elliptically clad fiber with a high transverse load sensitivity of 0.23±0.02 nm/(N/mm) (~25 % higher than any other PMF). This makes it an ideal embedded or surface mounted strain sensor. On the other hand, highest temperature sensitivity of 16.5±0.1 pm°C^{-1} (~27 % greater than any other fiber type) was reported for a FBG inscribed on Panda type PMF (Chehura et. al., 2004). In addition, simultaneous monitoring of strain and temperature was demonstrated using PMF with referral to the different dependences of two orthogonal polarisation modes (Ferreira *et al.*, 2000; Chen *et al.*, 2004). Multi-axis strain sensing based on PMF is possible and has been demonstrated in (Ye *et al.*, 2002; Mawatari & Nelson, 2008; Lawrence *et al.*, 1999). The measurement of three independent components of strain and temperature can be achieved using two gratings with Bragg wavelengths sufficiently spaced in the spectrum but co-located at the same position on a PMF (Lawrence *et al.*, 1999). Taking advantage of the two orthogonal modes in PMF, grating in PMF can be used for the generation of dual-wavelength laser and single linearly polarised laser (Zhao *et al.*, 2004; Liu *et al.*, 2004; Spiegelberg *et al.*, 2004; Yang *et al.*, 2012).

CHAPTER 3: FABRICATION OF REGENERATED FIBER BRAGG GRATING

Regenerated fiber Bragg grating (RFBG) is a temperature resistant grating suitable for operation in high temperature environment due to its high thermal stability. The operation temperature of the developed RFBG component can be as high as the regeneration temperature. The theory and mechanism of thermal regeneration has been studied intensively to understand and improve the performance of RFBGs. The studies have been conducted on various aspects such as the core dopants, the irradiation laser used for grating inscription (Barrera & Sales, 2013), fiber photosensitisation method (Cook *et al.*, 2012), thermal annealing methods (Bueno *et al.* 2013) and etc. The time required for thermal regeneration can take from several minutes up to few hours to complete depending on the chosen method. There is an array of heating equipment varieties that are capable of reaching thermal regeneration temperature for thermal annealing and characterisation of RFBG. This chapter elaborates the fabrication process of the RFBG in term of grating inscription, thermal regeneration and characterisation procedure on different type of fibers include a new type of photosensitive fiber and few modes fiber.

3.1 Hydrogen Photosensitisation

Hydrogen photosensitisation is an important pre-treatment procedure for the enhancement of the fiber photosensitivity so that fiber Bragg grating (FBG) with higher grating strength can be produced. By placing the fiber in a high pressure hydrogen gas chamber, the hydrogen gas molecules diffuse into the fiber core. The hydrogen molecules in the fiber core react with the silica and germanium oxide molecules in the glass matrix when the fiber is exposed to ultraviolet (UV) irradiation. This results in higher refractive index modulation in the produced FBG.

In general, hydrogen exists in the FBG in the form of hydroxyl (OH) and water. The UV exposure increases the concentration of OH group in the exposed region. After thermal annealing, most OH groups and water remain at the UV-exposed region (Lawrence *et al.*, 1999). The resultant periodic distribution of OH and water concentration in FBG might induce periodical crystallization (Wang *et al.*, 2011) or change of dopant diffusion in the FBG (Zhao *et al.*, 2004).

In this work, the fibers were placed inside a hydrogen chamber at a pressure of 1500 psi at room temperature for a week prior to the grating inscription process (see Figure 3.1). The large difference in concentration of hydrogen between the outside and inside of fiber core induces the diffusion of hydrogen molecules into the fiber core. Shortly after the fibers were withdrawn from the hydrogen chamber, FBG inscription was carried out using excimer laser and a phase mask.

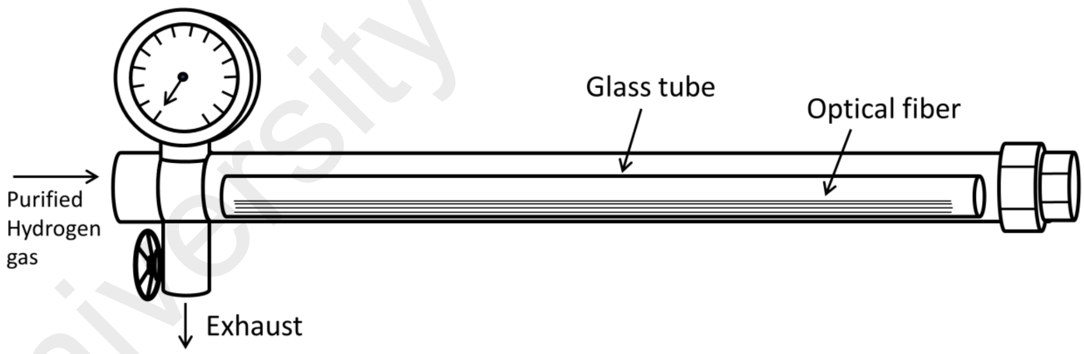

Figure 3.1 The schematic setup of hydrogen photosensitisation of optical fiber.

3.2 FBG Inscription

FBG inscription was carried out using excimer laser and a set of optical lenses for laser beam collimation. In this work, two different types of excimer lasers were used for FBG inscription, namely krypton fluoride (KrF) excimer laser and argon fluoride (ArF) excimer laser. The specifications and graphical user interface of both excimer lasers are summarized in Table 3.1 and Figure 3.2. The specifications of the phase mask and optical fibers used for the FBG inscription are summarized in Table 3.2 and 3.3 respectively.

Table 3.1 The specification of KrF and ArF excimer laser (UV CL 5100 excimer lasers, Optosystems Ltd.).

Excimer laser	KrF	ArF
Wavelength (nm)	248	193
Maximum output power (W)	4.0	2.5
Max repetition rate (Hz)	100	
Nominal pulse energy (mJ)	40	20
Pulse energy stability (%)	<2	
Beam size at FWHM (mm)	12 × 5	
Beam divergence at FWHM (mrad)	4 × 2	
Pulse duration (ns)	9-11	10
Premix Gas composition	Fluorine (F_2) 0.12 %, Krypton (Kr) 4.6 %, Helium (He) 2.33 %, Neon (Ne) balances.	F_2 0.2 %, Argon (Ar) 6.1 %, He 3.9 %, Ne balances.
Cooling	Air	
Power Consumption	220 V, 50 Hz, 1.5 kW	
Control	RS 232, Window	

Figure 3.2 Graphical user interfaces for the laser control panel for (a) KrF excimer laser and (b) ArF excimer laser.

Table 3.2 Specification of the phase mask used for the FBG inscription.

Specification	KrF excimer laser	ArF excimer laser
Material	UV-grade fused silica	Silica
Pitch (nm)	1068.8	1067
Pitch accuracy (nm)	±0.01	±0.001
Grating size (mm)	50×10	30×3
0^{th} order suppression	< 4 %	<3.05 %

Table 3.3 The specifications of optical fibers used. LP: Linearly polarised.

	PS1250/1500	ZWP-SMF	PS-PM980	2G	2S	4G	4S	Ga
Operating Wavelength (nm)	1260 - 1650	1260 - 1625	970 - 1550	1530-1565	1530-1565	1530-1565	1530-1565	1550
Mode field diameter (MFD) (μm)	8.8 - 10.6 @1550 nm	10.4 ± 0.5 @1550 nm	6.6 ± 1.0 @980 nm	LP_{01}: 11.0; LP_{11}: 11.0	15.5 @LP_{01}; 13.6 @LP_{11}	LP_{01}: 10.7; LP_{02}: 6.3; LP_{11}: 10.8; LP_{21}: 11.0	LP_{01}: 18.2; LP_{02}: 8.7; LP_{11}: 15.2; LP_{21}: 14.3	-
Numerical aperture (NA)	0.12-0.14	-	0.12	0.14	0.12	0.19	0.12	0.15

KrF excimer laser was used for FBG inscription on boron-germanium (B/Ge) co-doped photosensitive fiber (Fibercore Ltd: PS1250/1500), highly germanium (Ge)-doped fiber (Fibercore Ltd: SM1500 (4.2/125)), zero water peak single-mode fiber (OFS ZWP-SMF), photosensitive panda type polarisation maintaining fiber (PMF) (Thorlabs PS-PM980) and different types of few-mode fibers (OFS two modes/four modes/step index/graded index). Four types of few-mode fibers were used, namely two mode graded-index (2G), two mode step-index (2S), four mode graded-index (4G) and four mode step-index (4S). On the other hand, ArF excimer laser was used for the FBG inscription on gallium (Ga) doped fiber because of its higher absorption at the region of 193 nm compare to 240 nm (see Figure 3.3).

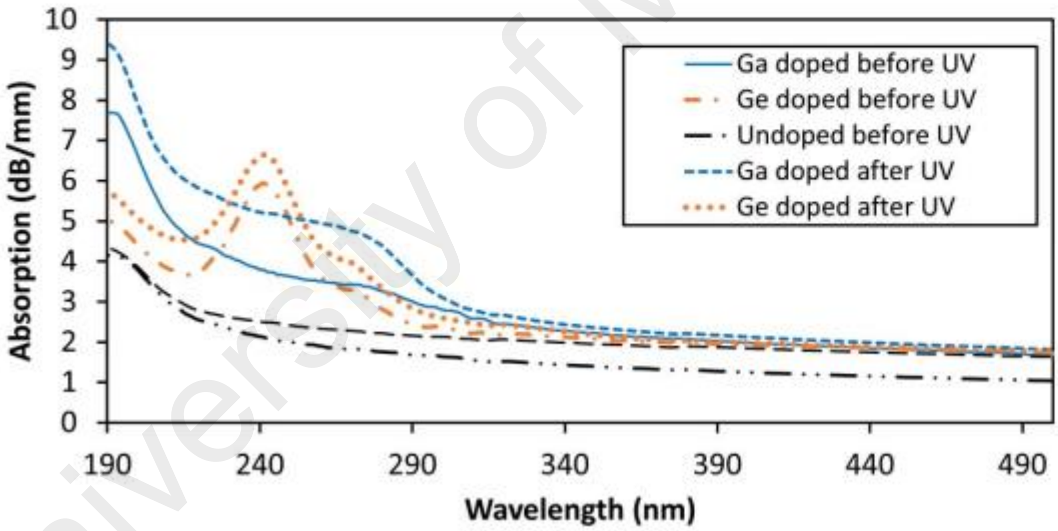

Figure 3.3 Photoabsorption of Ga and Ge doped glass in the range of 190-500 nm.

The fibers were photosensitised with hydrogen-loading before the FBG inscription. The fibers were loaded into a pressurized hydrogen gas chamber at 1500 psi under room temperature for one week. The average energy and beam width of the laser were 20 mJ and 5 mm (10 mJ and 15 mm for Ga doped fiber) respectively. The experimental setup of the FBG inscription is shown in Figure 3.4.

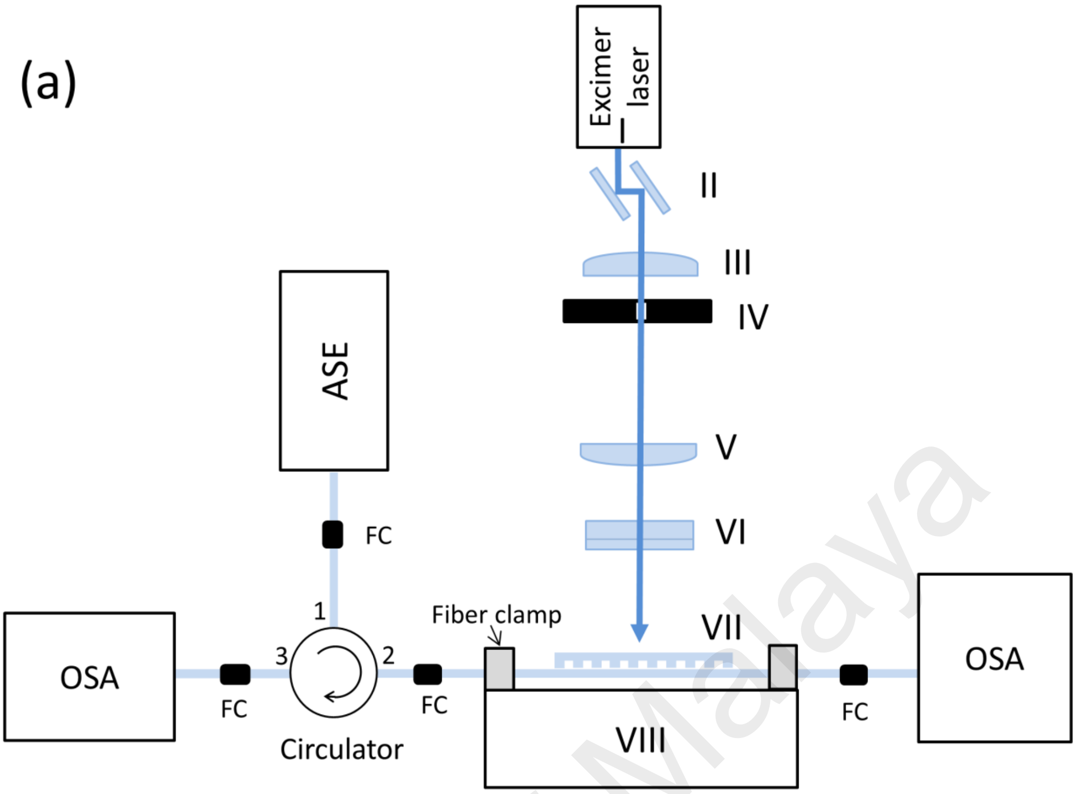

Figure 3.4 Schematic setup of the FBG inscription using excimer laser and phase mask. (a) Schematic diagram, (b) Side view, (c) Closer view of phase mask. I: Laser aperture, II: UV mirror, III, V, VI: Fused silica plano-convex cylindrical lens, IV: Vertical slit, VII: Phase mask, VIII: Three axis positioning stage, OSA: Optical spectrum analyser, ASE: Amplified spontaneous emission source, FC: Fiber coupler.

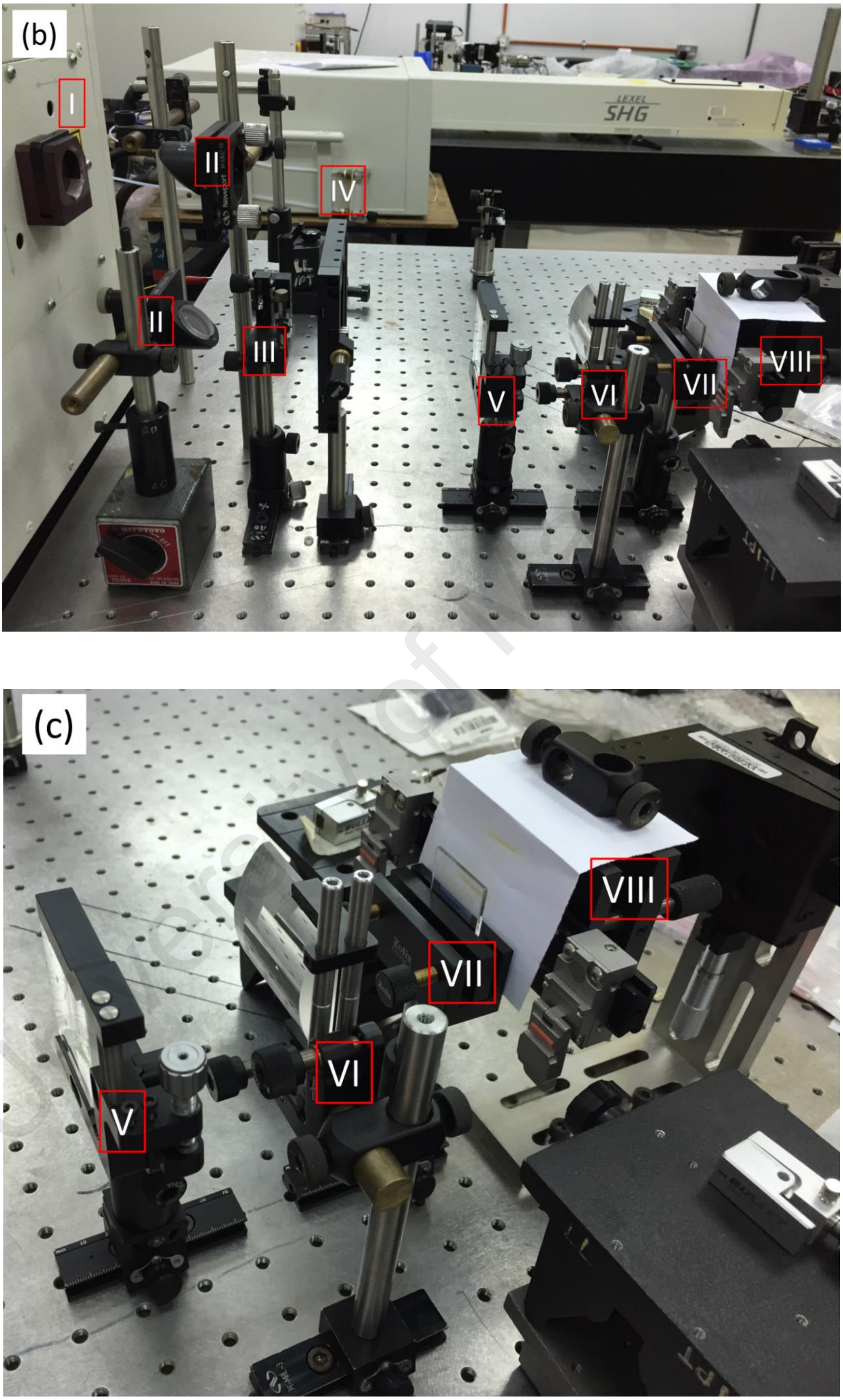

Figure 3.4, continued.

The height of the laser beam was first aligned using two UV mirrors. After that, the laser beam size was controlled with an adjustable vertical slit. The laser beam was collimated and focused using three plano-convex cylindrical lenses into a ~5 mm (15 mm for Ga doped fiber) long narrow and horizontal laser beam. Subsequently, the phase mask was used to create an interference field for optical fiber located behind the phase mask. The periodic variation of the laser beam intensity on the optical fiber induced periodic refractive index modulation on the fiber core is as shown in Figure 3.5.

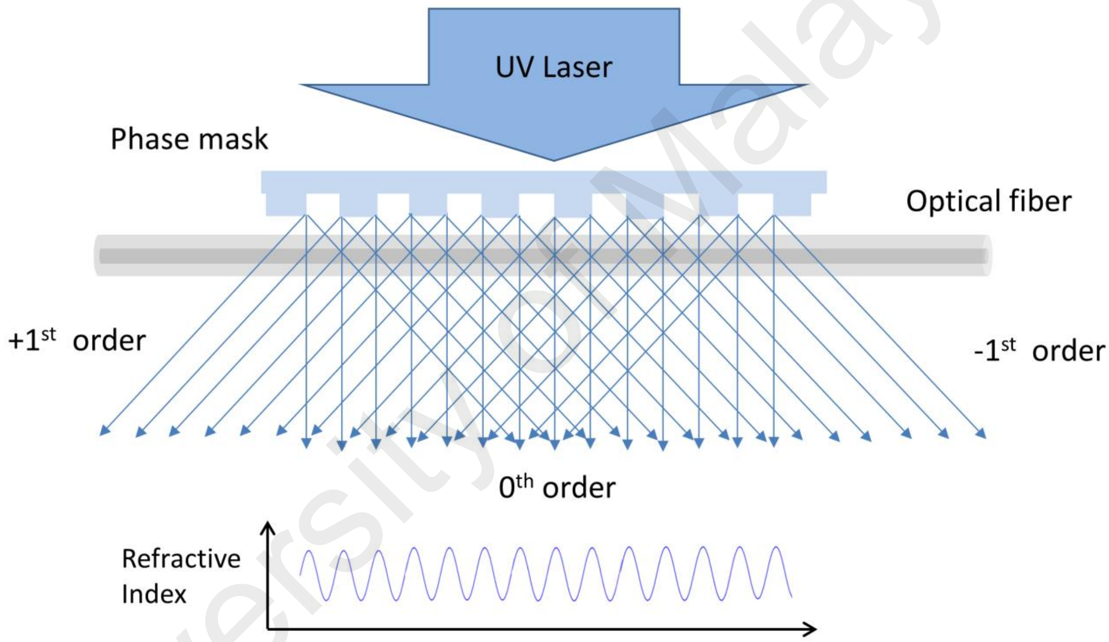

Figure 3.5 Illustrative diagram of interference pattern created by diffraction of UV laser beam through phase mask.

FBGs with a grating length of 5 mm (15 mm for Ga doped fiber) and Bragg transmission loss of 45 dB (corresponds to 99.997 % of reflectivity) (25 dB for Ga doped fiber) were produced. For PS-PM980 fibers, two transmission dips were formed in the transmission spectrum that correspond to the two polarisation modes in the fiber with refractive indices. In the observation, the two transmission dips became deeper and broader as the UV fluence increased. Therefore, the inscription process was halted before two transmission dips merged together. This precaution was to ensure that the associated wavelengths of the two polarisation modes were distinguishable in transmission and reflection spectra of the FBG.

After FBG inscription, these fibers were annealed in an oven at a temperature of 80 °C for more than eight hours to remove the residue hydrogen in the fibers. The process of dehydrogenation stabilised the Bragg wavelengths and the reflectivities of the FBGs. The FBGs produced was used as the seed grating for the thermal generation process.

3.3 Thermal Regeneration

The FBGs produced were used for the thermal regeneration treatment. Thermal regeneration of FBG was carried out in a high temperature tube furnace (LT Furnace STF25/150-1600). The temperature ramping and cooling rate and heating duration can be controlled by the in-built program. The seed grating was spliced to the optical circulator which was connected to a broadband ASE source and OSA as shown in Figure 3.6. The seed grating was positioned at the centre of the heating zone in tube furnace where the temperature was stable and spatially homogenous. Thermal regeneration using high temperature tube furnace was carried out on the seed grating inscribed on various types of fibers. Two different annealing schemes can be used for the thermal regeneration, namely isochronal and constant rate annealing (see Figure 3.7). For isochronal annealing, the annealing temperature was increased in the step wise manner from room temperature up to the regeneration temperature. The annealing temperature was maintained constant at each small step (~5 min) until the temperature stabilised before the annealing temperature was incremented. On the other hand, the annealing temperature was increased at a constant rate from room temperature to the regeneration temperature. The regeneration temperature for each fiber is listed in Table 3.4.

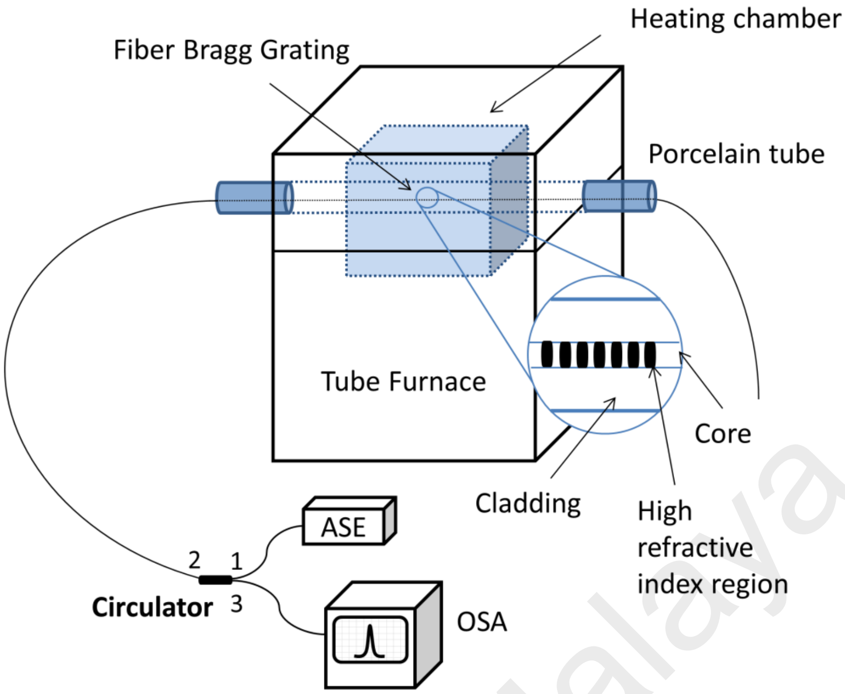

Figure 3.6 Experimental setup of thermal regeneration using tube furnace. ASE: Amplified spontaneous emission source. OSA: Optical spectrum analyser.

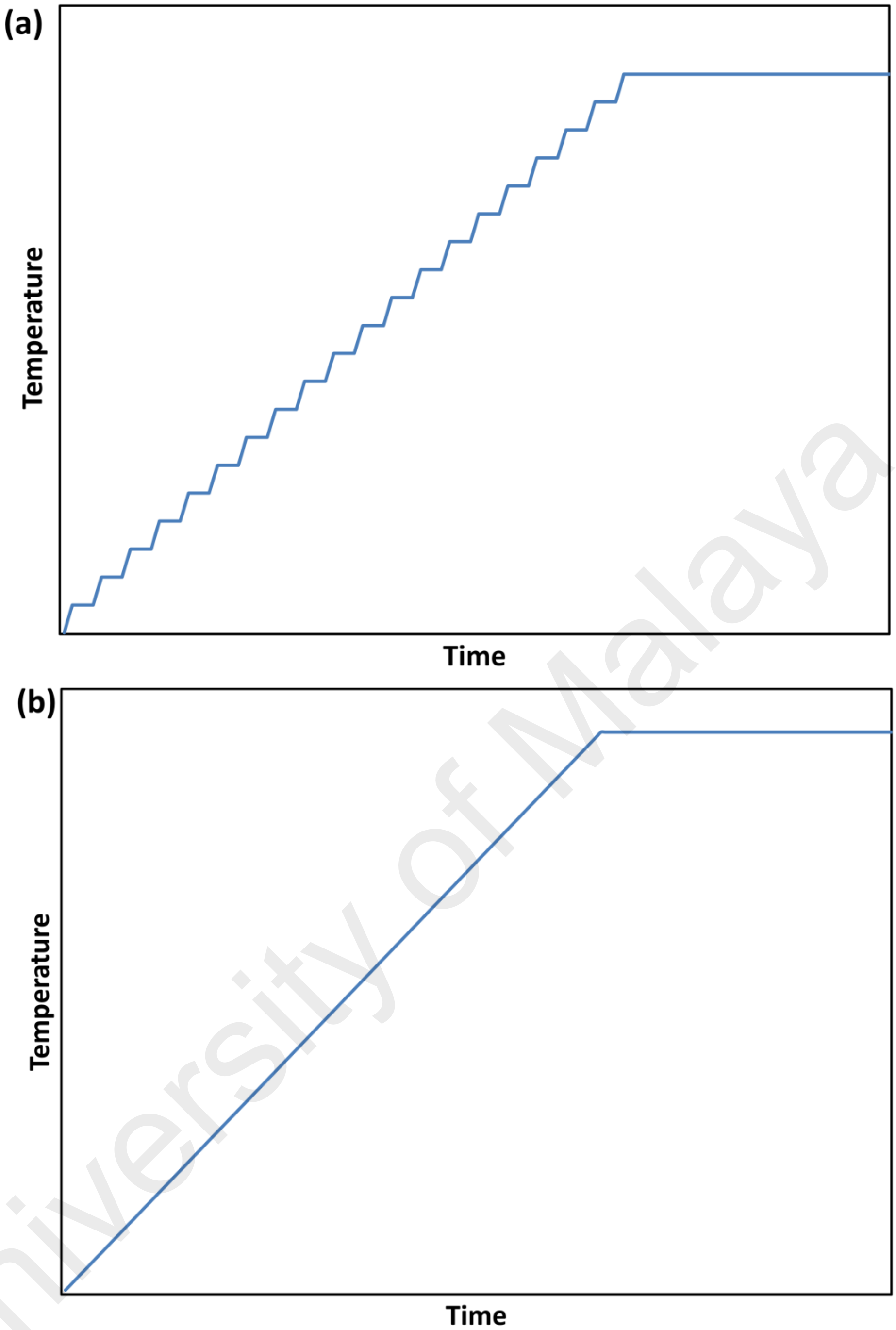

Figure 3.7 The annealing schemes used for thermal regeneration. a) Isochronal annealing, b) Constant rate annealing.

Table 3.4 Regeneration temperature for each type of FBGs.

Type of FBG	ZWP-SMF	PS1250/1500	PS-PM980	2G	2S	4G	4S	Ga
Regeneration temperature (°C)	~950	~850	~850	~920	~910	~900	~890	~720

The reflectivity of the seed grating gradually decreased with increasing annealing temperature and plummeted once it approached the regeneration temperature. Subsequently, the annealing temperature was held constant at the regeneration temperature for a given duration depending on the thermal response of the gratings. The grating reflectivity decayed rapidly until the Bragg reflection was totally erased. Shortly after that, a new reflection peak emerged from the noise level and increased continuously. The furnace was turned off after the reflectivity of the regenerated grating stabilised. The reflection spectra were then recorded continuously using an OSA controlled by a LabVIEW program via General Purpose Interface Bus (GPIB) interface card.

3.3.1 ZWP-SMF

During the thermal regeneration of ZWP-SMF FBG, the annealing temperature was increased from room temperature up to the regeneration temperature at a constant rate. The temperature increased from room temperature up to the regeneration temperature within ~100 min. As the annealing temperature increased, the reflectivity of the seed grating gradually decreased and plummeted when it approached the regeneration temperature as shown in Figure 3.8. The reflection spectra before and after regeneration process are compared in Figure 3.9. The Bragg wavelength of the regenerated grating is blue-shifted compared to that before regeneration. This is due to the stress relaxation and decay in grating strength after the regeneration process. The UV-induced stress between the high and low refractive index regions was built up in the grating during grating inscription process. This effect contributed to the red-shift in Bragg wavelength during the grating inscription process. However, during the subsequent thermal annealing process, the UV-induced stress and refractive index modulation of the grating was reduced. As a result, the Bragg wavelength of the RFBG was blue-shifted to a shorter wavelength than the seed grating.

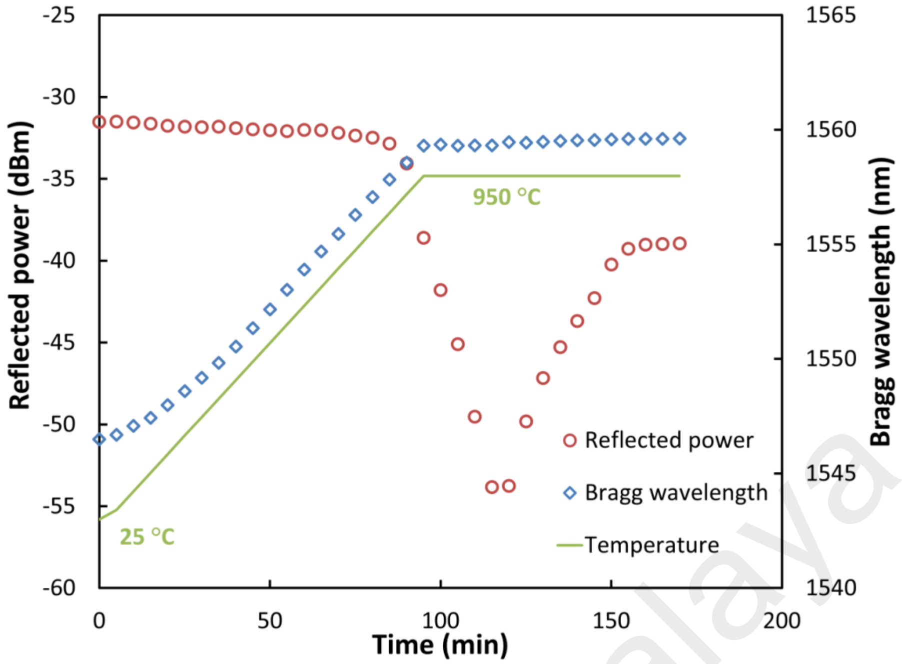

Figure 3.8 Output responses of ZWP-SMF FBGs during regeneration process.

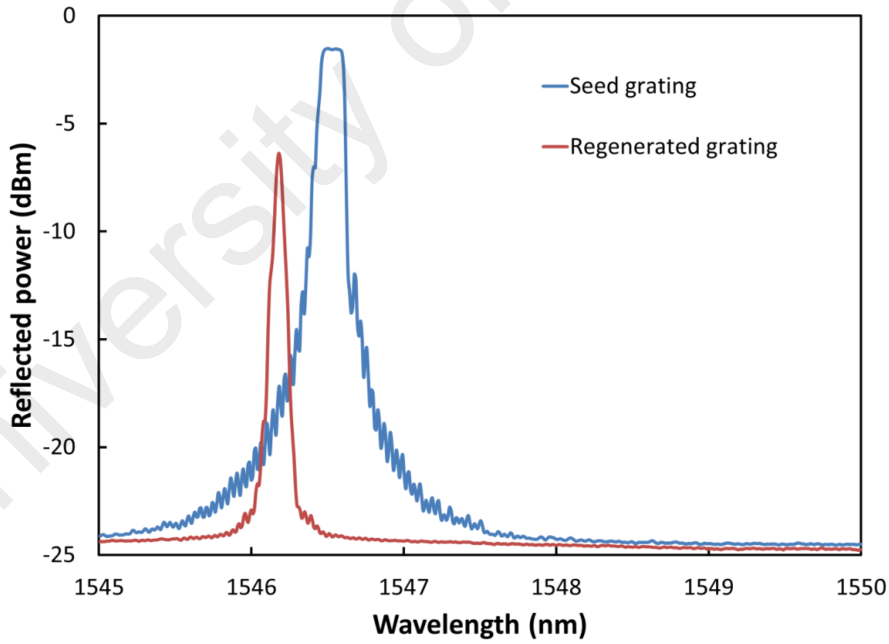

Figure 3.9 The comparison of reflection spectrum before (seed grating) and after (regenerated grating) thermal regeneration at room temperature.

3.3.2 PS1250/1500

For PS1250/1500, isochronal annealing was used for the thermal regeneration. The annealing temperature was increased in steps of ~59 °C every 30 s from room temperature up to 850 °C. The output response of the grating during thermal regeneration process is presented in Figure 3.10.

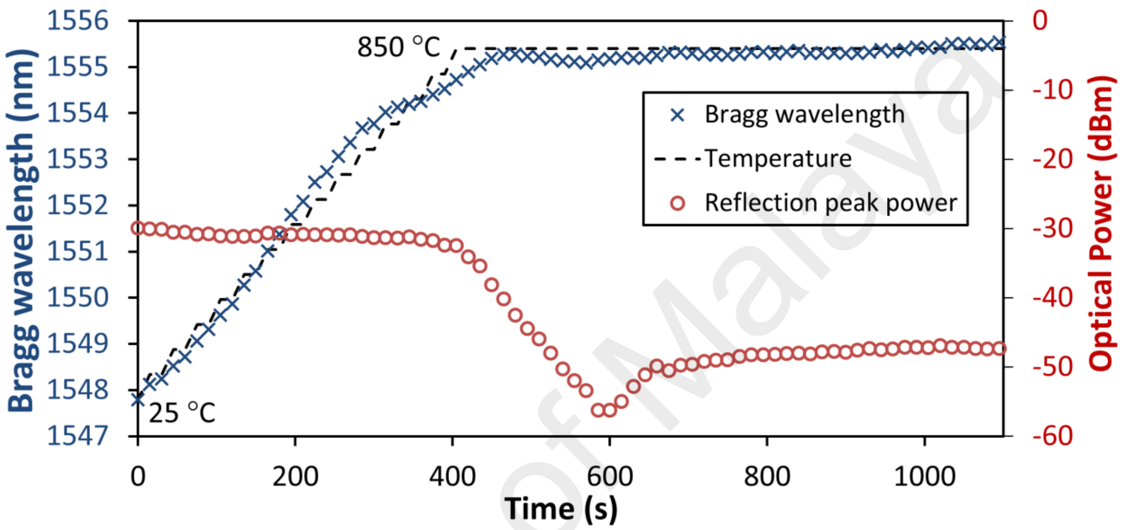

Figure 3.10 Output responses of a grating (PS1250/1500) during the regeneration process.

At 850 °C, the reflected power of the PS1250/1500 FBG started to decay continuously until it dropped to its minimal value. Shortly after that, a new reflection peak (regenerated grating) emerged from the noise level. This reflection peak gradually grew and stabilised at ~-47 dBm. The RFBG was cooled down to room temperature inside the furnace. The reflection spectra of the PS1250/1500 RFBG before and after thermal regeneration are presented in Figure 3.11. The reflection peak power of the RFBG is ~12 dB lower than the seed grating. The side lobes in the seed grating diminished after the thermal regeneration process. The bandwidth of the RFBG is also smaller than the seed grating. In overall, the results show that the grating strength of the RFBG was weakened after the thermal regeneration process.

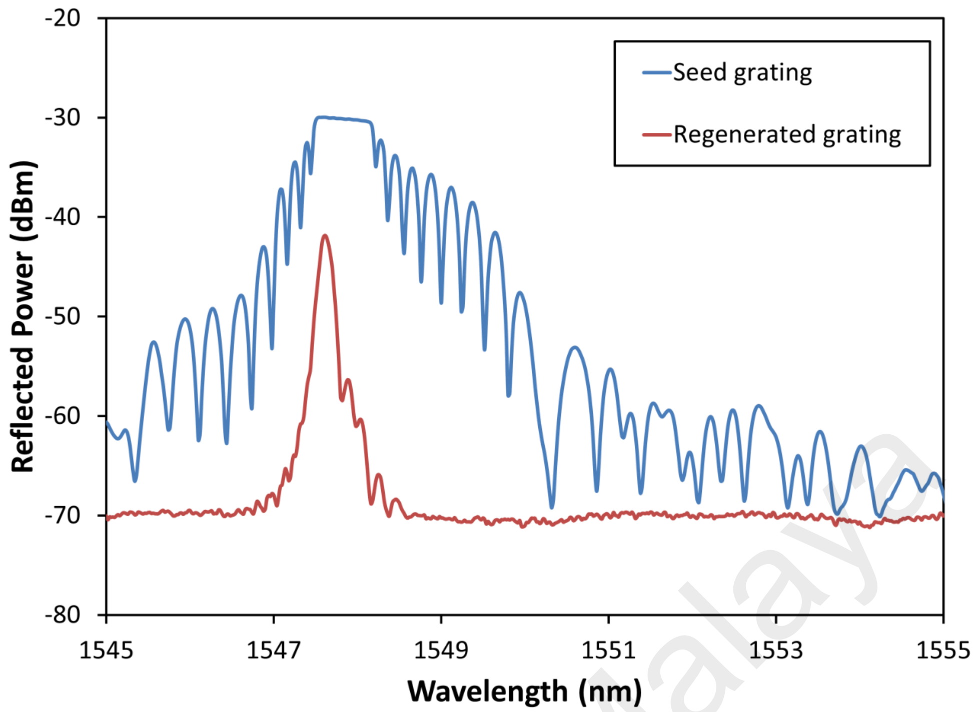

Figure 3.11 The reflection spectra of the PS1250/1500 FBG before and after the thermal regeneration process.

3.3.3 PS-PM980

A FBG inscribed on panda type polarisation maintaining fiber (PS-PM980) was used a subject for the demonstration of thermal regeneration on high birefringent fiber using high temperature furnace. The cross sectional micrograph of this fiber is shown in Figure 3.12. During the regeneration process, the annealing temperature was increased in steps from room temperature to ~850 °C, with a step of ~10 °C every minute. The grating strength decayed slowly until it was completely diminished. Shortly after that, a progressive growth was observed and stabilisation was achieved after 7–8 hours. It was observed that the birefringence of PMF was reduced to zero at ~850 °C (see Figure 3.13). This indicates the complete elimination of stress applying part (SAP)-induced stress in the fiber core due to the reduction in the viscosity of SAPs at high temperature.

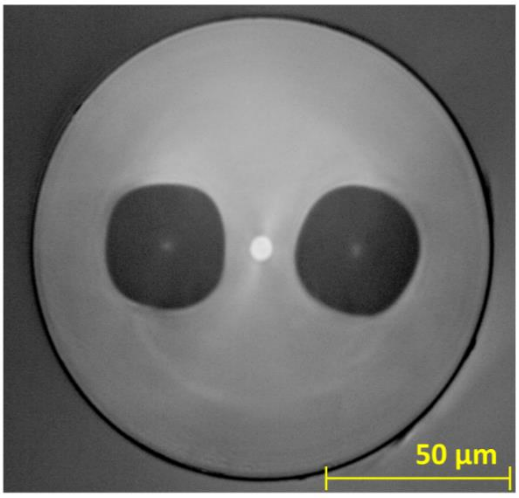

Figure 3.12 The cross sectional micrograph of photosensitive panda type PMF (Thorlabs PS-PM980).

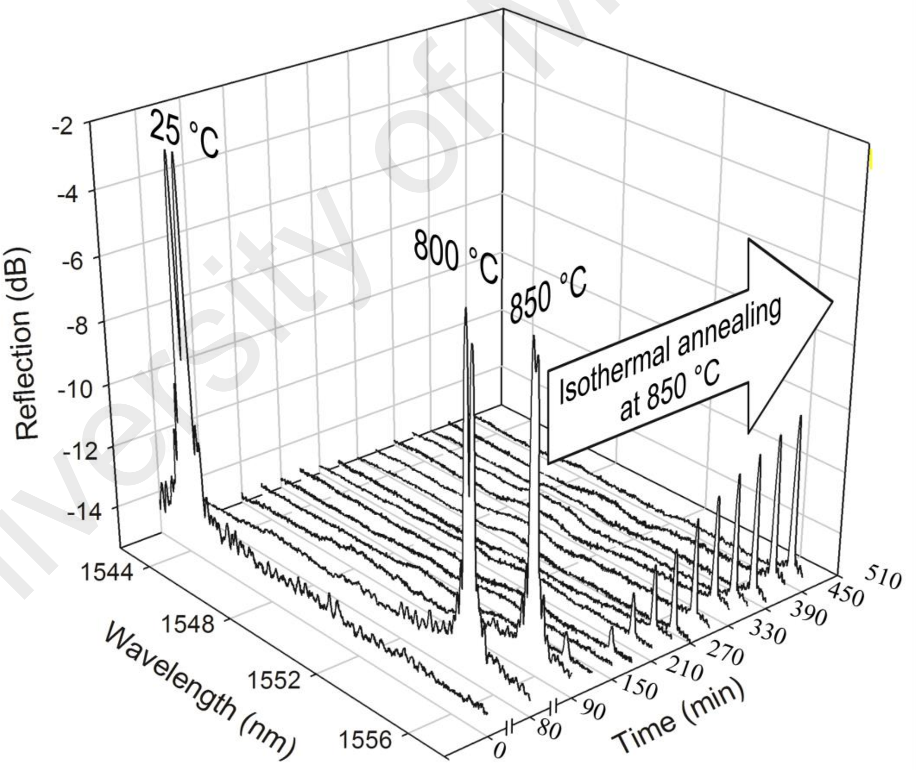

Figure 3.13 Spectral evolution of PS-PM980 during regeneration process.

Due to high concentration of boron dopant in SAP (~7.32 wt%), the glass transition temperature of SAP is lower and stress relaxation occurs at lower temperature than that in fiber core. After the onset of regeneration process at ~850 °C, the reflection peak decayed to below the noise level. It took ~30 minutes for the formation of a new grating and an additional 7–8 hours for the regrowth and stabilisation of the regenerated grating. Thereupon, the furnace was switched off and the produced regenerated grating in PMF (RGPMF) was left in the furnace to cool down to room temperature. The birefringence was re-introduced into RGPMF during the cooling process after grating regeneration because of the increment in viscosity of SAP. Figure 3.14 shows that, the birefringence increases from 3.37×10^{-4} to 4.56×10^{-4} after regeneration process based on the Bragg wavelength spacing between two orthogonal modes.

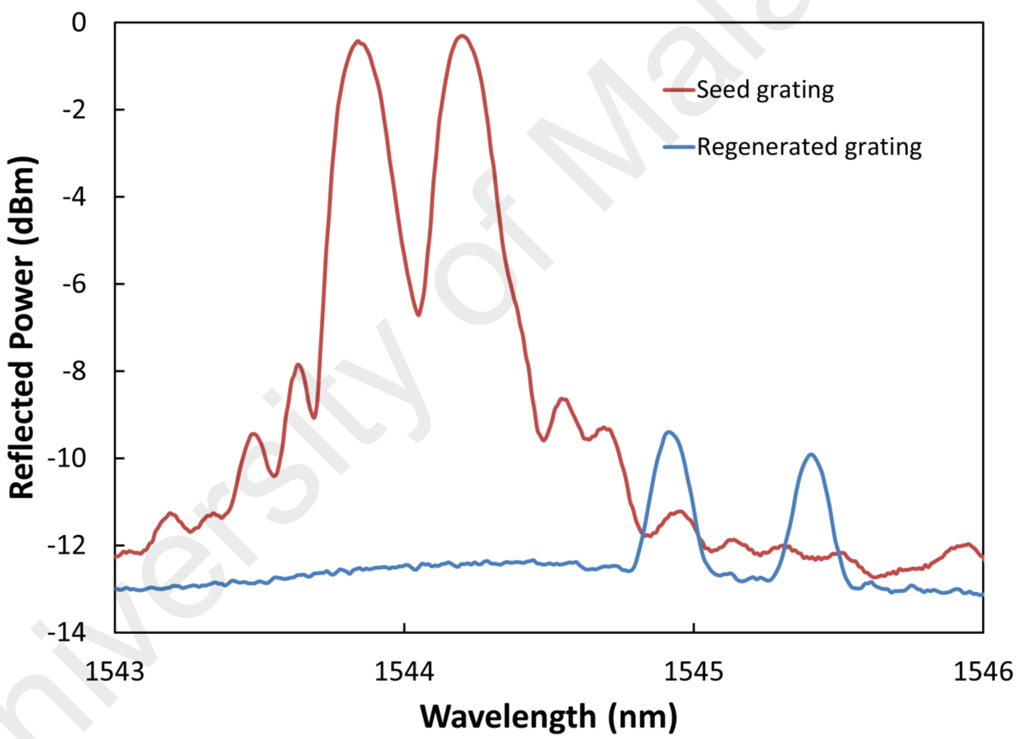

Figure 3.14 Reflection spectra of seed grating and regenerated grating written in PS-PM980.

This is due to the longer cooling process (slower cooling rate) after the regeneration treatment, as compared to the quenching rate during fiber pulling. Therefore, the compaction (or volume shrinkage) in SAPs due to slower cooling rate enhanced the birefringence. Besides that, a red shift in Bragg wavelength was observed after regeneration instead of the blue shift which was observed in the non-polarisation maintaining fiber. The slow cooling process after the regeneration might be the reason for the red shift in Bragg wavelength, which was due to the thermal stress relaxation.

3.3.4 Few-Mode Fiber

FBGs inscribed on four different type of few-mode fibers (2S. 2G, 4S, 4G) were used for the study of thermal regeneration on few-mode fiber. During the thermal regeneration treatment, the annealing temperature was incremented in a constant rate from room temperature to the regeneration temperature, where the grating reflectivity decayed rapidly until the Bragg reflection was totally erased. The grating was annealed at this temperature until the regeneration process was completed. The observed regeneration temperatures of 2G, 2S, 4G and 4S were 920 °C, 910 °C, 900 °C and 890 °C respectively. The annealing temperature was ramped up from room temperature to regeneration temperature in 100-175 min (see Figure 3.15 (a) green line). As shown in Figure 3.15, the reflected power of each type of few-mode grating (FMG) diminished once the annealing temperature reached the regeneration temperature.

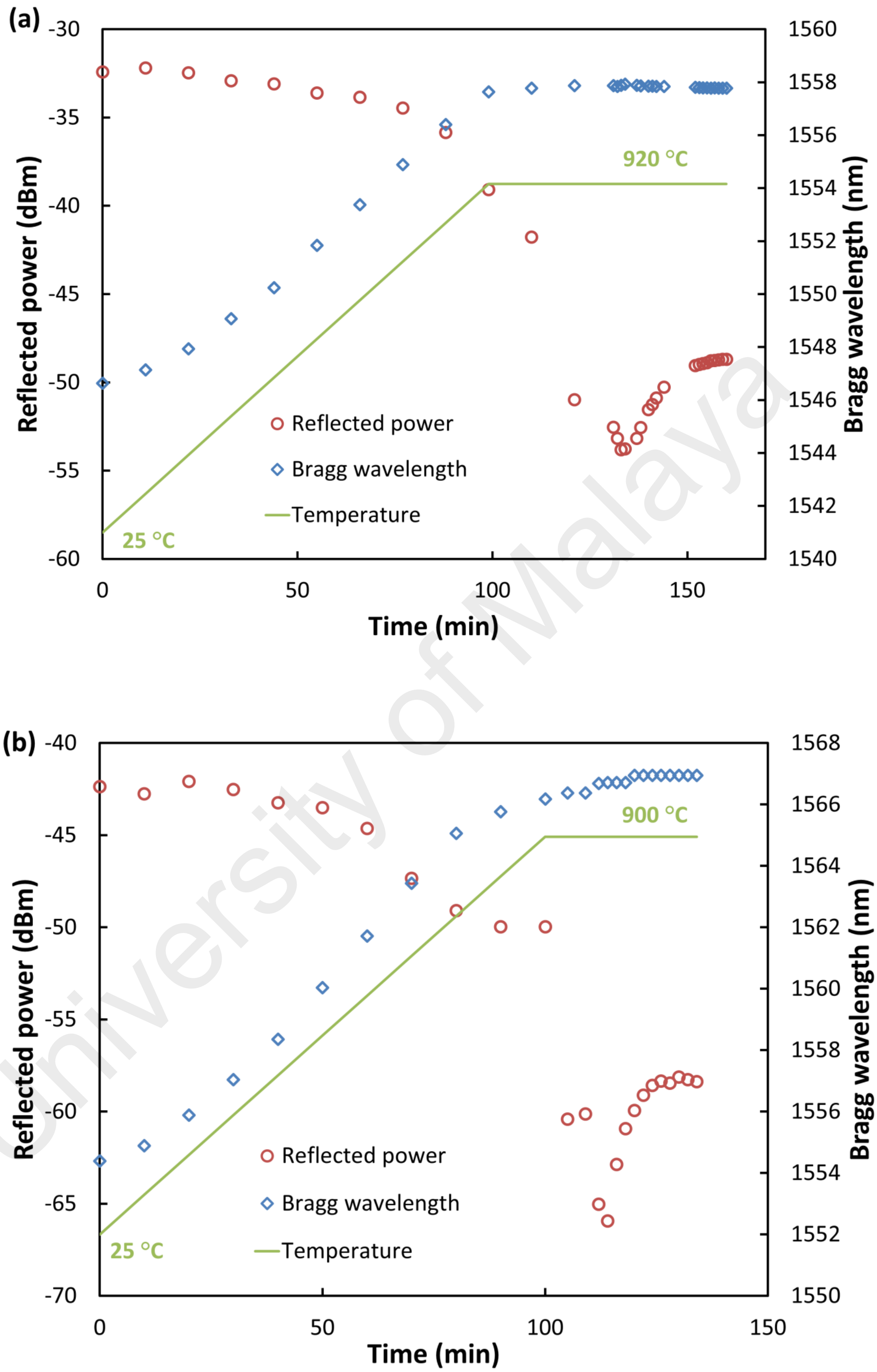

Figure 3.15 Output responses of (a) 2G, (b) 4G, (c) 2S and (d) 4S FBGs during regeneration process.

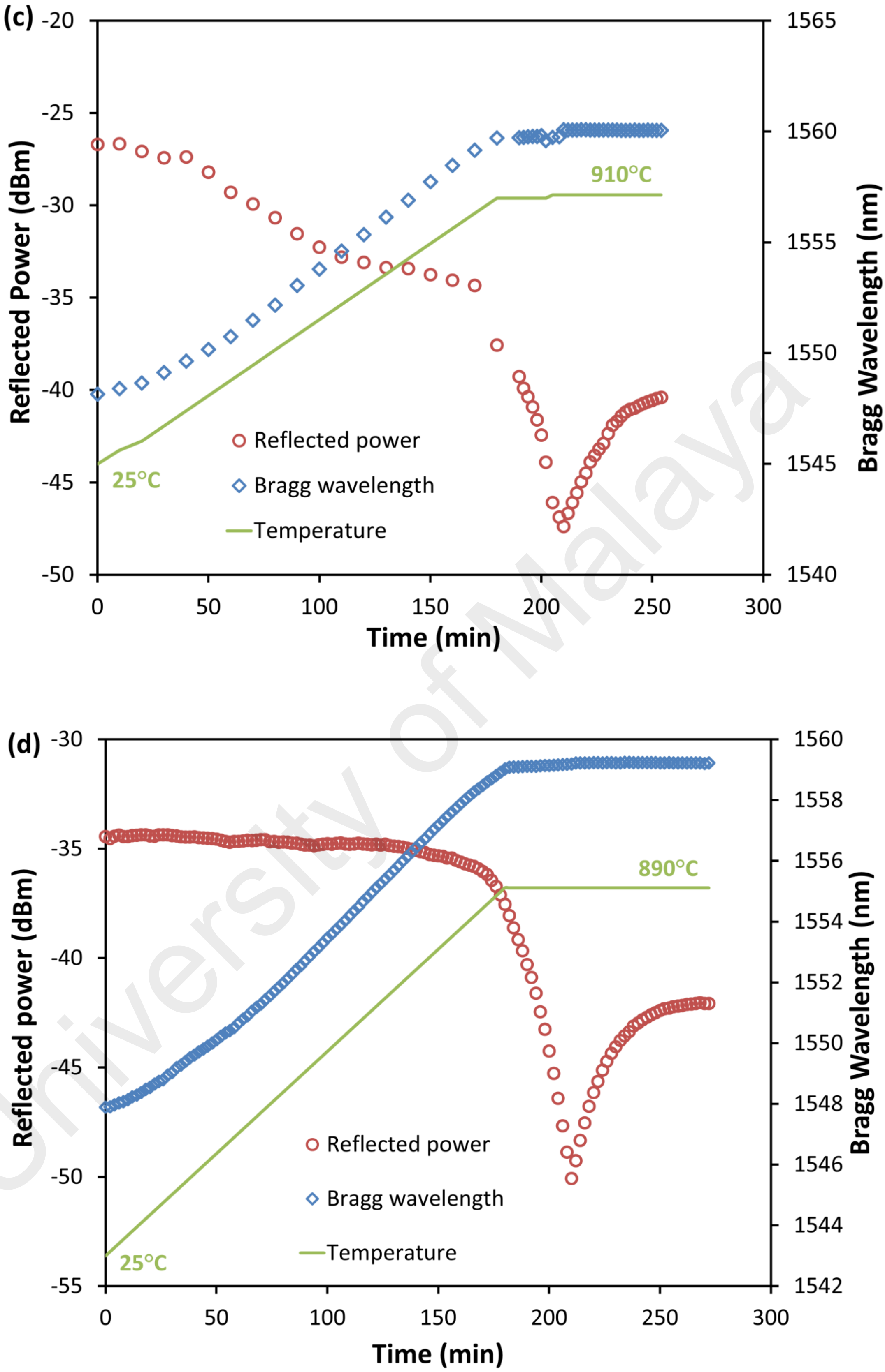

Figure 3.15, continued.

During thermal regeneration, a continuous variation in the grating reflectivity and Bragg wavelength was observed throughout the process. An OSA was used to continuously record the reflection spectra of the grating and the measurement of the grating reflected power during the regeneration process. After the regeneration process, the FMGs are gradually cooled down to room temperature. The UV-induced refractive index modulation in the FBG diminished to a minimum at the regeneration temperature. Subsequently, a regenerated reflection peak was recorded in the reflection spectrum when the fiber was isothermally annealed at its corresponding regeneration temperature for 5–10 min. As the annealing temperature increased from room temperature to regeneration temperature, the UV-induced refractive index modulation in FMGs decayed and the reflectivity of the grating reduced. Meanwhile, the Bragg wavelength variation during thermal annealing is due to the thermal-induced refractive index change (Ferreira *et al.*, 2000). It was observed that the UV-induced refractive index change of the seed grating decreased rapidly at an annealing temperature of 900 °C and eventually erased at the regeneration temperature (see Table 3.4). At this temperature, stress relaxation and structural rearrangement might have occurred as indicated by the diminishing UV-induced index modulation of the seed grating (Chen *et al.*, 2004). After 35–75 min of isothermal annealing at its regeneration temperature, a RFBG emerged from the noise level where the reflectivity gradually increased and finally stabilised. The reflection spectra of the seed gratings and the RFBGs are shown in Figure 3.16.

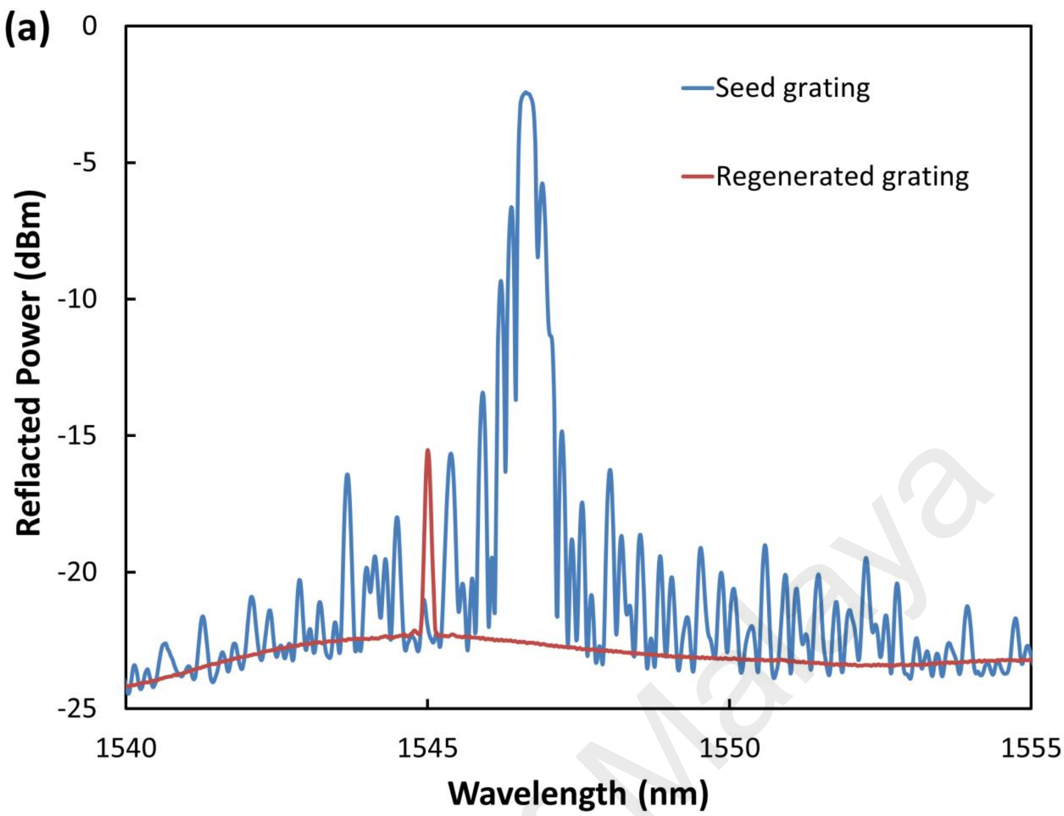

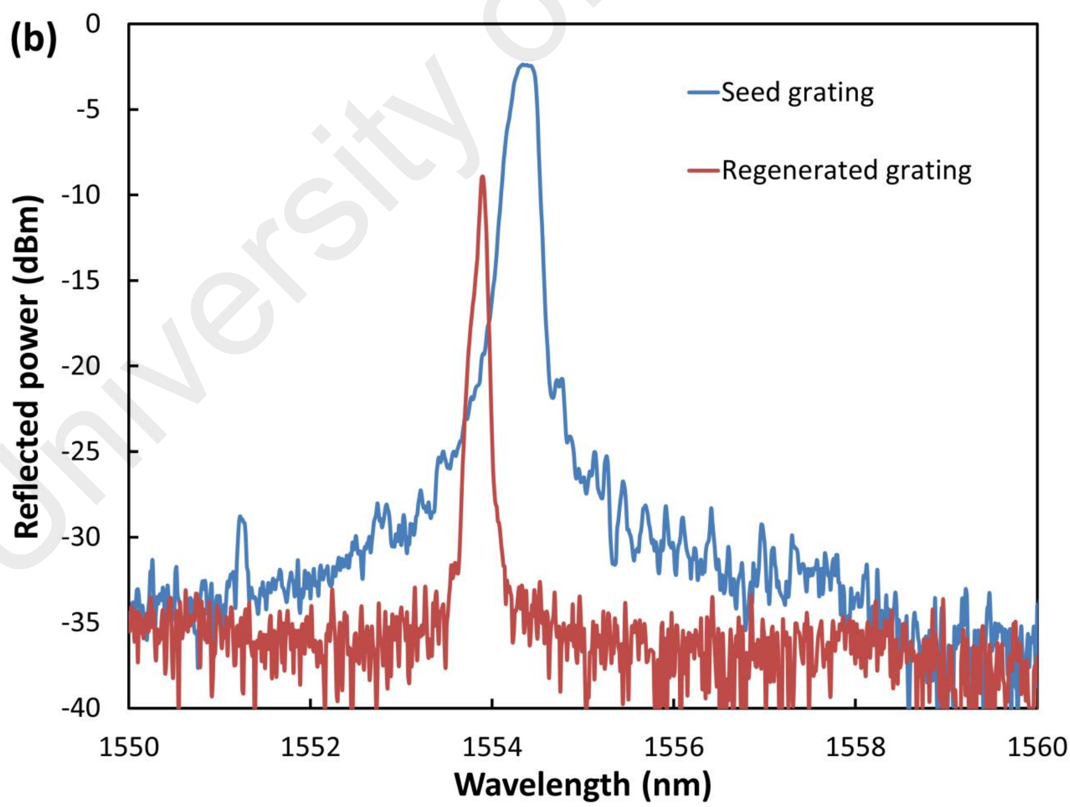

Figure 3.16 Reflection spectra of seed and regenerated gratings for (a) 2G, (b) 4G, (c) 2S and (d) 4S fiber at room temperature of 25 °C.

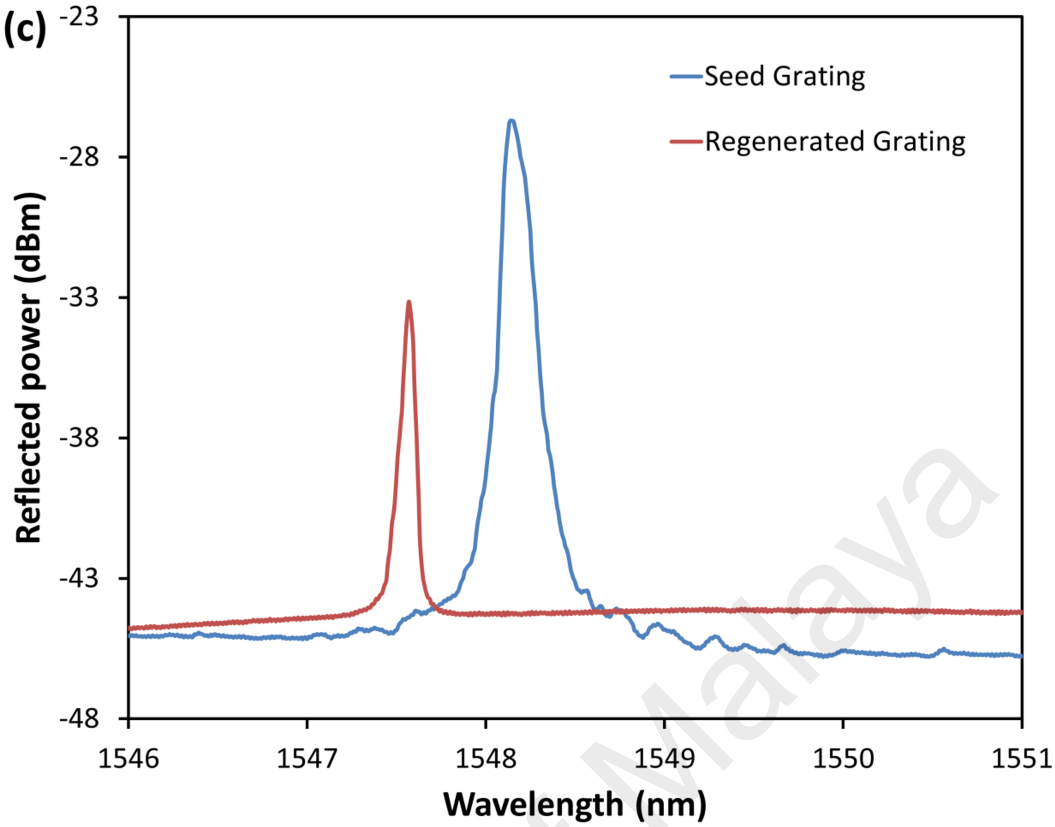

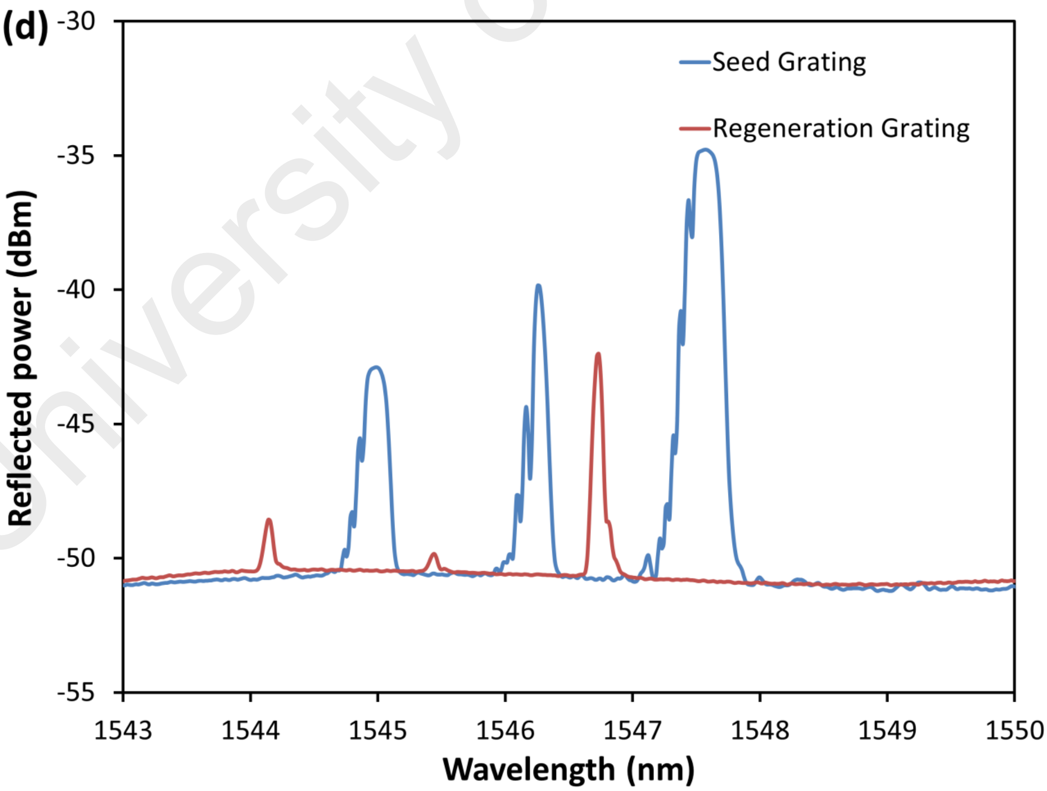

Figure 3.16, continued.

The reflection peaks of RFBGs have blue-shifted with respect to their seed gratings. This is due to the combined-effect of UV-induced index change at the fiber core and the alteration of the grating period after regeneration (Turnbull & Cohen, 1961). The peak reflectivity of the Bragg wavelength and the side lobes of RFBGs were drastically reduced compared with the seed gratings. This indicates the reduction of the grating strength (Chen *et al.*, 2004). The reflection peaks of higher order modes in 2G, 2S and 4G fibers were unobservable after the regeneration process because of their low grating strength. The reflection peaks of higher order modes in 4S become smaller after thermal regeneration process. It was observed that the bandwidth and reflected peak power of the RFBGs have been reduced. This indicates that the regenerated grating has a lower refractive index modulation. This can be attributed to the structural rearrangement of the glass during high temperature treatment of the gratings. Besides the excellent capability of extreme temperature detection, the proposed regenerated FMG can potentially be employed for multi parameter sensing. Each transverse mode in an etched FMG exhibited different sensitivity to the ambient refractive index change (Ourmazd *et al.*, 1983). The refractive index (RI) sensitivities of the transverse modes in the core can be enhanced by reducing the etched diameter of the fiber. Similar etching treatment can be applied to regenerated FMG to equip this grating with the RI sensing capability.

3.3.5 Gallium (Ga) doped fiber

Ga is an alternative dopant to Ge as an index raiser and photosensitive element in the fiber core. Ga doped fiber can be fabricated by using modified chemical vapour deposition (MCVD) and standard solution doping method reported by Townsend *et al.*, 1987. The fabrication of fiber preform begins with flowing silicon tetrachloride ($SiCl_4$) vapour and oxygen (O_2) gas into a rotating substrate tube (Heraeus F300) while it is heated by an external flame source moving along the substrate tube at temperature of 1700-1750 °C. A porous layer of silica (Si) layer (soot) is formed on the inner layer of the substrate tube. Afterwards, solution doping is carried out by soaking the soot preform into the solution of consist of 1.5 M of Gallium (III) nitrate hydrate solution (Sigma-Aldrich 99.9 %) Ga $(NO_3)_3.xH_2O$ diluted with ethanol/water (H_2O) mixture. After the drying process using nitrogen (N_2) gas, the preform is oxidized, sintered and collapsed into a glass rod following the standard MCVD process. The optical fiber is then drawn from the glass rod using standard fiber drawing tower. In this section, a Ga doped fiber was used in the investigation of thermal regeneration. The fiber has a Ga concentration of ~ 5 wt%, the fiber core diameter, cladding diameter and NA are ~11.8 µm, ~125 µm and ~0.15 respectively.

The thermal regeneration of Ga doped fiber was carried out in a high temperature tube furnace. The temperature in the furnace was controlled by an in-built program. During thermal regeneration process, the temperature was increased constantly at a rate of ~4.16 °C/min from room temperature up to 720 °C. The grating started to diminish as the annealing temperature reached 400 °C. A new reflection peak was formed after the initial peak disappeared. As soon as the grating reflectivity stabilised, the furnace was switched off and the regenerated grating was cooled down to room temperature inside the furnace. The evolution of the grating reflection spectra were recorded continuously throughout the whole annealing process using an OSA, controlled by a LabVIEW program via GPIB interface. The thermal response of the grating reflectivity and Bragg wavelength are presented in Figure 3.17.

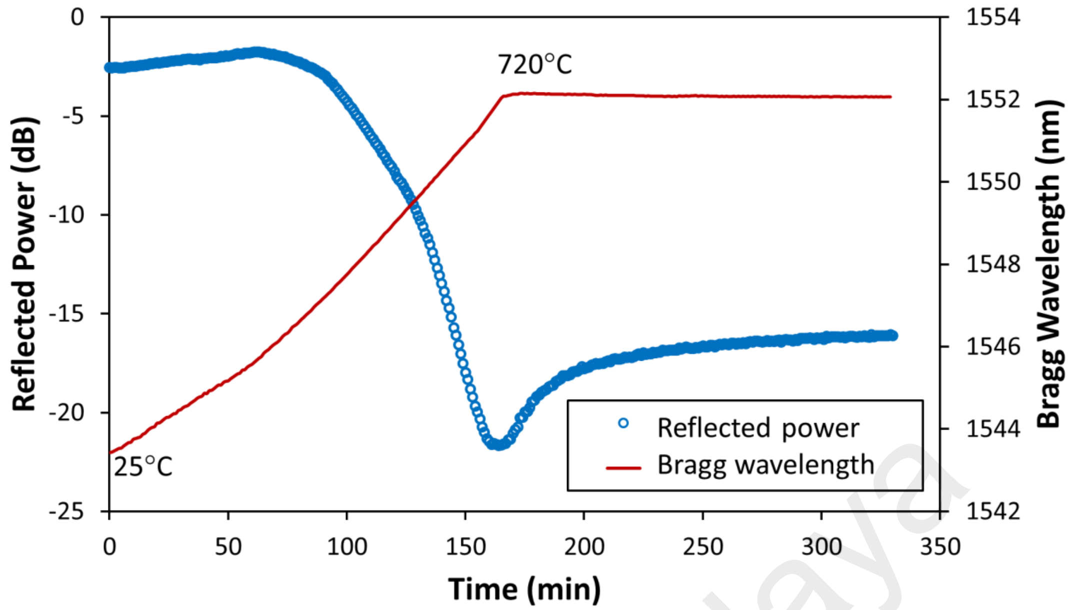

Figure 3.17 The evolution of reflected power and Bragg wavelength of the gallosilicate FBG during thermal regeneration.

After the grating regeneration stabilised, the Bragg wavelength of the regenerated grating was red-shifted by ~9 nm from that of the seed grating at room temperature. Figure 3.18 presents the comparison between the reflection spectra of the Ga doped FBG before (seed grating) and after (regenerated grating) thermal regeneration at room temperature. The regenerated grating has lower reflection peak power, fewer side lobes and smaller bandwidth compared to the seed grating. This is due to the decay in grating strength and UV-induced index modulation after the thermal regeneration process.

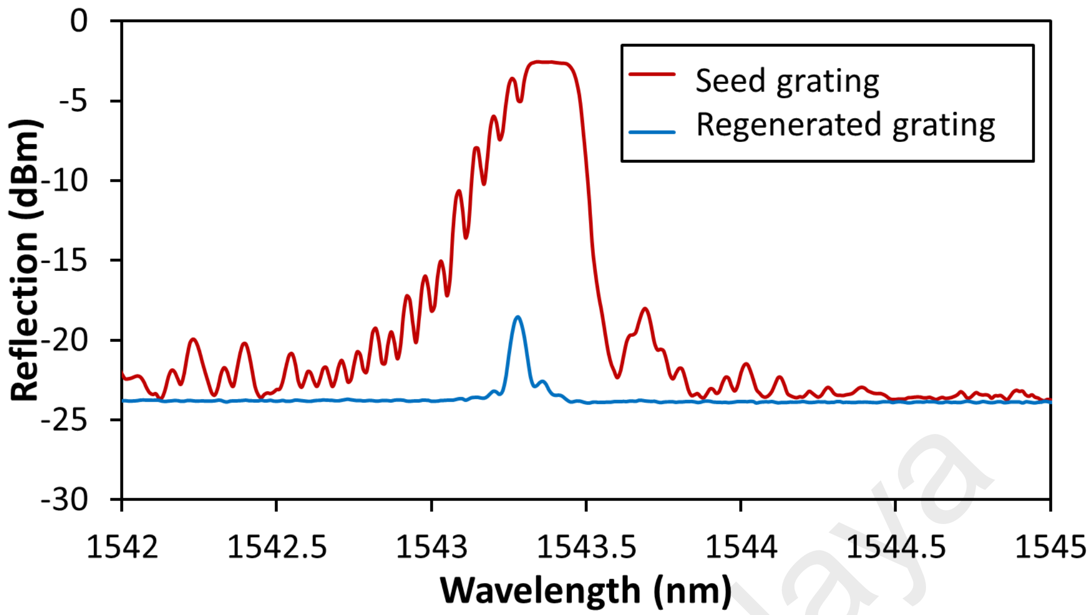

Figure 3.18 Comparison between the reflection spectra of the gallosilicate FBG before (seed grating) and after (regenerated grating) thermal regeneration at room temperature.

Thermal regenerated Ga doped FBG opened up a new avenue of research in fabricating high temperature-resistant FBG components using new dopant as refractive index raiser. The Ga can be used as a substitute for Al dopants in co-doped rare-earth fiber. Thermal regeneration on these Ga co-doped rare-earth fibers is useful in fabrication of high temperature-resistant fiber lasers and related devices.

3.4 Thermal Characterisation of RFBG

Thermal characterisation is the follow-up test for the freshly manufactured RFBGs to investigate their performance in terms of thermal sensitivity, wavelength stability and reflectivity stability. Nonetheless, another intention of performing thermal characterisation on RFBG is to investigate the hysteresis phenomenon in thermal response of the RFBG. This can be achieved by repeating the thermal characterisation tests for several cycles. A good RFBG temperature sensor should have a consistent thermal response with negligible hysteresis that they can be used for accurate temperature measurement.

The thermal sensitivity of the RFBG was characterised using the experimental setup for thermal regeneration using a high temperature furnace. The annealing temperature was elevated from room temperature to the target temperature at a specific rate. Shortly after that, the annealing temperature was reduced to room temperature gradually. The Bragg wavelength of the RFBG was recorded using OSA controlled by LabVIEW program via GPIB interface.

Figure 3.19 shows the wavelength response of PS1250/1500 RFBG in temperature ranges 100 – 700 °C. The annealing temperature was increased at a rate of 50 °C every 5 minutes. It is observed that there is no significant hysteresis during heating and cooling of the regenerated grating. Regenerated grating exhibits temperature sensitivity of between 11.5 pm/°C (heating) to 11.8 pm/°C (cooling).

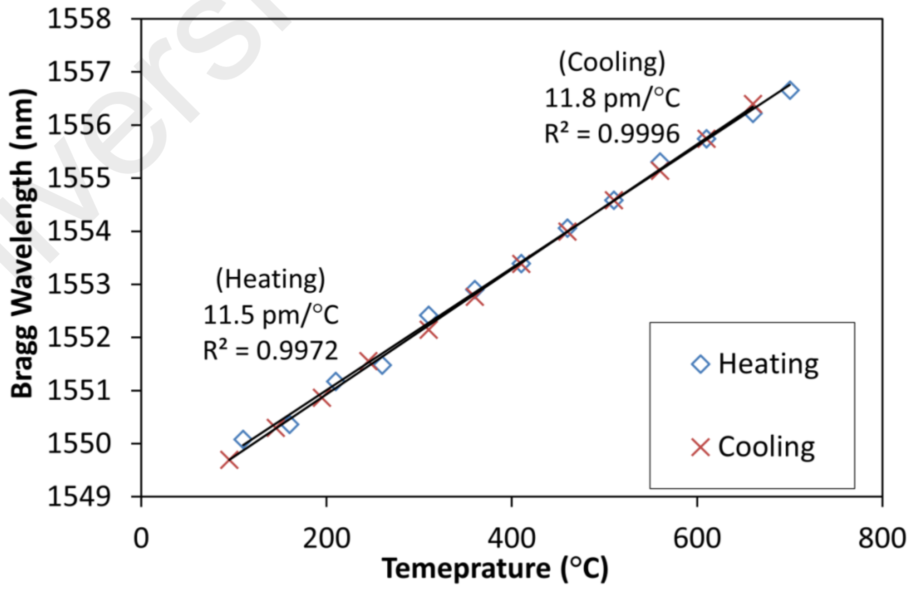

Figure 3.19 Wavelength response of regenerated grating (PS1250/1500) in the range of 100-700 °C.

Thermal characterisation of RGPMF was carried out from room temperature to 800 °C. The plots of Bragg wavelengths for both orthogonal polarisation modes against temperature are presented in Figure 3.20.

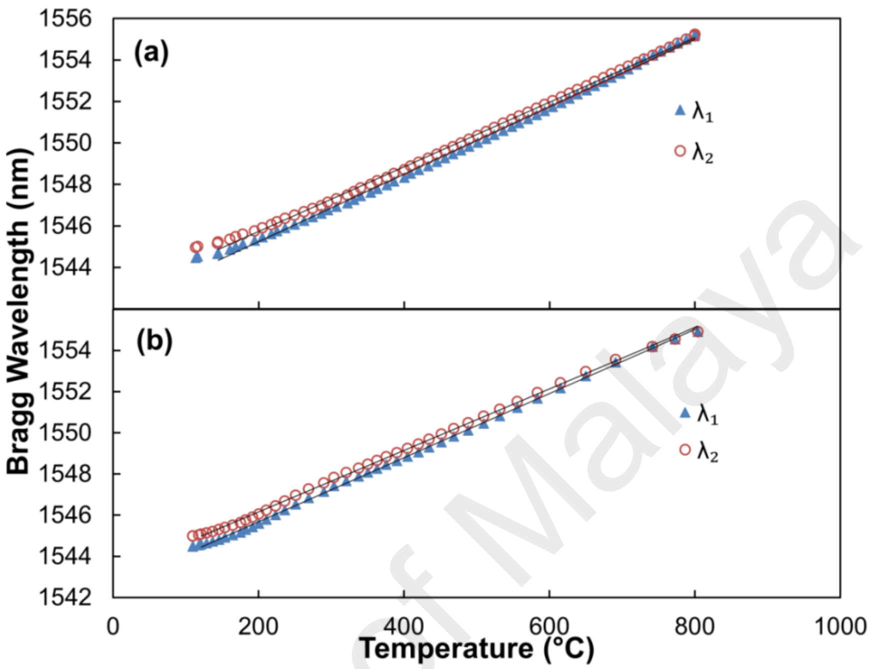

Figure 3.20 Thermal calibration of RGPMF (a) heating-thermal sensitivity of 15.6 pm/°C for λ_2 and 16.3 pm/°C for λ_1 and (b) cooling-thermal sensitivity of 14.9 pm/°C for λ_2 and 15.6 pm/°C for λ_1. 1 (○): Fast axis Bragg wavelength. 2 (▲): Slow axis Bragg wavelength.

During heating process, the thermal sensitivity of Bragg wavelengths in fast and slow axes are 15.6 pm/°C and 16.3 pm/°C respectively, whereas, during the cooling process, the thermal sensitivity of Bragg wavelengths in fast and slow axes are 14.9 pm/°C and 15.6 pm/°C respectively. Generally, the slow axis Bragg wavelength has a higher thermal sensitivity compared to the fast axis Bragg wavelength. Eventually, the two Bragg wavelengths merged at high temperature (~850 °C), where the birefringence eventually reduced to zero. In the comparison with the grating before regeneration, the temperature sensitivities for both axes are ~16.2 pm/°C. This shows that the temperature sensitivity of the grating does not change after the regeneration process. The maximum operating temperature of the regenerated grating in PMF is close to its regeneration temperature (~850 °C). At regeneration temperature, the birefringence of the grating completely disappears making the grating to lose its ability in multiparameter sensing. At this stage, the grating behaves like a grating in single mode fiber. Further increases in temperature beyond 1000 °C will result in a permanent decay of the grating strength of the grating and inaccurate temperature measurements.

For single mode (ZWP-SMF) and few-mode fibers, the annealing temperature was increased up in steps of 50 °C from room temperature to 900 °C. The thermal sensitivities of the regenerated gratings on single mode and few-mode fiber are presented in Figure 3.21 and summarized in Table 3.5. The thermal sensitivity of SMF, 2G, 2S, 4G and 4S RFBGs are 15.9 pm/°C, 16.1 pm/°C, 16.4 pm/°C, 15.5 pm/°C and 14.9 pm/°C respectively. The thermal sensitivities for heating and cooling process are consistent with each other.

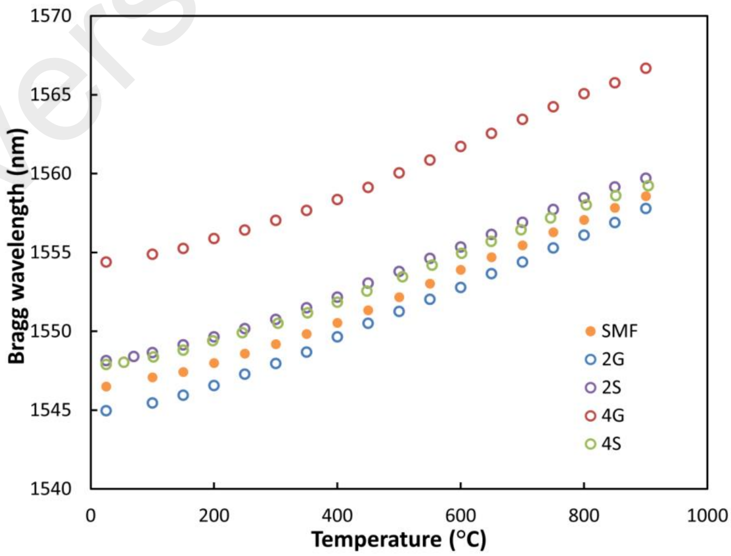

Figure 3.21 The thermal calibration of SMF, 2G, 2S, 4G and 4S. RFBGs from room temperature up to 900 °C. The thermal sensitivity of SMF, 2G, 2S, 4G and 4S RFBGs are 15.9 pm/°C, 16.1 pm/°C, 16.4 pm/°C, 15.5 pm/°C and 14.9 pm/°C respectively.

The characterisation of thermal sensitivity of Ga doped RFBG was carried out in the temperature range of 25 - 750 °C. The annealing temperature was gradually increased from 25 °C up to 750 °C, followed by cooling process down to 25 °C. This annealing and cooling cycle was repeated three times to analyse the hysteresis in thermal sensitivity. In addition, the Ga doped RFBG was annealed at 720 °C for 8 hours to investigate its Bragg wavelength stability. The plots of Bragg wavelength against temperature for heating and cooling are presented in Figure 3.22.

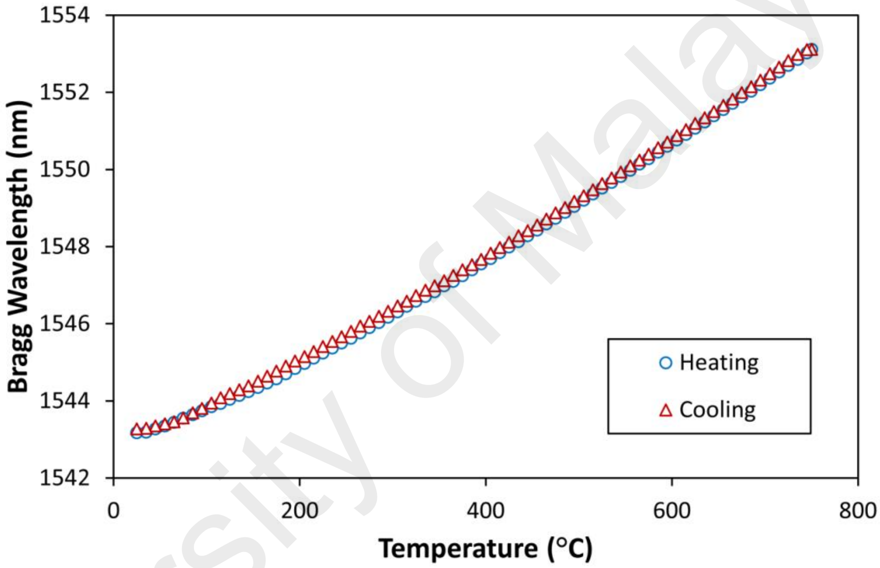

Figure 3.22 Thermal sensitivity characterisation of gallosilcate RFBG from 25 °C-750 °C.

The thermal sensitivities of the Ga doped RFBG during the heating and cooling processes are 15.2 pm/°C and 15.0 pm/°C. At 750 °C, the Bragg wavelength shift with respect to room temperature is 9.4 nm. The temperature gradient in the furnace may be responsible for the small difference in the thermal sensitivity between heating and cooling processes. The thermal sensitivity of the Ga doped RFBG shows a good linearity in the temperature range of 250 °C to 750 °C. On the other hand, the nonlinear thermal sensitivity below ~250 °C is due to the nonlinearity in thermo-optic response of silica glass (Leviton & Frey, 2008). Figure 3.23 shows the thermal sensitivity results for each cycle of annealing and cooling processes. The results in Figure 3.23 show a nearly perfect consistency in thermal sensitivity between each annealing and cooling cycle. The Bragg wavelength stability of Ga doped RFBG at 720 °C for 8 hours is presented in Figure 3.24. The result shows that the variation in Bragg wavelength over the 8 hours of annealing is ±4.4 pm. This indicates that Ga doped RFBG is an excellent temperature sensor with good temperature linearity and stability.

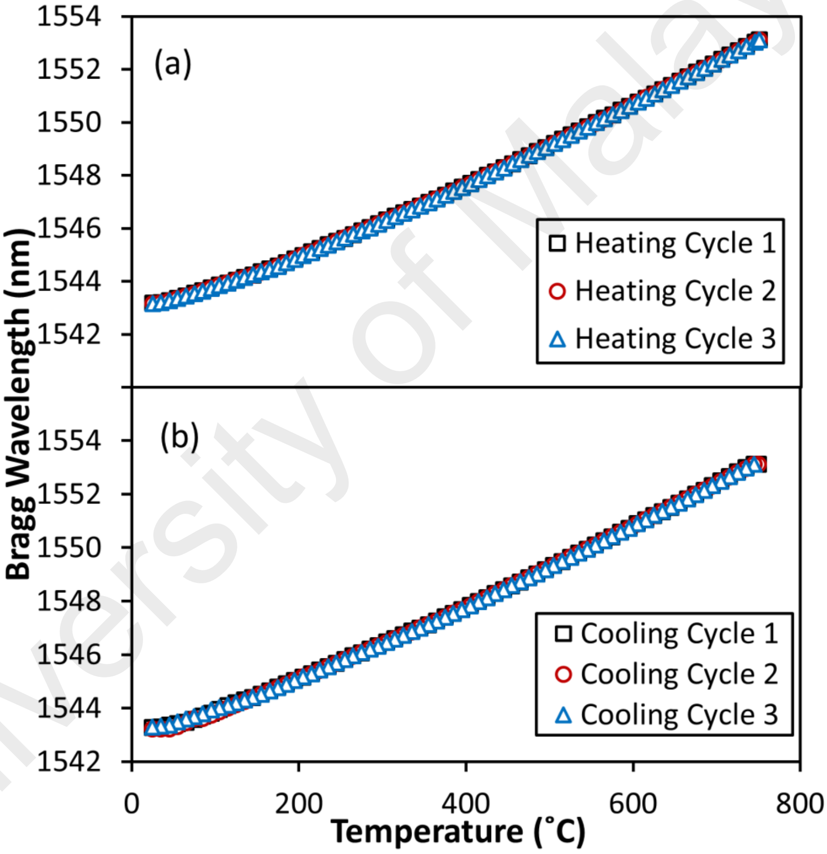

Figure 3.23 Thermal sensitivity calibration of the gallosilicate regenerated grating during (a) heating process and (b) cooling process.

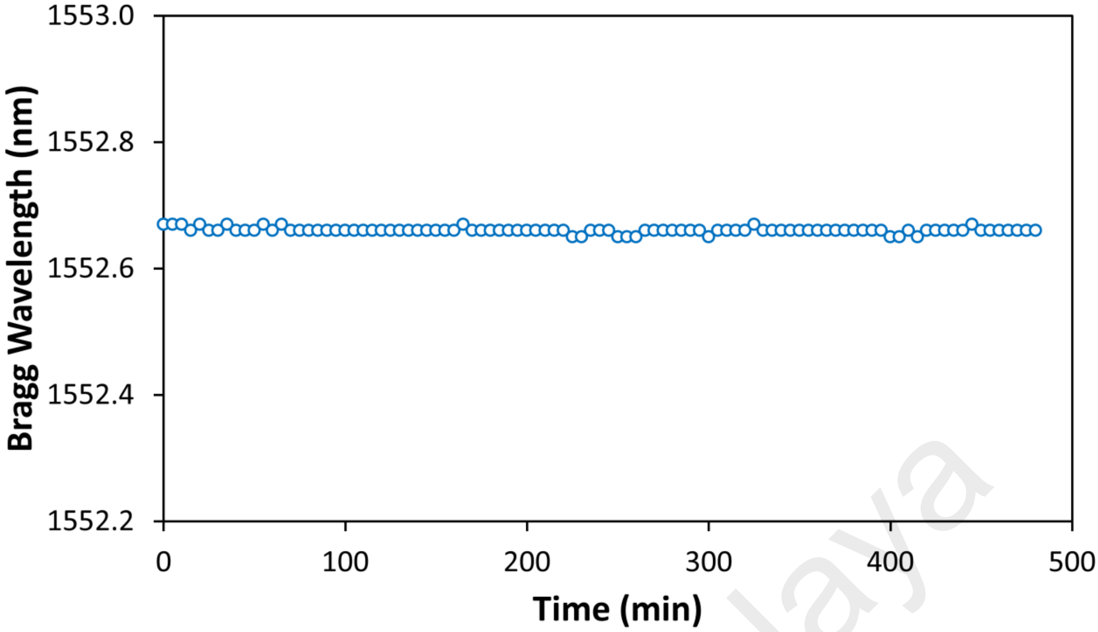

Figure 3.24 Bragg wavelength stability of Ga doped RFBG at 720 °C for 8 hours.

Table 3.5 Summary of thermal sensitivity for each type of RFBGs.

Type of FBG	ZWP-SMF	PS1250/1500	PS-PM980	Ga	2G	2S	4G	4S
Thermal sensitivity (pm/°C)	15.9	11.5-11.8	Heating: 15.6 - 16.3 Cooling: 14.9 - 15.6	15.0-15.2	16.1	15.5	16.4	14.9

3.5 Summary

The regenerated gratings had been successfully developed in different fibers includes ZWP-SMF, PS1250/1500, PS-PM980, few-mode graded index fiber, few-mode step index fiber and Ga doped fiber. Two types of annealing schemes were used in this work, namely isochronal annealing and constant rate annealing. For every type of seed grating, the thermal response during thermal regeneration was presented. All fibers showed similar thermal response during thermal regeneration process. The grating reflectivity decayed rapidly at regeneration temperature. Shortly after the grating was completely diminished, a new reflection peak was formed and its reflectivity increased gradually until it stabilised at lower reflectivity level. The reflection spectra of the grating before and after thermal regeneration are compared. The blue shift in Bragg wavelength after thermal regeneration can be attributed to the reduction in UV-induced index modulation and stress relaxation in the grating. The birefringence change after thermal regeneration in PMF shows that the stress condition in the fiber depends on the cooling process after annealing. The thermal responses of the RFBGs were characterised to investigate the thermal sensitivity and the hysteresis effect. The details of the regeneration temperature and thermal sensitivity of each fiber are summarized in Table 3.6.

Table 3.6 Summary of regeneration temperature and thermal sensitivity for each type of RFBGs.

Type of FBG	ZWP-SMF	PS1250/1500	PS-PM980	2G	2S	4G	4S	Ga
Regeneration temperature (°C)	~950	~850	~850	~920	~910	~900	~890	~720
Thermal sensitivity (pm/°C)	15.9	11.5 - 11.8	Heating: 15.6-16.3 Cooling: 14.9-15.6	15.0-15.2	16.1	15.5	16.4	14.9

CHAPTER 4: CO_2 LASER ANNEALING TREATMENT ON OPTICAL FIBER

Mie theory model (Bohren & Huffman, 1983) and geometric model (Grellier *et al.*, 1997) are generally used for describing the heat transfer in optical fiber during carbon dioxide (CO_2) laser irradiation. Grellier *et al.* (1998) modelled and examined the heat transfer in optical fiber during CO_2 radiation using both models. The optical fiber is treated as a one-dimensional (1-D) thin rod during CO_2 laser annealing where the laser beam is irradiated perpendicularly to the fiber axis. This approximation has been verified by thermal thinness condition (Myers, 1998). The temporal thermal response of the fiber Bragg grating (FBG) towards the CO_2 laser annealing appeared to be independent from the laser power and final annealing temperature. The direction of CO_2 laser irradiation also plays a vital role in fiber annealing. Asymmetric annealing will induce birefringence to the fiber due to non-uniform refractive index modification. In this chapter, CO_2 laser is used as the heating source in the study of thermal regeneration and thermal stability enhancement in FBG.

4.1 Experimental Setup

The experiment setup of the CO_2 laser annealing is presented in Figures 4.1 and 4.2. The laser source for the experiment is a fan-cooled CO_2 laser system (SYNRAD 48-2 SAM). The cooling of the CO_2 laser is enhanced through the heat dissipation to the stainless steel optical table. The maximum output power and power stability of the laser are 35 W and < ± 2 % respectively. The laser beam from the laser source was first expanded and collimated using a combination of two spherical zinc selenium (ZnSe) convex lenses from beam diameter of ~1 mm to ~10 mm. Subsequently, the laser beam was compressed horizontally using a plano-convex cylindrical lens (focal length: 50.8 mm) into a 1 mm × 10 mm long vertical beam with a maximum intensity of ~18 W. On the other hand, the fiber was clamped on a three axis positioning stages in which the grating region was located at the centre of the laser beam where the laser intensity was optimum. The other end of the grating was attached to a small plasticine load with a weight of ~0.2 g to ensure that the fiber remained straight throughout the annealing process and the grating region was fully exposed to the CO_2 laser beam. The mass of plasticine load should be made light, sufficient heavy to straighten the fiber but not to induce lengthening effect to the fiber during laser annealing process. In order to prevent swinging of fiber caused by air currents, the plasticine load gently leaned against another small metal block but remained straight and vertical. This is to ensure that the fiber is absolutely still during the laser annealing process. The grating used was connected to a circulator and an optical spectrum analyser (OSA) as shown in Figure 4.1.

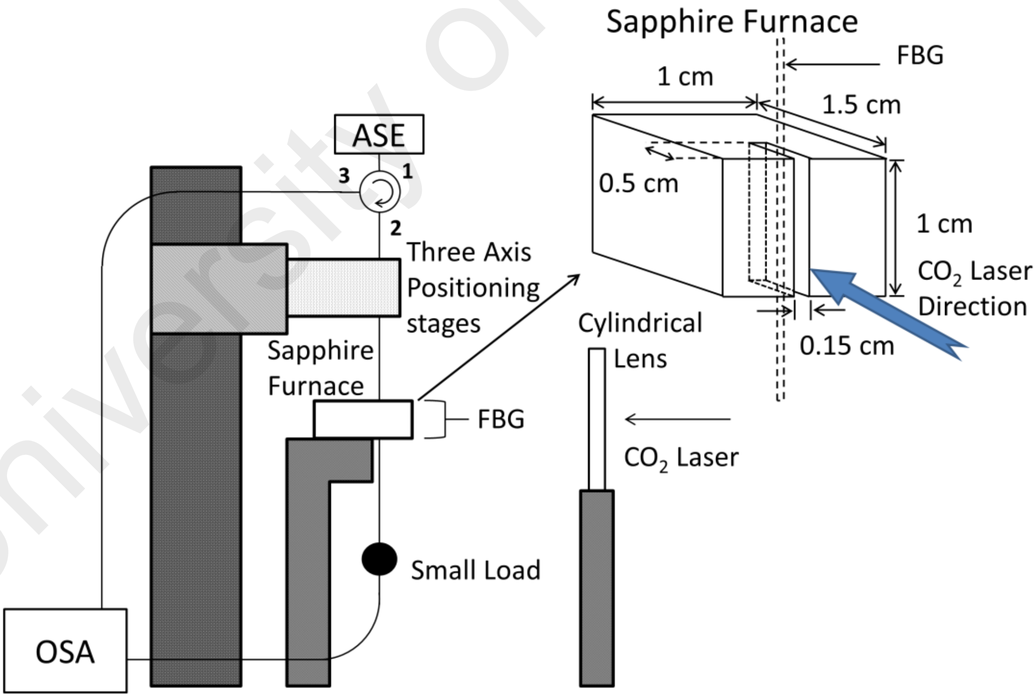

Figure 4.1 Schematic diagram of the experimental setup for CO_2 laser annealing. ASE: Amplified spontaneous emission source. Inset shows the dimension of the sapphire furnace.

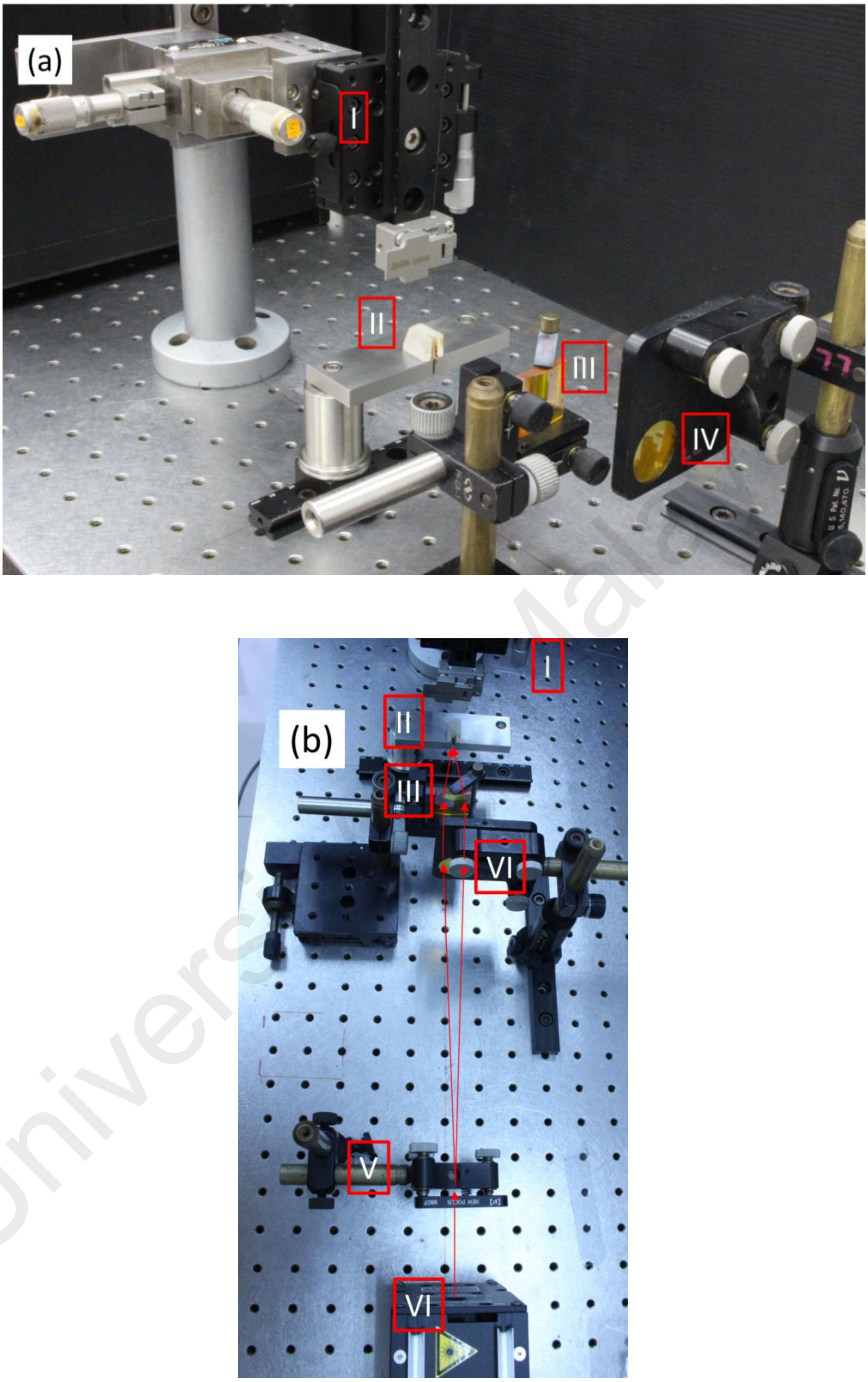

Figure 4.2 Illustration of CO_2 laser annealing setup from (a) top view, (b) side view. I: Three axis positioning stage, II: Sapphire mini furnace, III: ZnSe plano-convex cylindrical lens, IV & V: ZnSe plano-convex spherical lens, VI: CO_2 laser aperture.

4.2 Thermal Response of FBG to CO_2 Laser Annealing

CO_2 laser annealing has great advantages compared to the conventional furnace annealing. For instance, CO_2 laser annealing is based on the principle of radiative absorption and it is capable of providing instantaneous heating and cooling relaxation. Flexibility in the beam manipulation enables the heating to be applied in a more focus and small area. However, CO_2 laser annealing technique suffers a drawback of susceptibility to ambient air turbulence which leads to temperature instability. This problem can be addressed by employing a mini sapphire furnace in the annealing setup. Sapphire has a very high absorption to CO_2 laser radiation (Dobrovinskaya *et al.* 2009), it is capable of absorbing the scattered ray from the CO_2 laser and to generate additional heat to the system. This helps in maintaining the high temperature and reducing the influence of the ambient air perturbation within the vicinity of the grating in the slit.

Prior to the investigation of thermal regeneration, stress relaxation and birefringence modification in FBG using CO_2 laser, the thermal response of the FBG during CO_2 laser annealing has been characterised. In the annealing process, a mini sapphire furnace with a dimension of 1.5 cm × 1 cm × 1 cm was used. The small slit of the furnace has a depth of 0.5 cm and a width of 0.15 cm (see Figure 4.3) and that was where the seed grating positioned during the annealing process.

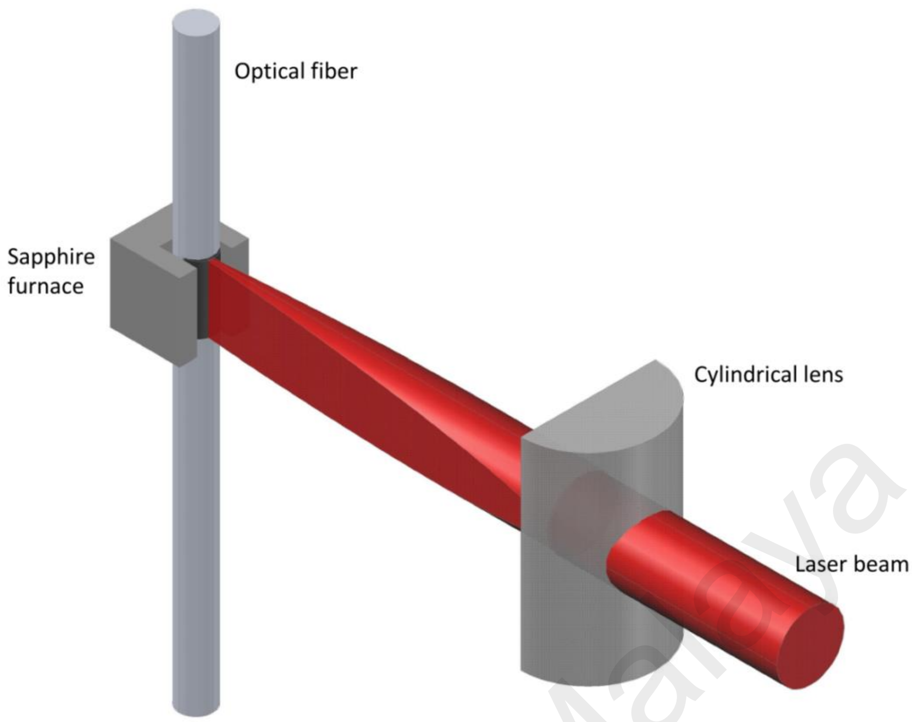

Figure 4.3 Illustrative diagram of CO_2 laser annealing setup.

The blue arrow in Figure 4.1 indicates the direction of the laser to the sapphire furnace. In the characterisation, the CO_2 laser was set at the power of ~7 W. A PS1250/1500 regenerated fiber Bragg grating (RFBG) was carefully translated (perpendicular to the direction of the laser) through the laser beam waist from the spatial position of −0.5 mm to 0.5 mm with reference to the focal point. Ten reflection spectra with a time interval of 10 s were recorded at every position to determine the average Bragg wavelength and standard deviation. The annealing temperature was estimated based on the thermal sensitivity and CO_2 laser-induced Bragg wavelength shift of the RFBG. Figure 4.4 (a) compares the thermal response of the RFBG at different spatial position in the laser annealing system with and without the assistance of a sapphire furnace.

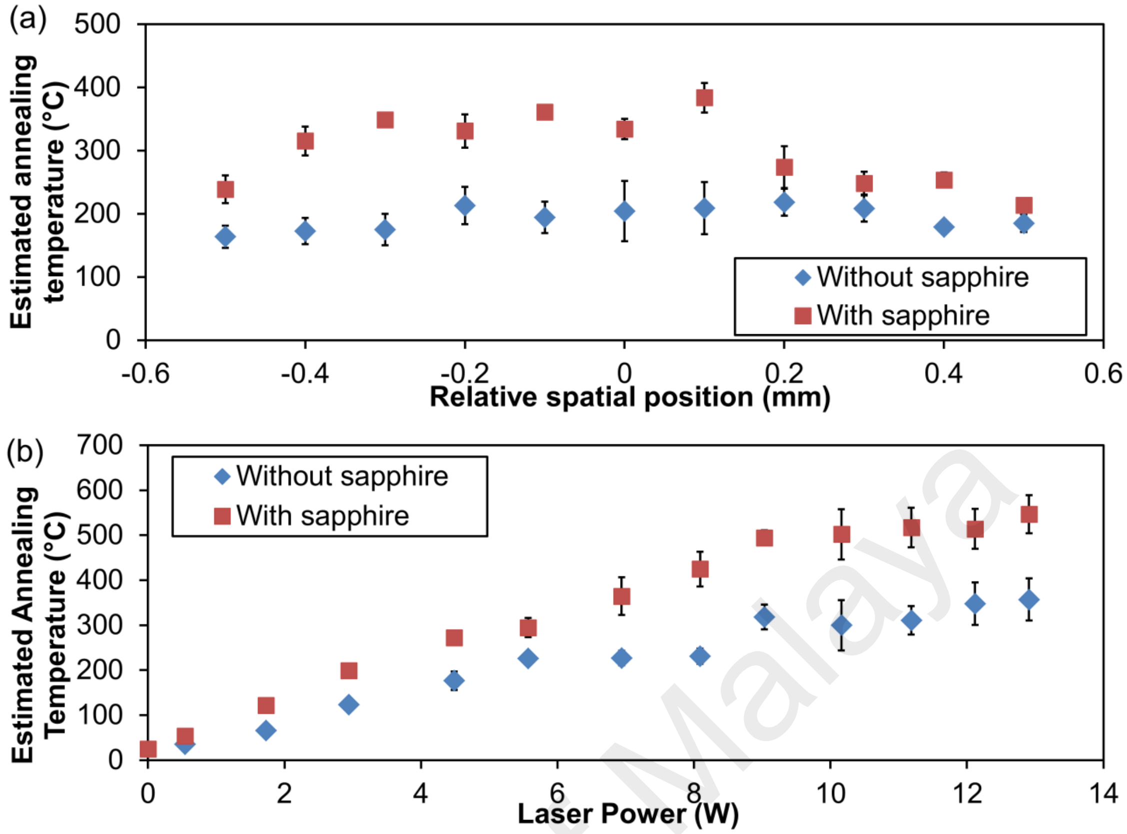

Figure 4.4 (a) Thermal response of the RFBG (PS1250/1500) scanning through beam waist of the focused CO_2 laser (b) The output response of RFBG (PS1250/1500) with increasing laser power with and without the assistance of sapphire furnace.

It was observed that the laser annealing with sapphire furnace yielded larger wavelength shifts than that without sapphire furnace. This indicates that the induced temperature on the RFBG is higher with the aid of the sapphire furnace. The average uncertainties in annealing temperature (σ / ΔT) is ~12.5 % for direct laser annealing without sapphire furnace and it is ~8.2 % for direct laser annealing with sapphire furnace. This finding indicates that sapphire furnace plays an important role in enhancing and stabilising annealing temperature on the grating. Therefore, the sapphire furnace was employed for laser annealing for the rest of this investigation. To optimize the efficiency of the laser annealing, RFBG was positioned at the centre of the laser beam where the intensity is maximum. This was achieved by positioning the RFBG where the shift in Bragg wavelength is the highest during the laser annealing treatment.

In the characterisation test with increasing laser power, the RFBG was positioned at the beam waist (determined from the optimum wavelength shift). The power of the CO_2 laser beam was ramped up from 0 W to 13 W, with a step size of 0.5 W. The Bragg wavelength of the RFBG was recorded after it stabilised for 2-3 minutes before the laser power was further increased. It was found that the annealing with sapphire furnace yielded higher estimated annealing temperature than that without sapphire as shown in Figure 4.4 (b). The temperature fluctuation grew larger with increasing laser power due to the large temperature difference between the irradiated region and ambient air. Figure 4.5 (a) presents the rapid thermal response of a grating written in PS1250/1500 fiber under the irradiation of a modulated ~4 W CO_2 laser, with a period of 1.5 s. The estimated annealing temperature from the Bragg wavelength shift is ~140 °C. The output spectra of the grating were analysed and recorded using a high speed FBG interrogation analyser (BaySpec) at a scanning rate of 10 Hz.

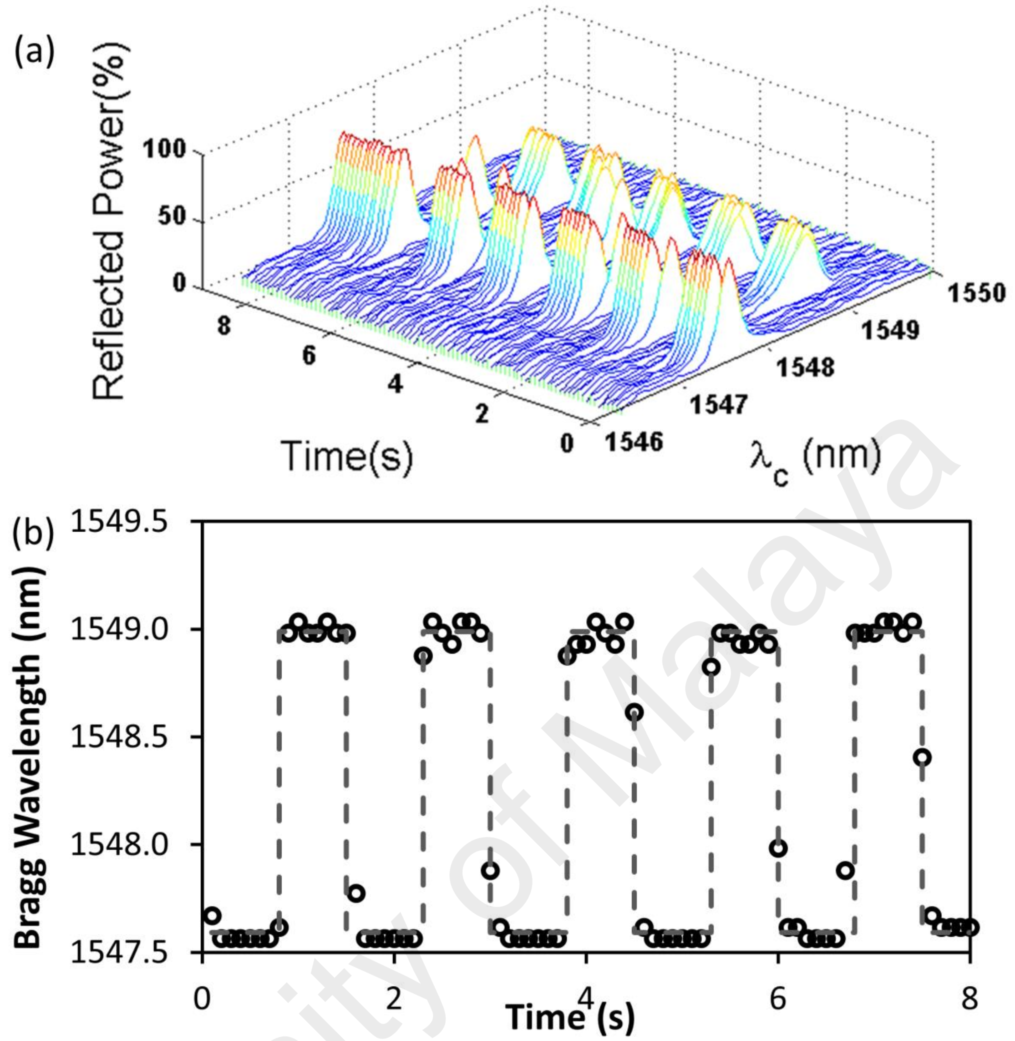

Figure 4.5 (a) The spectral response of grating and (b) variation of the Bragg wavelength under the irradiation of on-off CO_2 laser.

According to the results obtained, the variation of Bragg wavelength shift is in agreement with the CO_2 laser modulation. This shift of the Bragg wavelength indicates negligible thermal relaxation time constant of the glass fiber by the CO_2 laser irradiation. The fluctuation of the Bragg wavelength during heating (on-time) can be attributed to the small ambient air perturbation. Figure 4.5 (b) shows the Bragg wavelength variation to the modulated CO_2 laser. Similar study had been carried out for type II-IR grating under the irradiation of CO_2 laser. The results obtained from the hydrogen loaded type I grating were compared with the existing non-hydrogen loaded type II-IR grating and similar phenomenon was observed (Liao *et al.* 2009).

The temporal thermal response of the FBG towards the CO_2 laser annealing appeared to be independent from the laser power and final annealing temperature. The direction of CO_2 laser irradiation also plays a vital role in fiber annealing. Asymmetric annealing induces birefringence to the fiber due to non-uniform refractive index modification. The effect of axial asymmetry to the grating was studied by measuring the temporal thermal response to CO_2 laser irradiation while rotating the FBG in steps (Liao *et al.*, 2009).

4.3 Thermal Regeneration using CO_2 Laser Annealing Technique

The CO_2 laser annealing technique is deemed as an alternative solution for RFBG fabrication in which a CO_2 laser is used as heating source to replace the conventional furnace in the thermal regeneration process. In the investigation of thermal regeneration with CO_2 laser annealing, the power of CO_2 laser was increased in steps to escalate the annealing temperature (isochronal annealing). The annealing temperature was estimated based on the grating temperature sensitivity and its wavelength shift (correlation: ~0.997). The increment of the laser power was stopped when the peak power in reflection spectrum began to decrease rapidly. After the regeneration process, the laser was switched off and the reflection spectrum was recorded continuously until the spectrum completely stabilised. The recorded transmission spectra throughout the regeneration process were analysed. The time-varying reflected power, Bragg wavelength and transmitted power are plotted. Figure 4.6 shows the output response of a grating inscribed in PS1250/1500 photosensitive fiber under CO_2 annealing process.

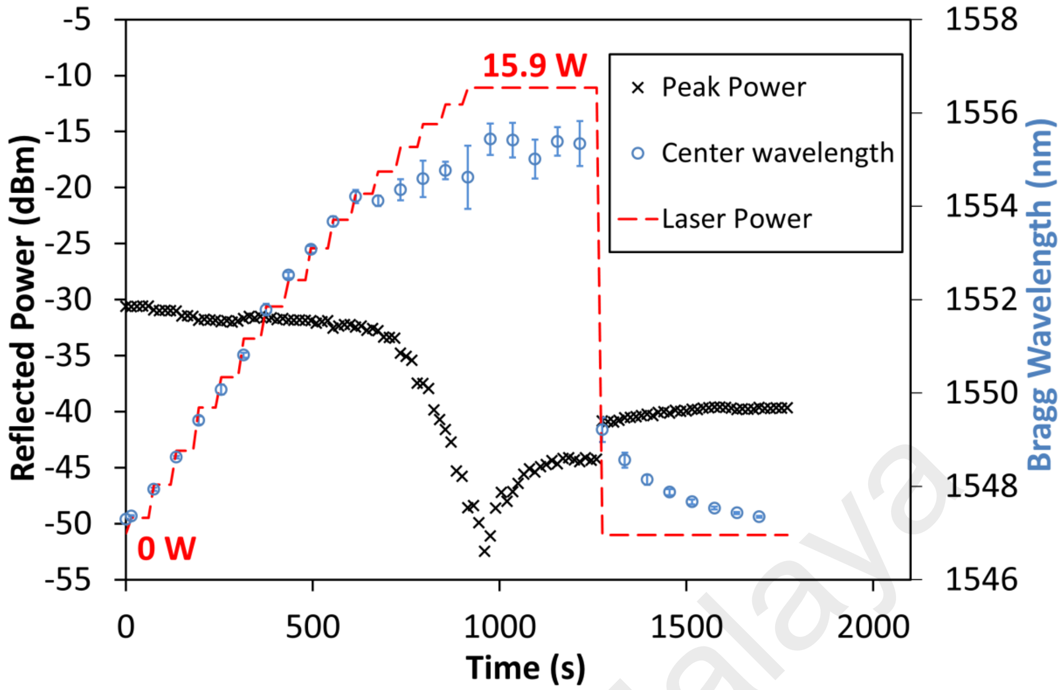

Figure 4.6 Output responses of a grating (PS1250/1500) during CO_2 laser annealing process. The laser power was incremented at rate of 1 W per minute until 15.9 W.

During the regeneration process, it was observed that the maximum wavelength shift of the RFBG in PS1250/1500 fiber that corresponds to a laser power of 15.9 W was ~8 nm. The estimated irradiation intensity of CO_2 laser on the fiber was ~1272 Wcm^{-2}. There was an agreement between the wavelength shift and laser power when the power was elevated from 0 to 13 W. The Bragg wavelength began to fluctuate and the grating peak power plummeted after 13 W, this was when the induced temperature on the grating was approaching the regeneration temperature. The grating peak power decayed rapidly until it dropped to its minimal value. Shortly after that, a new reflection peak emerged from the noise level and the grating peak power increased continuously. The CO_2 laser was turned off after the reflectivity of the regenerated grating stabilised. After regeneration process, the peak power has dropped by ~10 dB as shown in Figure 4.7. The drop in the side lobes' power in reflection spectrum indicated that the grating strength had decayed.

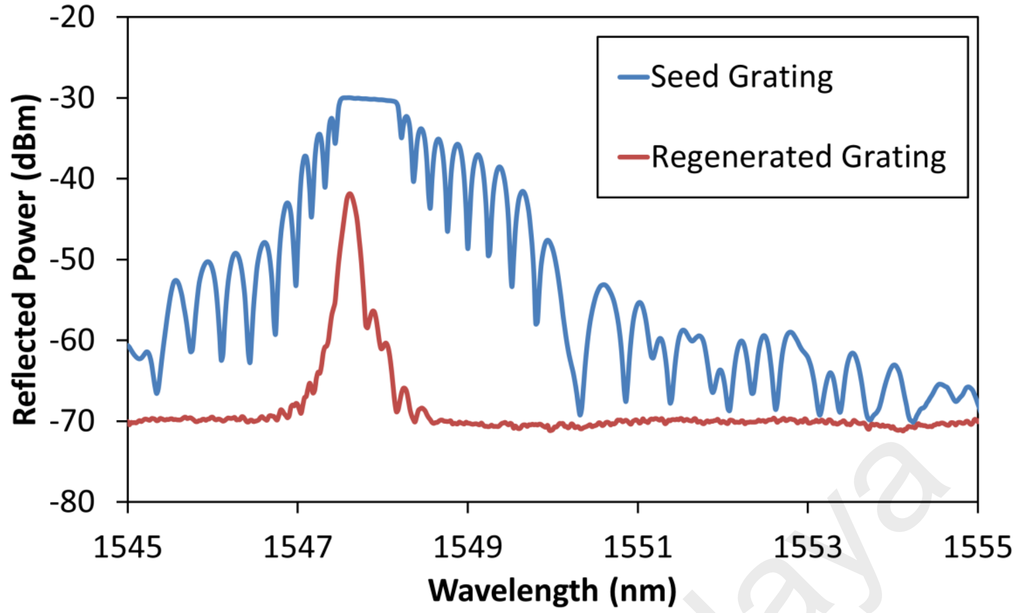

Figure 4.7 The reflection spectra of the grating (PS1250/1500) before and after regeneration process.

At the power of 15.9 W, the estimated temperature at the irradiated grating was ~730 °C which was higher than the regeneration temperature of the fiber. The CO_2 laser power was incremented at the rate of 1 W per unit time, which ranges between 15 s and 90 s. In addition, an isothermal annealing process was carried out on a PS1250/1500 fiber and the wavelength responses of the gratings are presented in Figure 4.8 for comparison purpose.

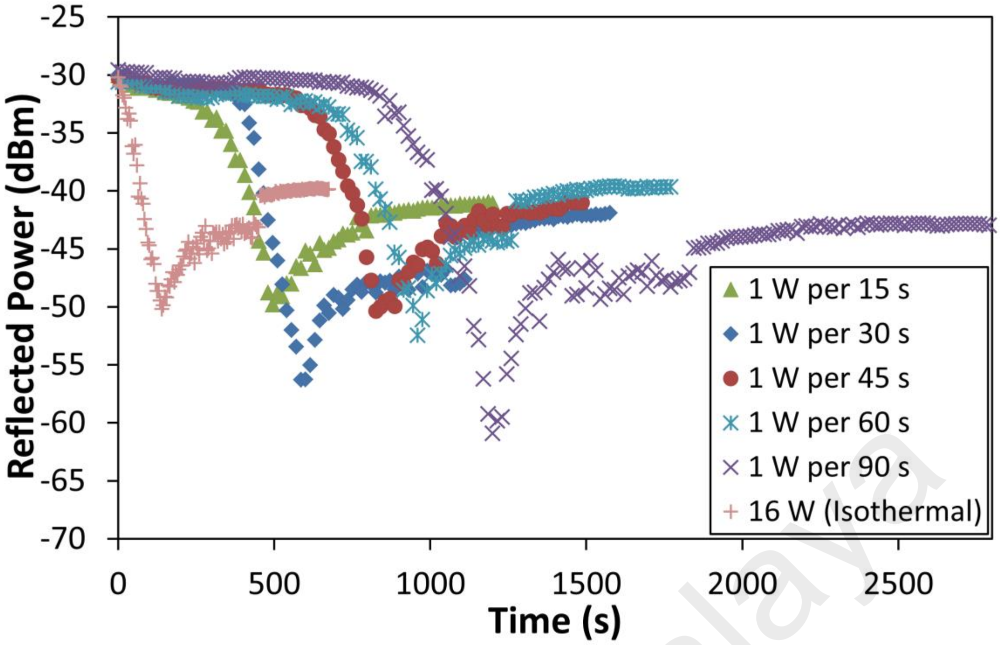

Figure 4.8 The regeneration process of the grating (PS1250/1500) at different heating rates.

All gratings show similar thermal response during thermal regeneration process using CO_2 laser annealing. The grating started to decay continuously at regeneration temperature until it dropped to its minimal value, followed by a progressive regeneration of reflection peak. During the isothermal annealing, the grating was directly irradiated by a focused laser beam with a constant power of ~15.9 W until the regeneration process was completed. The developed regenerated grating based on isothermal annealing shares similar performance as that of produced based on isochronal annealing. According to Figure 4.6 and Figure 4.8, there is a continuous fluctuation in the peak power during regeneration. This effect can be seen as a result of the residual stress relaxation induced rearrangement of glass structure and temperature fluctuation during high temperature annealing process. Moreover, since CO_2 laser annealing was carried out in an open environment, the ambient air turbulence might disrupted the annealing temperature. Gaussian-like beam shape might induced spectral chirping of the grating which led to peak power fluctuation during the regeneration process. When the grating was inscribed onto the core of the fiber, ultraviolet (UV) irradiation induced a chemical reaction between the hydrogen molecules and oxygen atoms in the silica glass and produced hydroxyl ions which relaxed the residual frozen stress in the fiber glass. The glass density at processed region increased after the exposure to UV irradiation (Douay *et al.*, 1997). This difference in residual stress between processed and unprocessed regions introduced a residual elastic stress between these two regions (Fonjallaz *et al.*, 1995). During the CO_2 laser annealing for PS1250/1500 fiber, UV induced stress between these processed and unprocessed regions had been relaxed (Yablon, 2004). However, since the intensity profile of the CO_2 laser beam took the form of a Gaussian distribution, every region of the grating experienced a slightly different annealing temperature. Therefore, different location positions of the grating were annealed at different rates. The centre part of the grating which received higher CO_2 laser intensity was treated at a faster rate compared to both ends of the grating. As the result of stress relaxation, the treated part of the grating had slight higher refractive index and longer Bragg wavelength. This can be observed from the two reflection peaks in Figure 4.9 (the spectra are offset in the y-axis direction for better clarity in presentation). The peak at the longer wavelength is contributed by the treated part of the grating.

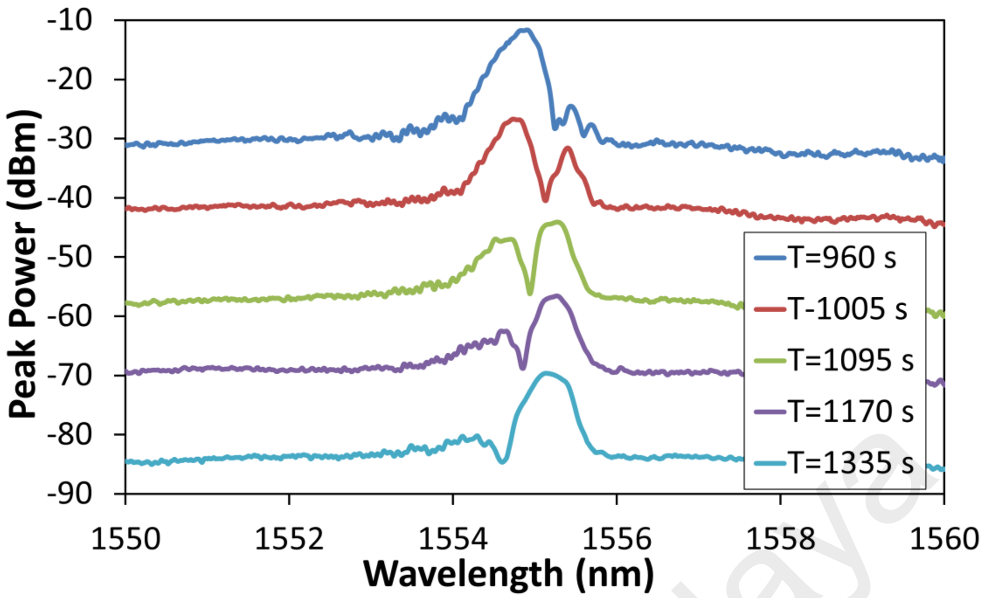

Figure 4.9 The evolution of reflection spectra during regeneration process of the grating (PS1250/1500).

4.4 Thermal Stability Enhancement

In this section, the thermal stability enhancement in FBG based on CO_2 laser pre-treatment is discussed. The FBG in PS1250/1500 fiber was used as the subject for the investigation of thermal stability enhancement. The fiber was irradiated by a 15 mm long vertical sheet beam with increasing power from 0 W to 14.4 W at an increment rate of 0.18 W/s (Detailed experimental setup is presented in Section 4.1). The annealing scheme used was isochronal annealing (Figure 3.7) with a 5 min dwelling time between each ramping step. Afterwards, the fiber was slowly cooled down to room temperature by reducing the laser power at a rate of 0.09 W every 10 s. After CO_2 laser treatment, hydrogen photosensitisation treatment was carried out on the treated and non-treated fibers at 1800 psi for 10 days. Subsequently, 10 mm long FBGs were inscribed on both types of fibers using argon fluoride (ArF) excimer laser. The fibers were irradiated by 8 mJ of UV laser beam at a repetition rate of 1 Hz until a grating with reflectivity of ~40 dB was formed. The transmission spectra of the fibers were recorded continuously using

OSA controlled by a LabVIEW program via a General Purpose Interface Bus (GPIB) interface. After the grating inscription process, all produced FBGs were annealed in an oven at 80 °C for 8 hours to remove the residual hydrogen (H_2) from the fibers.

The refractive index changes in the fiber core for both CO_2 laser treated and non-treated fibers during the FBG inscription process are presented in Figure 4.10.

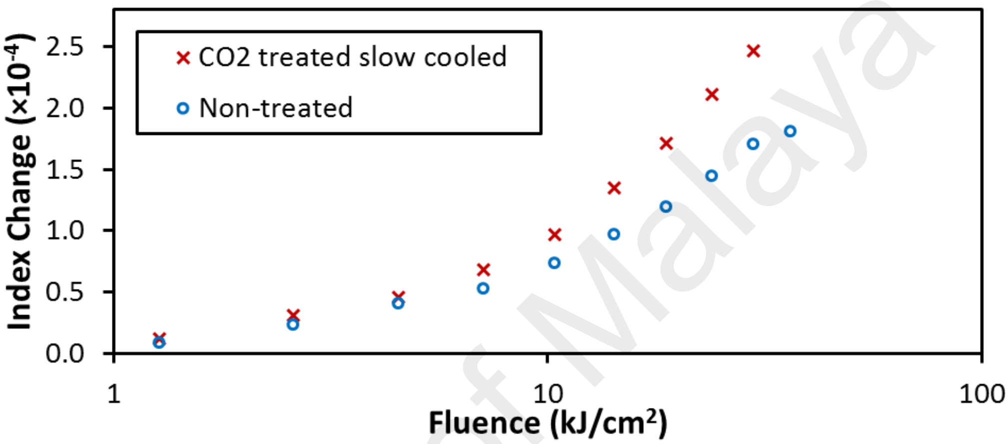

Figure 4.10 The growth of UV-induced refractive index change of CO_2 laser treated and non-treated fiber during FBG inscription using ArF excimer laser.

It was observed that the CO_2 laser treated fiber showed a higher refractive index change at higher UV fluence compared to that in non-treated fiber. The refractive index change is calculated using the following formula

$$\Delta n_{\mathrm{mod}} = \frac{\lambda_C(F)\tanh^{-1}(\sqrt{R})}{\eta\pi L} \qquad \textbf{(4.1)}$$

where $\lambda_c(F)$ is the Bragg wavelength which is a function of the cumulated UV fluence, R the reflectivity of the FBG, η the mode overlap parameter and L the FBG length. The mode overlap parameter can be expressed as

$$\eta = \frac{\pi^2 d^2 k^2}{\lambda^2 + \pi^2 d^2 k^2} \qquad \textbf{(4. 2)}$$

where d, k and λ indicate the fiber core diameter, the numerical aperture (NA) of the fiber and Bragg wavelength respectively. The photosensitivity enhancement after CO_2 laser irradiation is due to the increment of germanium oxygen-deficient centre (GODC) population (Brambilla *et al.*, 1999). These defects which can be bleached only at high UV fluence provide the supportive proof of the occurrence of multiphoton absorption during FBG inscription using ArF excimer laser.

The thermal stability test was carried out using high temperature tube furnace (Figure 3.6). Both types of fibers were annealed from 25 °C to 100 °C in 5 min. The annealing temperature was held constant for 3 hours before it was further increased to 200 °C and 300 °C. Similarly, the annealing temperature was held constant at 200 °C and 300 °C for 3 hours. The transmission spectra of the FBG were recorded continuously using an OSA. The Bragg transmission depth (BTD) of the FBG is analysed and presented in Figure 4.11. Furthermore, the thermal degradation of the CO_2 laser treated FBGs was examined at 100 °C, 150 °C and 250 °C. The result is presented in Figure 4.12.

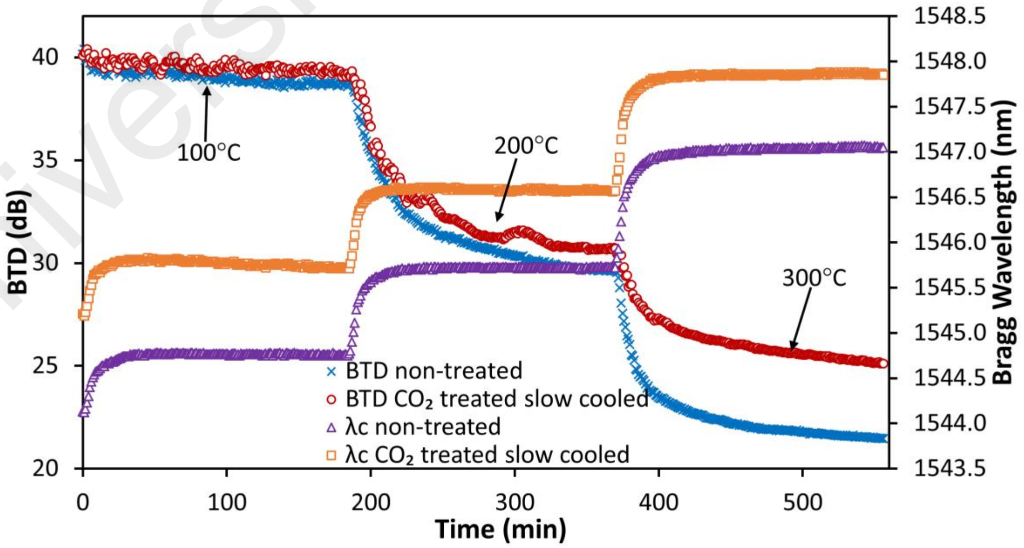

Figure 4.11 The variations of BTD and Bragg wavelengths of the CO_2 laser treated and non-treated FBGs at 100 °C, 200 °C and 300 °C.

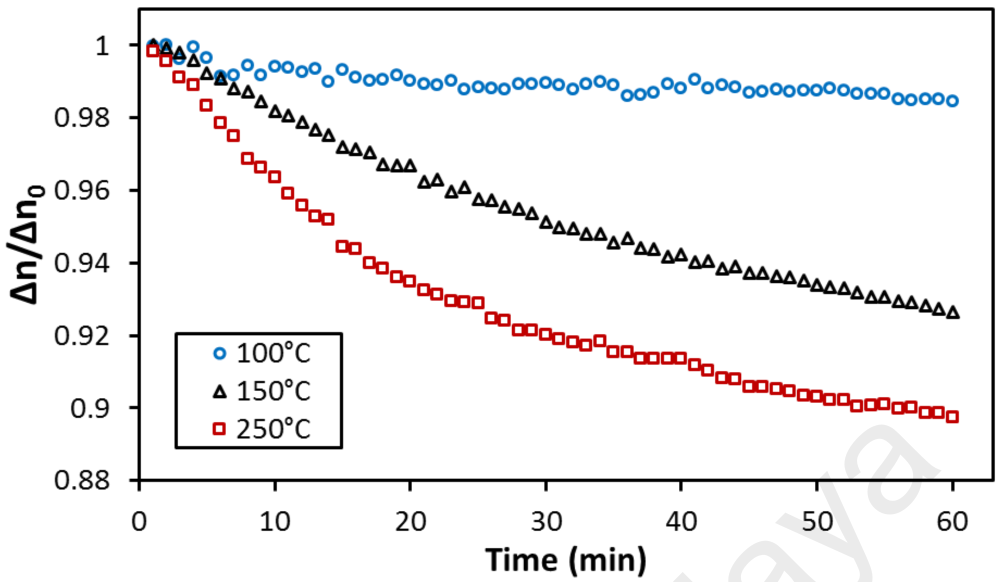

Figure 4.12 The thermal degradation of refractive index modulation ratio for CO_2 laser treated FBG at 100 °C, 150 °C and 250 °C. $\Delta n/\Delta n_0$: Refractive index modulation ratio.

In Figure 4.11, the BTD for both treated and non-treated FBGs show similar trend of progression at 100 °C and 200 °C. However, at 300 °C the non-treated FBG decayed more than the treated FBG. The BTD of the non-treated FBG is ~4 dB lower than the treated FBG after 3 hours of isothermal annealing at 300 °C. Besides that, the Bragg wavelength of the treated FBG is ~1 nm longer than that in non-treated FBG at every annealing temperature condition. This is due to the stress relaxation happened during the CO_2 laser annealing and the subsequent slow cooling process. The reduction of the thermal stress in the fiber core led to red-shift in the Bragg wavelength. Figure 4.12 presents the evolution of the normalized refractive index modulation ratio = (Instantaneous refractive index modulation, Δn)/(Initial refractive index modulation, Δn_0), at different annealing temperature. The treated FBG has highest stability at 100 °C in which the refractive index modulation ratio decreased for ~1 % after 1 hour of annealing. In comparison, the refractive index modulation ratio is decreased for ~8 % and ~10 % after annealing at 150 °C and 250 °C respectively for 1 hour. In conclusion, the thermal stability enhancement using CO_2 laser annealing technique is very useful for the fabrication of grating components with long lifespan, particular important for the operation in high temperature environment.

4.5 Summary

Thermal regeneration and thermal stability enhancement of FBG based on CO_2 laser annealing has been successfully demonstrated. In the investigation with FBG inscribed in PS1250/1500, thermal regeneration using CO_2 laser annealing at different heating rate have been investigated. It was observed that the thermal responses of the gratings during regeneration shared similar characteristics to that produced using conventional method (hot furnace). Under isothermal annealing using CO_2 laser, thermal regeneration can be completed within ~12 minutes. In conclusion, CO_2 laser offers the advantages of dynamic control in heating and cooling, as well as flexibility in the beam manipulation which enables the heating to be applied in a small and more focused area on the grating region. In addition, the CO_2 laser annealing was used for the thermal stability enhancement on FBGs (PS1250/1500). The results show that CO_2 laser treated FBG has higher photosensitivity within the vicinity of ~193 nm and lower reflectivity degradation at high temperature. The refractive index modulation ratio of the CO_2 laser treated FBG is reduced by ~1 %, ~8 %, ~10 % after annealing at 100 °C, 150 °C and 250 °C respectively for 1 hour. At annealing temperature of 300 °C, non-treated FBG showed greater degradation in reflectivity than the treated FBG by ~4 dB after 3 hours. CO_2 laser annealing is useful for enhancing the thermal stability of FBGs and prolonging their lifespan in high temperature environment.

CHAPTER 5: THERMAL STRESS AND BIREFRINGENCE MODIFICATION

The characteristic of the glass material is defined by its viscosity at different temperature. The strain point of the glass is defined as the temperature at which the viscosity of the glass equal to $10^{14.5}$ poises. At any temperature below this point, no permanent strain (and hence thermal stress) can be introduced to the glass. In addition, beyond the glass transition temperature (T_g) (viscosity $=10^{13}$ poises), atomic diffusion in the treated glass is sufficiently fast and any residual stresses can be removed within ~15 min. Thermal stress can be completely removed if the glass is uniformly heated under controlled conditions followed by cooling process at sufficiently slow rate (Ojovan, 2008; Callister & Rethwisch, 2008). The T_g and the volume of the glass are affected by the cooling process after annealing at elevated temperature (Ojovan, 2008; Brückner, 1970; Moynihan *et al.*, 1974; Yablon, 2004). Silica glass that is cooled at a slower rate has lower T_g and smaller volume compare to that of rapidly cooled. This can be attributed to the rearrangement of molecular structure of the glass matrix that takes place in the system that is slowly losing their kinetic energy. Rapid cooling from annealing temperature introduces more free volume in the molecular structure. In another words, less compaction in volume can be achieved with rapid cooling. However, this effect is reversible by reheating and then cooling at a slower rate.

In the fiber, thermal stress is built up in the fiber core and cladding due to the difference of thermal expansion coefficients (TEC) between the two regions. Generally, doped fiber core has higher TEC, lower viscosity and lower T_g than fiber cladding. During the drawing process, the cladding glass will solidify at a much higher temperature and hence earlier than the doped core glass. The liquid core will experience substantial thermal contraction as it cools. The constraint by the surrounding solidified cladding leads to the hydrostatic tension in fiber core at room temperature after drawing process (Krohn, 1970; Scherer & Cooper, 1980; Krohn & Copper 1969). The relationship between the axial thermal stress σ_z at the centre of fiber core, TEC difference between core and cladding, β and T_g is given by

$$\beta = \frac{1+\upsilon}{1-\upsilon}\left(\alpha_{core} - \alpha_{clad}\right) \qquad \textbf{(5.1)}$$

$$\sigma_z = -\frac{E\beta T}{1+\upsilon}\left(1-\frac{a^2}{b^2}\right) \qquad \textbf{(5.2)}$$

where $T = T_g - T_{ambient}$ is the difference between the transition temperature T_g and the ambient temperature, and α_{core} and α_{clad} are the TECs of the core and cladding, respectively. E is the Young's modulus of the fiber glass, and υ is the Poisson's ratio. a and b are the radii of core and cladding, respectively (Lim *et al.*, 2013). Equation (5.2) suggests that σ_z can be modified through manipulation of T_g by annealing at temperature above T_g followed by a specific cooling process.

Carbon dioxide (CO_2) laser annealing is well known for mechanical stress relaxation in optical fibers (Kim *et al.*, 2001). The annealing was achieved via radiative absorption of the laser intensity and heat generation in the irradiated fiber glass. The induced temperature on the target sample can be controlled by manipulating the intensity of the laser. Laser-annealing technique was also employed for long period grating (LPG) fabrication in which a focused laser beam was used to create periodical index modulation along a fiber.

The stress in polarisation maintaining fiber (PMF) due to the dopant concentration difference between each region in the fiber cross section induced birefringence (Chu & Sammut, 1984). The birefringence of stress-applied PMF can be described by Equations (2.5) and (2.6) in section 2.5.

In this chapter, the modifications of thermal stress and birefringence in regenerated fiber Bragg grating (RFBG) using CO_2 laser annealing treatment are demonstrated and discussed.

5.1 Thermal Stress Modification

Thermal stress in the optical fiber can be easily modified by using CO_2 laser annealing with different cooling process. Thermal stress modification process requires high temperature annealing which exceeds the glass transition temperature of the silica glass. In this section, thermal stress modification in a RFBG based on CO_2 laser annealing technique is discussed.

In the investigation, RFBG was used as the subject for the experiment because of its high temperature stability. The power of the CO_2 laser was controlled using a computer program to achieve the desired heating and cooling rates as well as the dwell time. The interface of the program is shown in Figure 5.1.

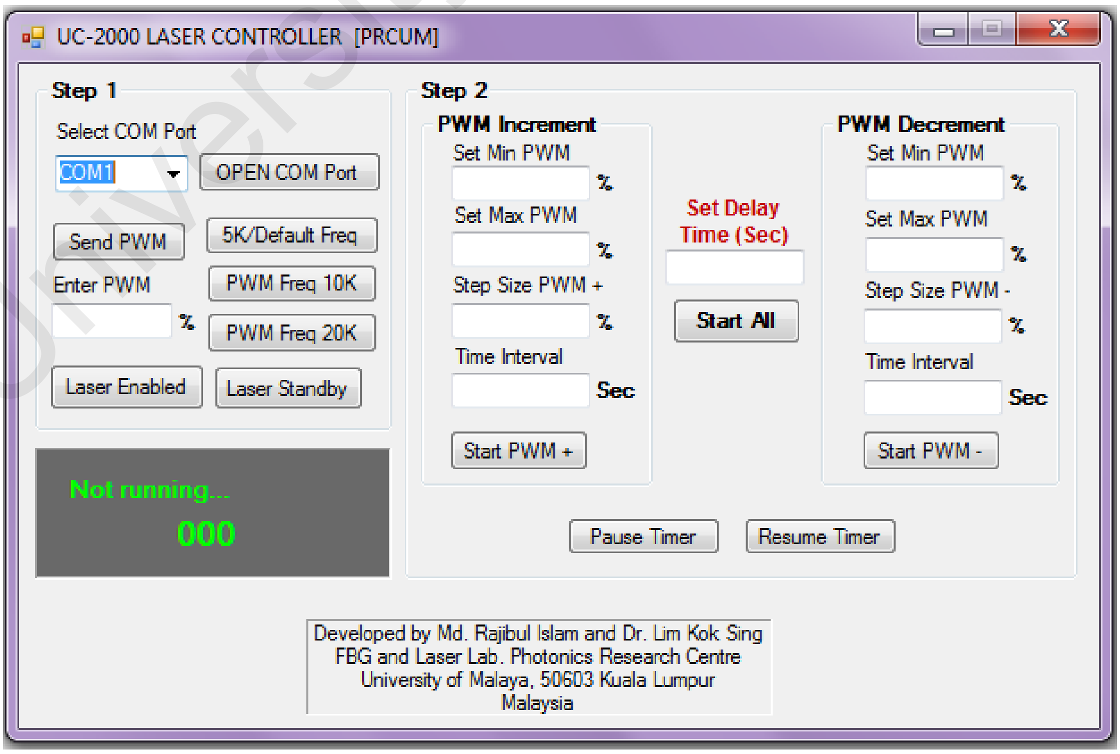

Figure 5.1 The interface of the program for CO_2 laser controlling.

During the annealing treatment, the irradiated laser power on the RFBG (PS1250/1500, fabricated in chapter 3.3.2) was increased at a rate of 1 W for every 15 s until the max power of 16 W was reached. Based on the Bragg wavelength shift of ~7.8 nm and calibrated temperature sensitivity of the RFBG, 10.6 pm/°C, the induced annealing temperature (T_a) on the RFBG is estimated to be ~760 °C. The T_a was deliberately set at a point between the glass transition temperature ~500 °C and regeneration temperature ~850 °C of boron-germanium (B/Ge) co-doped fiber (Bueno *et al.* 2013; Croswell *et al.* 1999; Wang *et al.*, 2013), to ensure the induced temperature was sufficiently high for structural relaxation in the core glass without degrading the grating strength of the RFBG. After 2 min of isothermal annealing, two different cooling approaches, namely slow cooling and rapid cooling, were investigated. For slow cooling, the laser power was reduced at the rate of~0.1 W per 15 s and the equivalent temperature reduction rate was ~4 °C per 15 s, whereas for rapid cooling, the laser power was rapidly reduced to zero by switching off the laser. Figure 5.2 (a) shows the wavelength response of the RFBG (blue curve) undergoing a series of annealing treatment. The wavelength response is in accordance to the programmed laser power denoted by the black curve in the Figure 5.2 (a).

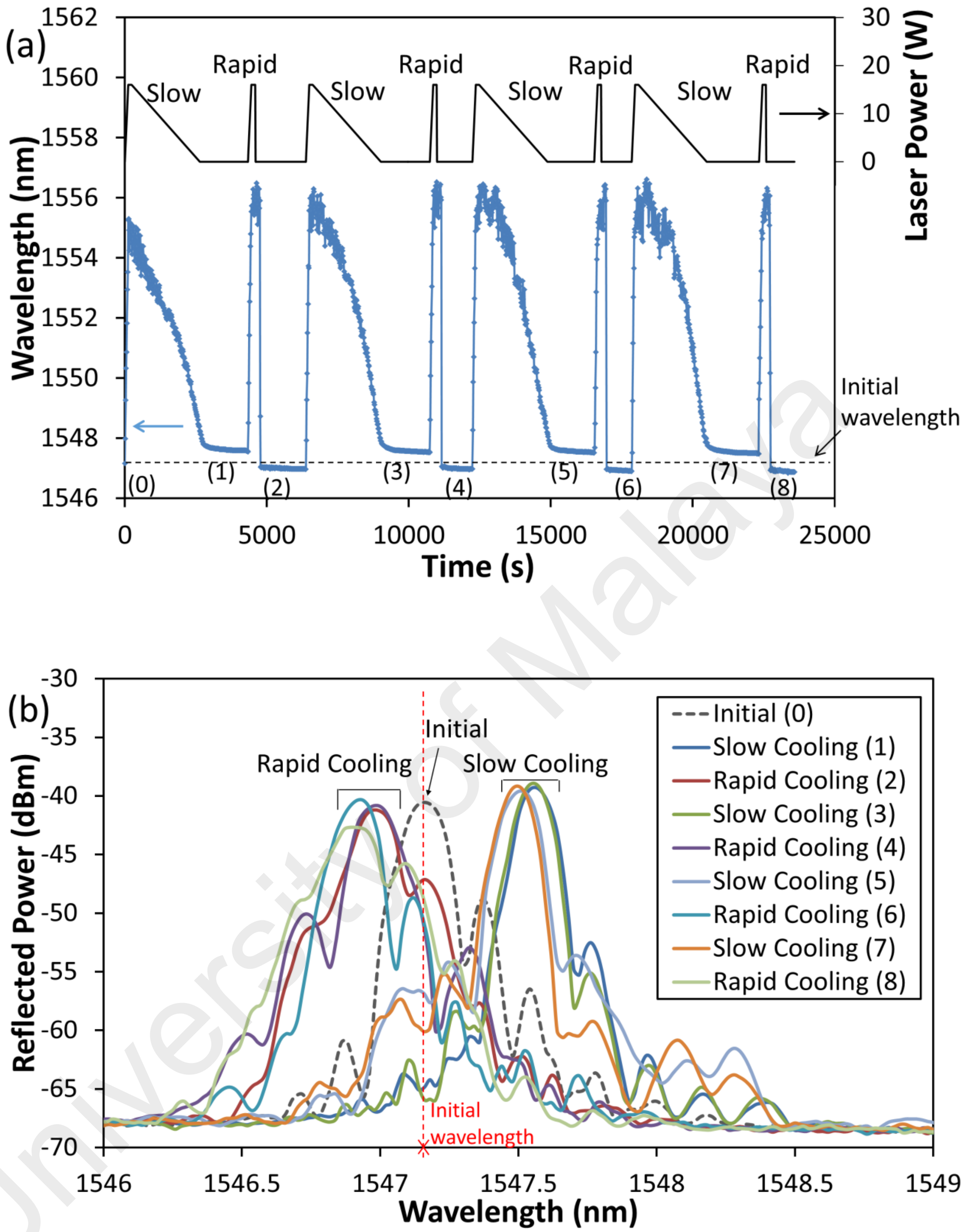

Figure 5.2 (a) Reflection wavelength of RFBG (PS1250/1500) treated by CO_2-laser radiation annealing with different cooling processes. (b) The reflection spectra of the RFBG correspond to the steady states (0)–(4) in (a).

In the first circle of treatment, the slow cooling process was implemented after 2 min of isothermal annealing. The Bragg wavelength was red-shifted from the initial wavelength of 1547.16 nm [denoted as (0) in Figure 5.2 (a)] to 1547.55 nm [at steady state (1)] after the treatment. It is worth noting that the RFBG has never been treated with laser annealing before state (0). In the second circle of treatment, the same annealing process was performed but it ended with a rapid cooling process. This time, the Bragg wavelength was blue-shifted [at (2) in Figure 5.2 (a)] in respect to the reference Bragg wavelength. Similarly, red-shift was observed after the ensuing treatments with slow cooling at (3), (5), (7) and then blue-shift after rapid cooling at (4), (6), (8). For the ease of comparison, the corresponding reflection spectra at steady states (0)–(4) are presented in Figure 5.2 (b). Slow cooling process has provided sufficient time for structural relaxation of the glass in low viscosity condition. As a result, the T_g of the fiber core was reduced. Decrement in T_g led to the reduction of both thermal stress (refer Equation 5.2) and negative stress-induced index change in the fiber core. This explains the red-shift of Bragg wavelength after the slow-cooling process. On the other hand, the T_g of the core glass was increased after rapid cooling process. Structural relaxation in core glass has been denied by the rapid cooling. As the result, greater thermal stress and negative stress-induced index change were induced in the fiber core. Thus, the Bragg wavelength was blue-shifted. In addition to the above analysis, the observations in Figures 5.2 (a) and (b) also indicate that the modification of thermal stress by means of T_g manipulation is reversible and repeatable. The Gaussian profile of CO_2 laser beam might produce a non-uniform distribution of T_g and spatially variant stress-induced index change along the treated grating structure. The greater the laser power reduction rate, the larger is the difference in cooling rates at different local points along the irradiated region. This effect is particularly obvious with rapidly cooling, and it explains the slightly broader reflection curves of rapidly cooled RFBG [see Figure 5.2 (b)]. The 15 dB-bandwidths of the RFBG after slow and rapid cooling processes are ~0.34 nm and ~0.67 nm, respectively. Slow cooling process provides a rather uniform treatment, and the T_g-distribution is more homogeneous along the irradiated region. The bandwidth of the slowly cooled RFBG has smaller reflection bandwidth. It is believed that the residual frozen-in mechanical stress induced by fiber drawing and ultraviolet (UV)-induced stress (UV densification) in the fiber has already been greatly reduced to a minimum level during the earlier thermal regeneration process (Yablon, 2004; Kim *et al.*, 2001; Dürr *et al.*, 2005; Kim *et al.*, 2002). Hence, it is reasonable to assume that thermal stress is the major contributor to the wavelength shift in the laser annealing treatment. Based on the Bragg wavelength shift of the RFBG after different cooling processes, the change of effective refractive index and the stress condition in the fiber can be described by the following equations:

$$\Delta n_T = n_{eff}\left(\frac{\lambda_a}{\lambda_b} - 1\right) \qquad \textbf{(5.3)}$$

$$\Delta \sigma_z = \left(\frac{2\Delta n_T}{3C_2 + C_1}\right) \qquad \textbf{(5.4)}$$

Δn_T is the change in effective refractive index, n_{eff} is the effective refractive index, λ_b and λ_a represent the Bragg wavelengths before and after a treatment, and $\Delta\sigma_z$ is change in axial thermal stress. Stress optic coefficients C_1: 4.102×10^{-5} mm^2/kg, C_2: 7.42×10^{-6} mm^2/kg (Lim *et al.*, 2013).

Based on the wavelength shifts presented in Figure 5.2 (b), the corresponding changes of thermal stress in the treated RFBG are estimated and as shown in Figure 5.3. Negative thermal stress change indicates that the thermal stress in RFBG had been relaxed during the slow cooling process, whereas positive stress changes indicate that larger thermal stresses have been developed in the core due to high T_g induced after the rapid cooling processes.

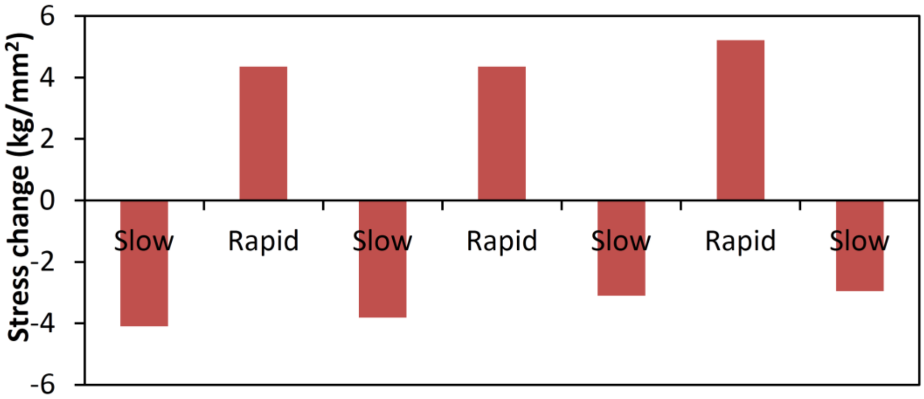

Figure 5.3 Changes in thermal stresses in the fiber core of the RFBG under a series of annealing treatments with alternating slow–rapid cooling processes.

The strain temperature of the cladding glass (fused silica) is ~1070 °C (Callister & Rethwisch, 2008), which is higher than the T_g of the core glass. It is beyond the regeneration temperature of the RFBG and the achievable T_a by the CO_2 laser in this investigation. Concerning the laser annealing treatment on RFBG at ~760 °C in Figures 5.2 and 5.3, it is reasonable to state that the structural relaxation is limited to the core but not the cladding. Figure 5.4 shows the output spectra of the RFBG treated at different annealing temperatures, T_a ~300 °C, ~700 °C, and~830 °C.

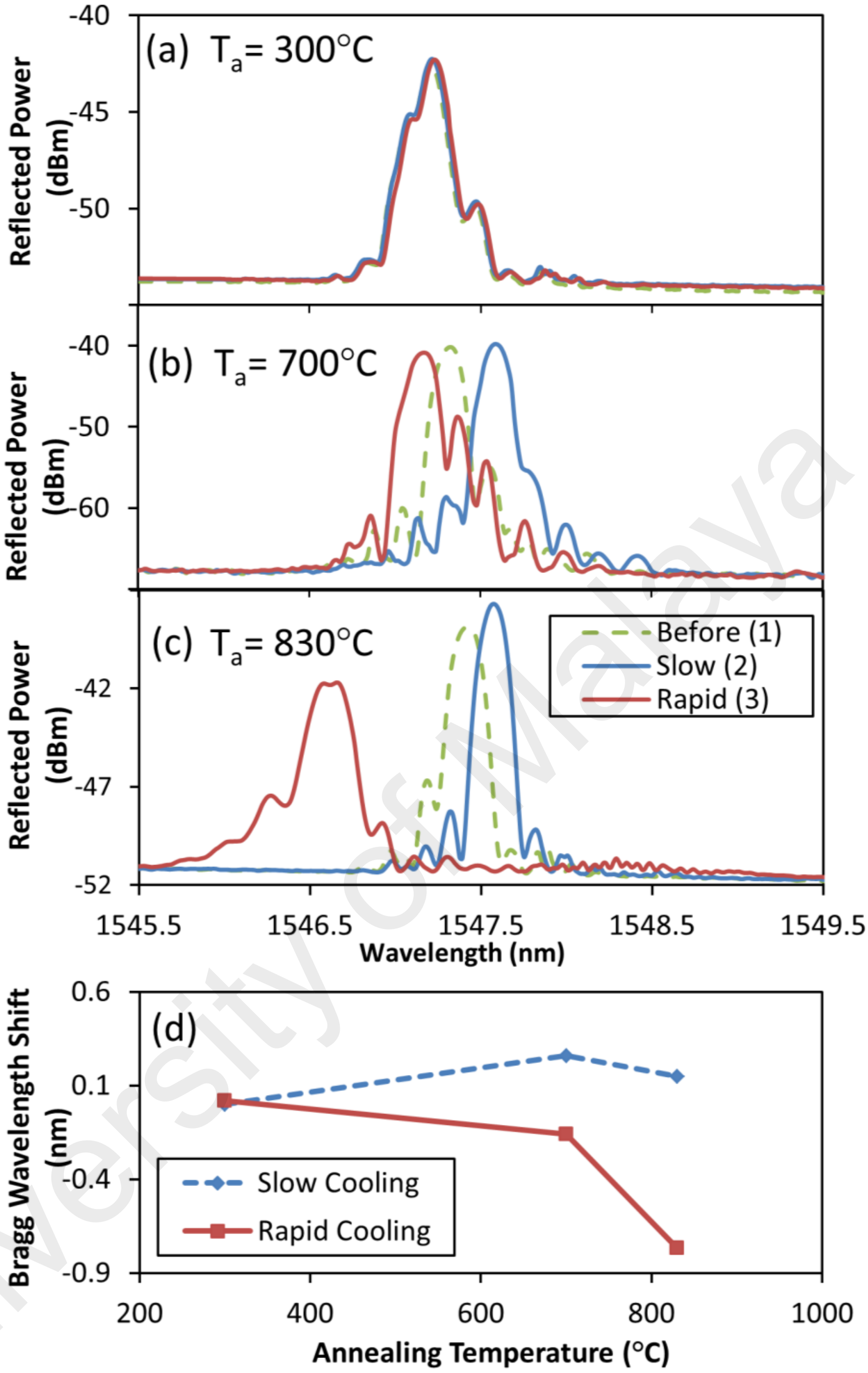

Figure 5.4 Bragg wavelengths at room temperature after annealing at T_a of (a) ~300 °C, (b) ~700 °C, (c) ~830 °C, followed by slow and rapid cooling processes to room temperature. The numbers in the parentheses indicate the sequence of the treatments. (d) Relation between wavelength shifts and T_a.

An isothermal annealing for 5 minutes had been implemented before the cooling process. For $T_a < T_g$, there was no significant shift in Bragg wavelength after annealing process [see Figure 5.4 (a)]. Apparently, the core glass was still at the highly viscous state, and thermal relaxation did not happen at this temperature. On the other hand, wavelength shifts were observed after the annealing and cooling processes at the temperature of T_a ~700 °C, higher than the T_g of RFBG [see Figure 5.4 (b)]. Larger blue shift in Bragg wavelength was observed when higher T_a (~830 °C) was adopted in conjunction with the rapid cooling process [red curve in Figure 5.4 (c)]. The relation between wavelength shifts and T_a is shown in Figure 5.4 (d). The difference in Bragg wavelengths induced by two different cooling processes may lead to inaccurate temperature measurement if the detail of the previous cooling process is unknown. Based on the temperature sensitivity of 10.6 pm/°C, the wavelength difference of ~0.96 nm in Figure 5.4 (c) could potentially lead to a misinterpretation and measurement error of ~91 °C. The finding in this investigation has proven the reversibility and repeatability of thermal stress modifications in the fiber core by different cooling rates. The knowledge of thermal stress modification and stochastic behaviour of RFBG in dynamic and high temperature environment should be considered in the design and handling of this device.

5.2 Birefringence Modification

Thermal stress modification by annealing can lead to the birefringence modification in PMF. This is because the stress applying part (SAP)-induced thermal stress in the fiber core has been modified after the annealing treatment. In this section, modification of birefringence in a regenerated grating inscribed in polarisation maintaining fiber (RGPMF) based on post- CO_2 laser annealing treatment is demonstrated and discussed.

First, a RGPMF (PS-PM980) was fabricated by using a high temperature furnace based on the annealing procedure presented in Chapter 3.3.3. After that, the fabricated RGPMF was used in the investigation birefringence modification by CO_2 laser annealing with a sapphire mini furnace. The details of laser power increment and decrement rates, isothermal annealing laser power and time used in the investigation are tabulated in Table 5.1. The estimated temperature in Table 5.1 was determined using a thermocouple. During the CO_2 laser annealing process, the sensing probe of the thermocouple was placed directly in contact with the sapphire mini furnace to measure its current temperature. The estimated annealing temperature shown in Table 5.1 is the calibrated data from the thermocouple. Two annealing treatments were carried out using RGPMF. In the first annealing experiment, a treatment cycle of F1-F2-F3-F4-F5 was performed. This treatment sequence was used to investigate the annealing power dependence of birefringence variation in RGPMF. In the second annealing treatment, a sequence of F5-S1-F5-S2-F5-S3-F5-S4 was carried out and the cooling rate dependency of birefringence in RGPMF was investigated.

Table 5.1 Summary of CO_2 laser annealing treatments.

Treatment	Laser power increme nt rate (%/s)	Relative annealing power (%) / estimated temperature (°C)	Annealing time (min)	Laser power decrement rate
F1	1	20 / ~163	5	20 % /s
F2	1	40 / ~302	5	20 % /s
F3	1	60 / ~421	5	20 % /s
F4	1	80 / ~520	5	20 % /s
F5	1	95 / ~581	5	20 % /s
S1	1	95 / ~581	5	0.5 % /s
S2	1	95 / ~581	5	0.5 % /3 s
S3	1	95 / ~581	5	0.5 % /10 s
S4	1	95 / ~581	5	0.5 % /30 s

The slow cooling process leads to volume contraction in the SAPs at room temperature, thus increasing the stress induced birefringence in the fiber core (Ourmazd *et al.*, 1983). When the RGPMF was annealed with a high power CO_2 laser, the stress relaxation occurred in SAP before fiber core. Referring to Equation (2.5), different cooling rates altered $T_{g(SAP)}$ and TEC of SAP, hence modifying the birefringence of RGPMF. The observation of higher birefringence in RGPMF induced by slower cooling rate, indicates that the product of ΔT and the difference of TEC between cladding and SAP had increased as well (Equation (2.5)). However, the slower cooling process lowered the $T_{g(SAP)}$ (Ourmazd *et al.*, 1983). Apparently, the influence of TEC change in SAP to the birefringence by different cooling rates is greater than that of $T_{g(SAP)}$.

Figure 5.5 shows the reflection spectrum and birefringence change with different annealing laser power and cooling rate. Figures 5.5 (a) and (c) show that the birefringence of RGPMF decreases with increasing annealing laser power when a fast cooling rate (~3.6 W per second) is used. The relationship between the annealing laser power and birefringence change shows a power threshold between 7.2–10.8 W of annealing laser power (estimated temperature 302–421 °C). The highest and lowest birefringences recorded throughout the annealing process are 4.72×10^{-4} and 3.46×10^{-4}, respectively (birefringence difference = 1.26×10^{-4}). It marks the onset of the glass transition region, viscosity change and stress relaxation of the SAPs, where the SAPs are transformed from the glassy state to the rubbery state as the temperature increases. Beyond the glass transition temperature, the viscosity of SAP decreases exponentially with increasing temperature, in accordance to Arrhenius Law. This explains the nonlinear curve in the change of birefringence with annealing power (temperature). On the other hand, Figures 5.5 (b) and (d) show that the birefringence increases exponentially with decreasing cooling rate. In between each slow cooling treatment (S1, S2, S3, S4), a fast cooling treatment (F5) was performed to reset the birefringence in RGPMF to the original state. Slower cooling rate enables more compaction in SAPs due to the longer relaxation time.

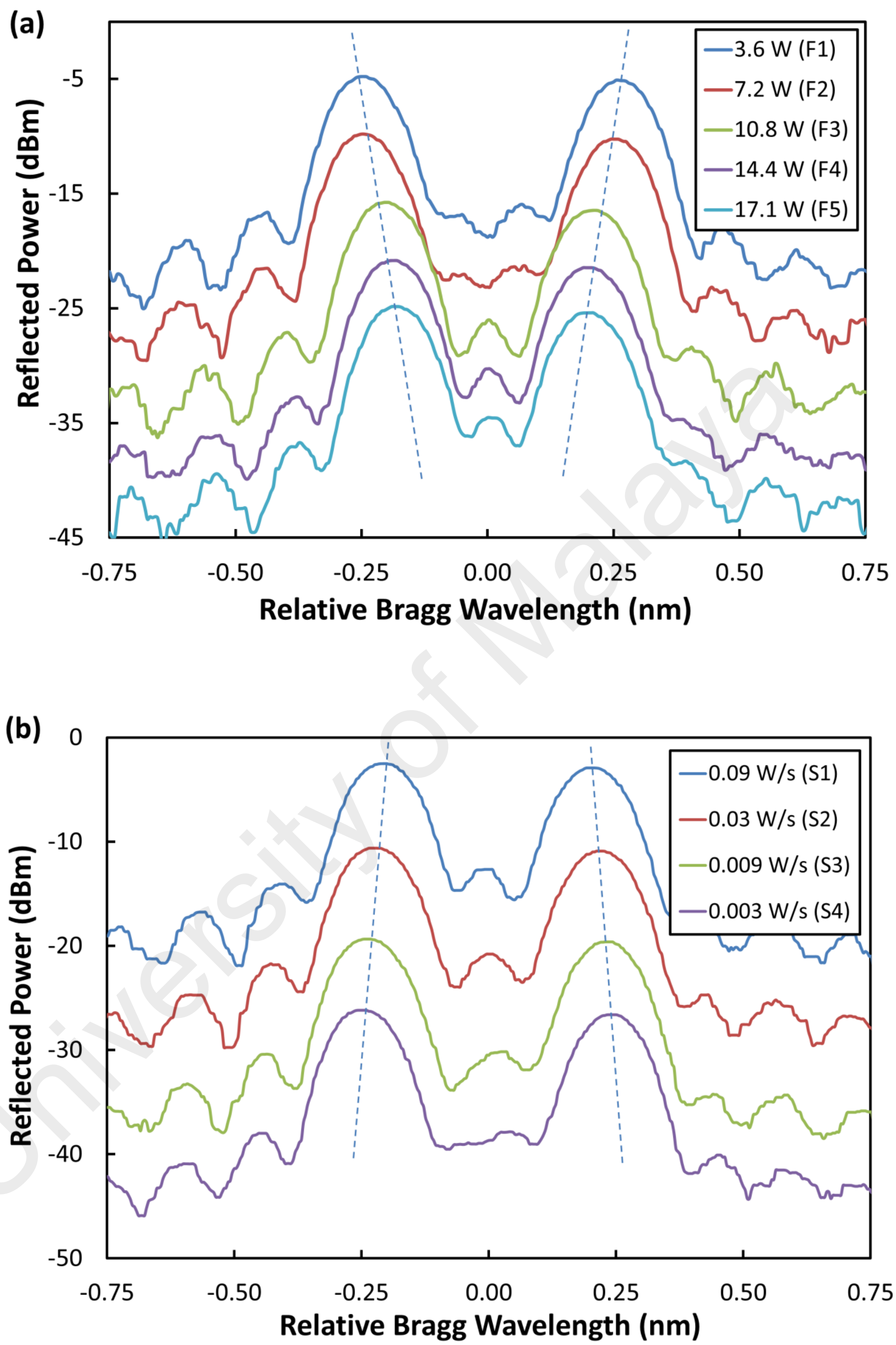

Figure 5.5 Spectral response and birefringence variation of RGPMF after the annealing treatments of (a), (c) F1-F5 and (b), (d) S1-S4. The dashed lines in (a) and (b) illustrate the variations of Bragg wavelengths by different treatments.

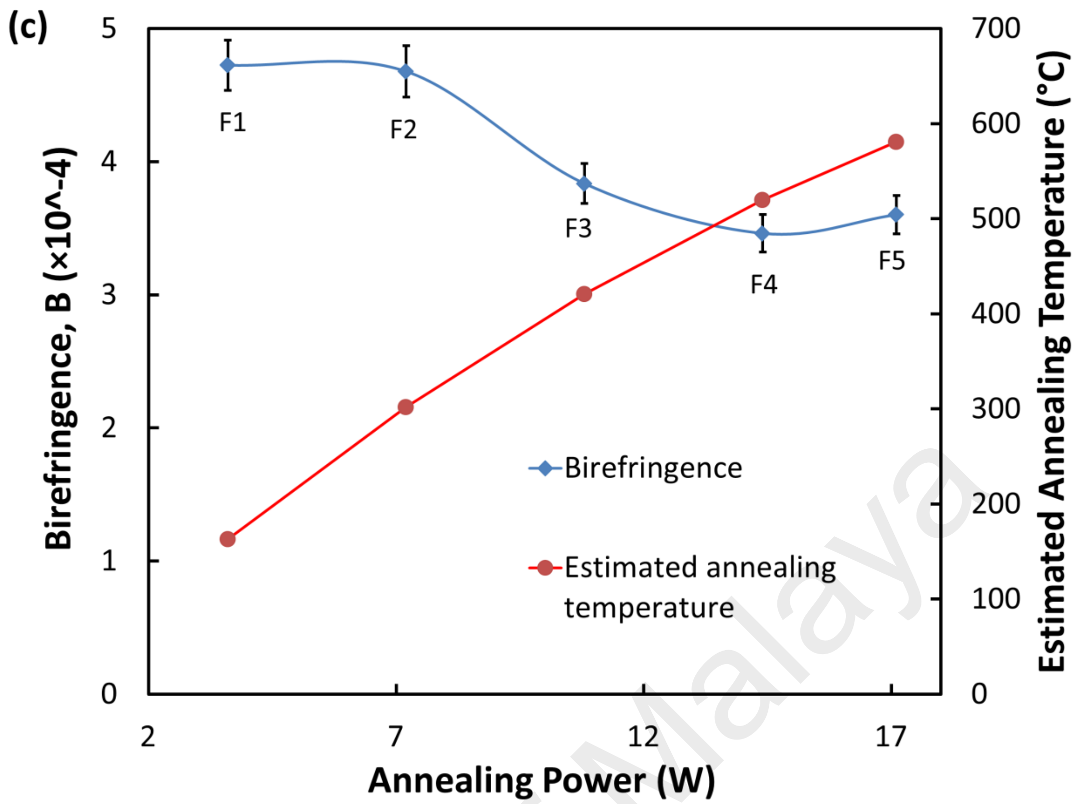

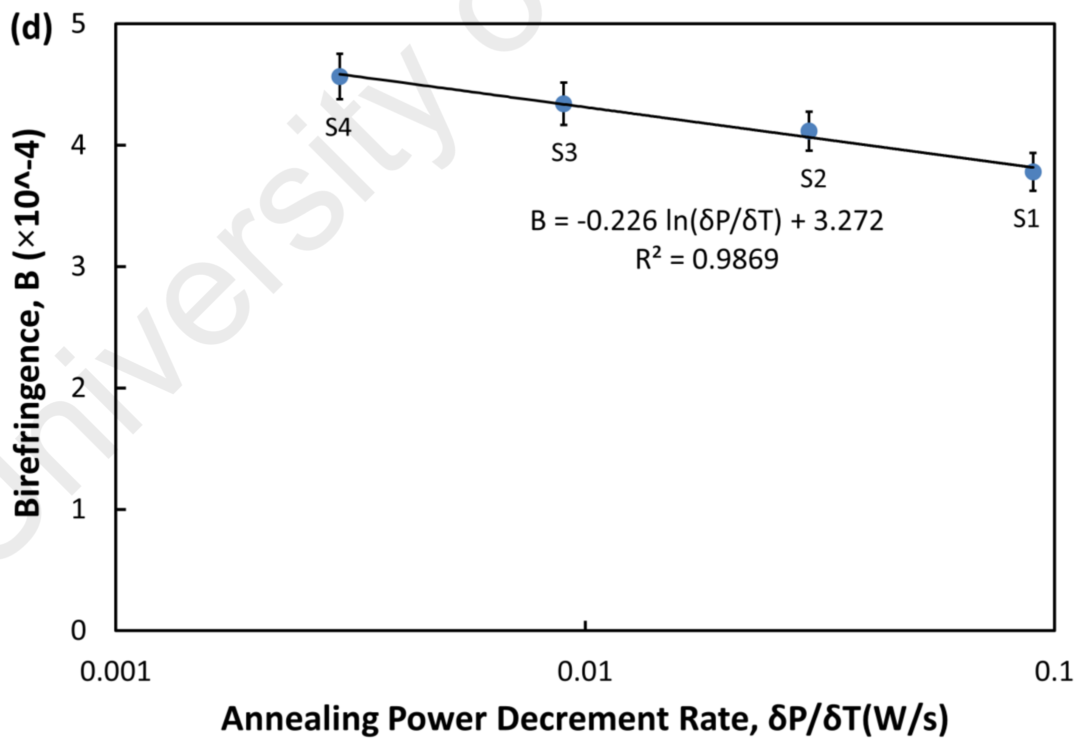

Figure 5.5, continued.

The birefringence in RGPMF is proportional to the TEC difference between fiber core and SAPs. The SAP has higher TEC than the fiber cladding due to its higher dopant concentration. Therefore, a compressive stress is exerted to the fiber core, which causes stress anisotropy in the fiber. The variation in birefringence after different cooling processes indicated that the TEC of SAP had been modified. The maximum temperature used for annealing was above the glass transition temperature of SAPs but below that of fiber core. As a result, the stress relaxation was limited to the SAPs. The TEC and glass transition temperature of fiber core in Eqn. (2.5) are assumed to be constant. The product of TEC and ΔT of SAP (birefringence) was increased because of slower cooling rate. Slower cooling promotes stress relaxation in glass structure of SAP, which in turn causes structural compaction due to longer relaxation time. The error in the birefringence change due to different annealing process is ~4 %. This error might be due to the uncertainty in laser power stability, ambient air turbulence, and alignment of the experimental setup. Additionally, the influence of laser irradiation angle was investigated. A series of annealing process was implemented on the RGPMF at different radial direction by rotating the fiber at an angle of 45° around its longitudinal axis after each annealing process (see Figure 5.6). The resultant birefringence at different irradiation angles using thermal treatment F5 is shown in Figure 5.7. The variation of birefringence due to different irradiation angles is 2.47 %, which is smaller than the largest birefringence difference (between F1 and F4) of 26.8 % presented in Figure 5.5 (c). The RGPMF was fixed on the experimental setup throughout the experiment. Hence, the fact of laser direction induced birefringence change can be eliminated from the results obtained.

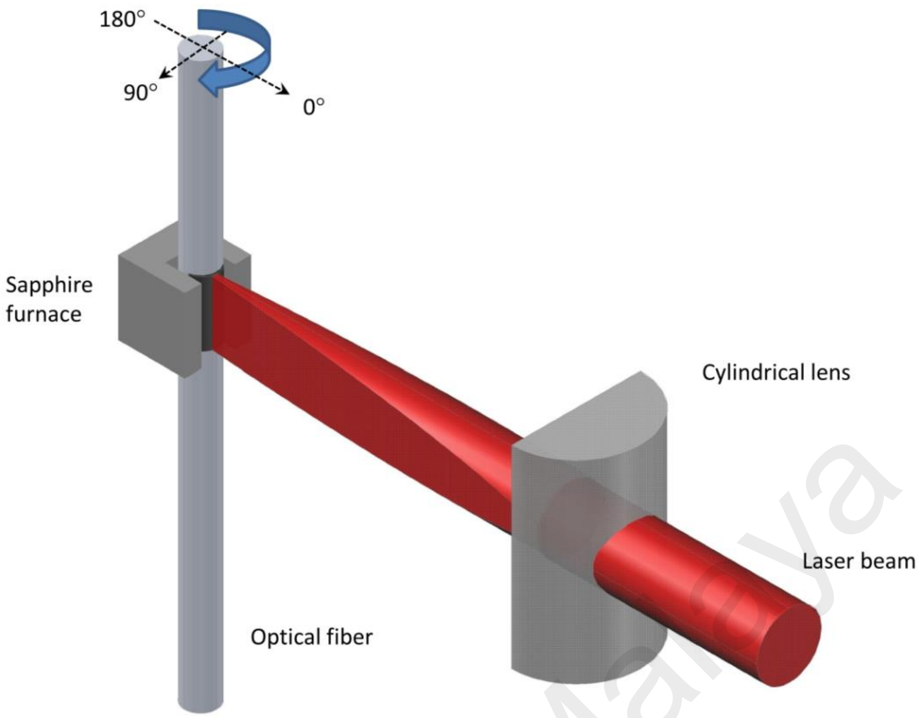

Figure 5.6 Schematic diagram of CO_2 laser annealing at different radial direction. The fiber was rotated clockwise to achieve radial direction ranging from 0 ° to 180 °.

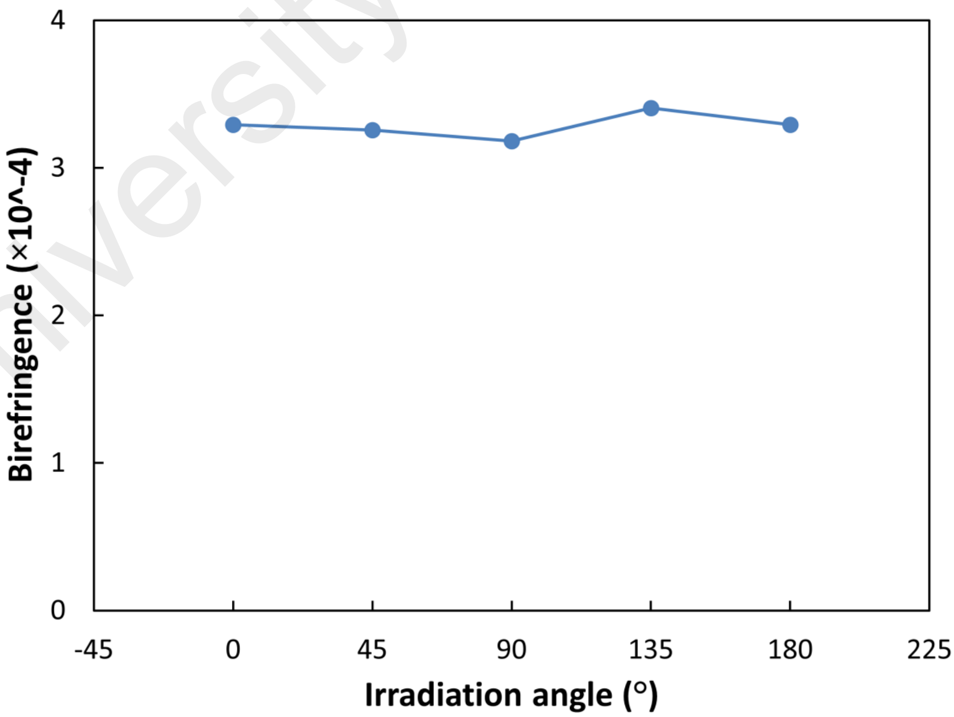

Figure 5.7 The birefringence of RGPMF after annealing at different radial direction followed by fast cooling (F5).

The CO_2 laser annealing technique provides an easy solution for modification of birefringence in PMF by means of manipulation of annealing rate, cooling rate, and annealing temperature. As a result, this modification technique makes the birefringence tuning feasible in PMF. This technique can be applied in the fabrication process of PMF as post processing treatment in order to tailor the birefringence of the fiber. Since the high annealing temperature is required, birefringence modification of the PMF is only possible to perform in RGPMF due to its high thermal sustainability. RGPMF is very useful for the application of polarisation maintaining in fiber laser operating in a high-temperature environment. It also provides an alternative solution for multi parameter sensing at high temperature.

5.3 Summary

Modification of thermal stress in PS1250/1500 with CO_2 laser annealing had been demonstrated. In the investigation, the Bragg wavelength of RFBG (PS1250/1500) served as an indicator for the change in fiber core refractive index. By manipulating the laser power decrement rate, the thermal stress in RFBG can be modified. Slower cooling process relaxes the thermal stress in the fiber core, which results to the red-shift in the Bragg wavelength and vice-versa. This effect is reversible and repeatable. Similarly, in the investigation of birefringence modification in RGPMF by CO_2 laser annealing, the dual Bragg wavelength of the RGPMF (PS-PM980) provided important information about the birefringence of the fiber. It was observed that the thermal stress relaxation in the SAPs was responsible for the changes in the birefringence after an annealing treatment followed by a cooling process. The birefringence modification can only be triggered when the annealing laser power exceeds the threshold power of ~7 W. It is believed that the operation of the RFBG in a dynamic temperature environment may result to hysteresis in the output response. Precaution and proper handling procedure for RFBG sensor are required to ensure accurate measurement in the dynamic and extreme temperature environment.

CHAPTER 6: CONCLUSION AND FUTURE WORK

This thesis focuses on experimental analyses of thermal regeneration and stress modification on regenerated fiber Bragg grating (RFBG). The conclusion for each chapter is given below. In the following section, recommendations of future work for this thesis are given to further improve the current achievement.

6.1 Conclusion

In this thesis, the research focuses on the thermal regeneration of several types of fibers include ZWP-SMF, PS1250/1500 fiber, PS-PM980, few-mode graded index fiber and few-mode step index fiber, as well as gallium doped fiber. Generally, the thermal regeneration temperature and thermal sensitivity for each type of RFBG are in the range of 850 °C – 950 °C and 11.5 pm/°C – 16.4 pm/°C respectively. All fiber Bragg gratings (FBGs) share similar thermal response during thermal regeneration process in which the grating reflectivity decayed rapidly followed by subsequent regeneration at regeneration temperature. The newly formed reflection peak gradually grew until it finally stabilised at lower reflectivity level compared to the seed grating. The comparison on the reflection spectra for each type of RFBGs at room temperature before and after thermal regeneration shows the degradation of grating strength and blue shift in Bragg wavelength. The blue shift in Bragg wavelength is due to the stress relaxation after thermal regeneration. Similarly, the stress relaxation reduced the birefringence of polarisation maintaining fiber (PMF) (PS-PM980) after the thermal regeneration process. This can be observed from the decrement in Bragg wavelength spacing for two orthogonal polarisation modes.

Thereafter, the CO_2 laser annealing was used for the thermal regeneration and thermal stability enhancement study of PS1250/1500 FBG. Prior to that, the thermal response of RFBG towards CO_2 laser annealing was characterised using on-off modulated CO_2 laser. The Bragg wavelength of RFBG showed a rapid response towards the variation of CO_2 laser power. In addition, a series of annealing processes have been carried out to investigate the effect of mini sapphire furnace on the performance of CO_2 laser annealing. The results show that the annealing temperature is higher and more stable with the aid of mini sapphire furnace. To optimize the efficiency of the laser annealing, RFBG was positioned at the centre of the laser beam where the intensity is maximum. This was achieved by positioning the RFBG where the shift in Bragg wavelength is the highest during the laser annealing treatment. Thermal regeneration was successfully demonstrated in PS1250/1500 FBG using CO_2 laser annealing at different heating rates. During thermal regeneration, the thermal response of the FBG shows similar behaviour to those produced using conventional method. Using isothermal annealing scheme, the duration of thermal regeneration was reduced to ~12 minutes. CO_2 laser offers the advantages of dynamic control and focused annealing area. That makes CO_2 laser annealing a good technique for thermal regeneration of FBG. Moreover, the investigation of thermal stability enhancement shows that CO_2 laser treated FBG has higher photosensitivity to the radiation at the wavelength range of ~193 nm and lower reflectivity degradation at elevated temperature. The refractive index change of the CO_2 laser treated FBG was higher compared to the non-treated FBG during grating inscription process. In thermal stability test, the CO_2-laser-treated-FBG has a reflectivity of ~4 dB higher than that in non-treated FBG after 3 hours of annealing at 300 °C. After annealing at 100 °C, 200 °C and 300 °C for 1 hour each, the refractive index modulation ratio of the CO_2-laser-treated-FBGs have been reduced by ~1 %, ~8 % and ~10 % respectively. This indicates that CO_2 laser annealing is useful for thermal stability enhancement of RFBG component to prolong its long lifespan in high temperature environment.

Beside thermal regeneration and thermal stability enhancement, CO_2 laser annealing was used in the studies of thermal stress modification (PS1250/1500) and birefringence modification (PS-PM980). The findings indicate that the ensuing cooling process after an isothermal annealing with CO_2 laser play an important part in modifying the thermal stress and birefringence of the RFBG. In the observation, the Bragg wavelength red-shifted after a slow cooling process and vice-versa. This phenomenon is reversible and repeatable by performing slow and rapid cooling treatments alternatively. This is due to the change in the thermal expansion coefficient (TEC), glass transition temperature (T_g) and density of the fiber core after different cooling process. This phenomenon only happen if the RFBG is cooled down from elevated temperature above its T_g. The stress relaxation of stress applying part (SAP) in PMF induces birefringence change in the fiber. The threshold laser intensity for the stress relaxation is ~560 W/cm^{-2}. The highest and lowest birefringences recorded at different cooling rates are 4.72×10^{-4} and 3.46×10^{-4}, respectively (a birefringence difference of 1.26×10^{-4}). The annealing-induced birefringence difference is much higher compare to that induced by different annealing direction (26.8 % compared to 2.47 %). As a result, the dynamic temperature change causes the hysteresis in the output response of RFBG components. Precaution and proper handling procedure for RFBG component are required to ensure accurate measurement in the dynamic and extreme temperature environment.

In overall, the thermal regeneration was performed on different types of FBG. That includes the first demonstrations of grating regeneration in few mode fibers and gallium doped fibers. The findings support the stress relaxation theory of thermal regeneration. Besides, a new RFBG fabrication technique based on CO_2 laser annealing was demonstrated and investigated. The performance of CO_2 laser annealing shows promising result in the fabrication of high quality RFBGs. CO_2 laser annealing was also proposed for the thermal stress and birefringence modification in boron-germanium co-doped fiber and panda type PMF. The result shows that the thermal stress and birefringence can be manipulated by using cooling process at different rate. This finding has opened a new perspective in the handling and operation of RFBG components and PMF-related fiber components in a high-temperature and dynamic environment. Overall, this research in RFBG and CO_2 laser annealing has achieved a great milestone.

6.2 Future Work

In the future, the thermal regeneration using CO_2 laser annealing should be performed on other types of fibers with different dopant and structures. The goal of the study is to understand the characteristics of thermal regeneration of different fibers and ultimately improve the fabrication technique in terms of productivity, flexibility and efficiency of the RFBGs. The production capacity of the current fabrication setup is limited to one FBG sample only. However, this limitation can be solved by splitting the laser source into several separate beams so that multiple FBG samples can be annealed at the same time. One of the shortcomings of CO_2 laser annealing technique is the stability of laser output power and susceptibility to the influence from environment. Hence, a fabrication setup with better shielding ability as well as higher and more stable laser output power should be developed. As extended work, the RFBG can act as an infrared laser beam profiler. This can be achieved by scanning laser beam with an RFBG, the thermal sensor to acquire the spatial and temporal thermal responses of the reflection spectrum from the RFBG.

Furthermore, the thermal stress and birefringence modification study can be extended to other type of fibers. This is because different types of fibers have different TEC and T_g due to different composition. Therefore, thermal stress modification treatment should have different effect on different types of fibers. This is important for the investigation of the effect of thermal stress on optical fiber components at different thermal condition.

In addition, the birefringence modification treatment using CO_2 laser can be applied on other types of PMFs such as bow tie, elliptical core, dumbbell core, elliptical cladding and flat cladding type PMF. The PMFs due to geometric birefringence are good subject for the birefringence modification study using CO_2 laser annealing technique. The thermal-induced stochastic effect in the stress properties of optical fiber components is an important parameter for high and dynamic temperature environment. More study should be dedicated into exploring and improving the functionalities of PMF components in high temperature environment.

REFERENCES

Abe, I., de Góes, R. E., Fabris, J. L., Kalinowski, H. J., Müller, M., Fugihara, M. C., Falate, R., Diesel, B. W., Kamikawachi, R. C., & Barbosa, C. L. (2003). Production and characterization of refractive index gratings in high-birefringence fiber optics. *Opt. Lasers Eng., 39*(5/6): 537–548.

Abe, I., Kalinowski, H. J., Nogueira, R., Pinto, J. L., & Frazao, O. (2003). Production and characterisation of Bragg gratings written in high-birefringence fiber optics. *Proc. Inst. Elect. Eng. —Circuits, Devices Syst., 150*(6): 495–500.

Abloud, J. H., Benyounis, K. Y., Obabi, A. G., & Hashmi, M. S. J. (2007). Laser surface treatments of iron-based substrates for automotive application original research article. *J. Mater. Process. Tech., 182* (1-3): 427-431.

Adams, M. J. (1993). CO_2 gas lasers: engineering and operation, Laser Processing in Manufacturing. *Springer Netherlands*, 115–139.

Apostolos, F., Panagiotis, S., Konstantinos, S., & George, C. (2012). Energy efficiency assessment of laser drilling process. *Phys Procedia, 39*: 776–783.

Archambault, J. L., Reekie, L., & Russell, P. St. (1993). 100% reflectivity Bragg reflectors produced in optical fibres by single excimer laser pulses. *Electron. Lett., 29*(5): 453-455.

Ascher, P. W., & Heppner, F. (1984). CO_2-Laser in neurosurgery. *Neurosurg. Rev., 7*(2-3): 123-133.

Åslund, M., & Canning, J. (2000). Annealing properties of gratings written into UV-presensitized hydrogen-out diffused optical fiber. *Opt. Lett., 25*(10): 692-694.

Baker, S. S., Muenzler, W. S., Small, R. G., & Leonard, J. E. (1984). Carbon dioxide laser blepharoplasty. *Ophthalmology, 91*(3): 238-244.

Bandyopadhyay, S., Canning, J., Stevenson, M., & Cook, K. (2008). Ultrahigh-temperature regenerated gratings in boron-codoped germanosilicate optical fiber using 193 nm. *Opt. Lett., 33*(16): 1917-1919.

Barlow, A. J. (1985). Optical-fiber birefringence measurement using a photo-elastic modulator. *J. Lightw. Technol., 3*(1): 135–145.

Barrera, D., & Sales, S. (2013). High-temperature optical sensor based in high birefringence regenerated FBGs and a simple interrogation scheme. *Proc. SPIE, 8794*: 87941K.

Bass, I. L., Guss, G. M., Nostrand, M. J., & Wegner, P. L. (2010). An improved method of mitigating laser induced surface damage growth in fused silica using a rastered, pulsed CO_2 laser. *Proc. SPIE 7842, Laser-Induced Damage in Optical Materials*: 784220.

Bayle, F., & Meunier, J. P. (2005). Efficient fabrication of fused-fiber biconical taper structures by a scanned CO_2 laser beam technique. *Appl. Opt., 44*(30): 6402-6411.

Beck, O. J. (1980). The use of the Nd-YAG and the CO_2 laser in neurosurgery. *Neurosurg. Rev., 3*(4): 261-266.

Benda, J. A., & Parasco, A. (2011). Long period fiber Bragg gratings written with alternate side IR laser illumination. US7946137 B2.

Benghalem, N. K., & Allag, W. (2015). Optimization of parameters CO_2 laser for drilling different types of glass. *New Journal of Glass and Ceramics, 5*(4): 75-83.

Bennett, T. D., & Li, L. (2001). Modeling laser texturing of silicate glass. *J. Appl. Phys., 89*(2): 942-950.

Bohren, C. F., & Huffman, D. R. (1983). Absorption and scattering of light by small particles, *Wiley-VCH Verlag GmbH & Co. KGaA*.

Brambilla, G., Pruneri, V., Reekie, L., & Payne, D. N. (1999). Enhanced photosensitivity in germanosilicate fibers exposed to CO_2 laser radiation. *Opt. Lett., 24*(15): 1023-1025.

Brusasco, R., Penetrante, B., Butler, J., Grundler, W., & Governo, G. (2002). CO_2 laser and plasma microjet process for improving laser optics. US20020070198 A1.

Brückner, R. (1970). Properties and structure of vitreous silica. I. *J. Non-Cryst. Solids, 5*(2): 123-175.

Bueno, A., Kinet, D., Mégret, P., & Caucheteur, C. (2013). Fast thermal regeneration of fiber Bragg gratings. *Opt. Lett., 38*(20): 4178–4181.

Busch, M., Ecke, W., Latka, I., Fischer, D., Willsch, R., Bartelt, H. (2009). Inscription and characterization of Bragg gratings in single-crystal sapphire optical fibres for high-temperature sensor applications. *Meas. Sci. Technol., 20*(11): 115301.

Butov, O. V., Dianov, E. M., & Golant, K. M. (2006). Nitrogen-doped silica core fibres for Bragg grating sensors operating at elevated temperatures. *Meas. Sci. Technol., 17*: 975-979.

Byron, K.C. (1997). Bragg gratings in waveguides. US5694502 A.

Cale, A. S., Danley, J. D., Dean, Jr., D. L., Cooke, T. L., Mabry, III, C. B., Miller, D. M. (2011). Laser based methods of stripping fiber optic cables. US8052836 B2.

Callister, W. D., & Rethwisch, D. G. (2008). Fundamentals of materials science and engineering: an integrated approach- 3rd ed. ISBN 978-0-470-12537-3.

Canning, J., Bandyopadhyay, S., Biswas, P., Aslund, M., Stevenson, M., & Cook, K. (2010). Regenerated fiber Bragg gratings. *Frontier in Guided Wave Optics and Optoelectronics*, B. Pal, Ed.–(INTECH): 365–384.

Canning, J., Sommer, K., & Englund, M. (2001). Fibre gratings for high temoerature sensor applications. *Meas. Sci. Tech., 12*: 824-828.

Canning, J., Stevenson, M., Bandyopadhyay, S., & Cook, K. (2008). Extreme silica optical fibre gratings. *Sensors, 8*: 6448-6452.

Chehura, E., Ye, C. C., Staines, S. E., James, S. W., & Tatam, R. P. (2004). Characterization of the response of fiber Bragg gratings fabricated in stress and geometrically induced high birefringence fibers to temperature and transverse load. *Smart Mater. Struct., 13*(9): 888–895.

Chen, G. H., Liu, L. Y., Jia, H. Z., Yu, J. M., Xu, L., & Wang, W. C. (2004). Simultaneous strain and temperature measurements with fiber Bragg grating written in novel Hi-Bi optical fiber. *IEEE Photon. Technol. Lett., 16*(1): 221–223.

Chen, X. (2013). Optical fibre gratings for chemical and bio-sensing, current developments in optical fiber technology. Dr. Sulaiman Wadi Harun (Ed.), InTech, DOI: 10.5772/54242.

Chiasera, A., Macchi, C., Mariazzi, S., Valligatla, S., Lunelli, L., Pederzolli, C., Rao, D. N., Somoza, A., Brusa, R. S., & Ferrari, M. (2013). CO_2 Laser irradiation of GeO_2 planar waveguide fabricated by rf-sputtering. *Opt. Mater. Express, 3*(9): 1561-1570.

Chryssou, C. (1999). Theoretical analysis of tapering fused silica optical fibers using a carbon dioxide laser. *Opt. Eng., 38*(10): 1645–1649.

Chu, P. L., & Sammut, R. A. (1984). Analytical method for calculation of stresses and material birefringence in polarization maintaining optical fiber. *J. Lightw. Technol., 2*(5): 650–662.

Coelho, J. M. P., Nespereira, M., Silva, C., Pereira, D., & Rebordão, J. (2013). Advances in optical fiber laser micromachining for sensors development, current developments in optical fiber technology. Dr. Sulaiman Wadi Harun (Ed.), InTech, DOI: 10.5772/52745.

Cohen, A. J., & Smith, H. L. (1958). Ultraviolet and infrared absorption of fused Germania. *J. Phys. Chem., 7*(4): 301-306.

Cook, K., Shao, L. Y., & Canning, J. (2012). Regeneration and helium: regenerating Bragg gratings in helium-loaded germanosilicate optical fibre. *Opt. Mater. Express, 2*(12): 1733–1742.

Cormont, P., Bourgeade, A., Cavaro, S., Donval, T., Doualle, T., Gaborit, G., Gallais, L., Lamaignère, L., & Rullier, J. L. (2015). Relevance of carbon dioxide laser to remove scratches on large fused silica polished optics. *Adv. Eng. Mater., 17*(3): 253-259.

Cormont, P., Combis, P., Gallais, L., Hecquet, C., Lamaignère, L., & Rullier, J. L. (2013). Removal of scratches on fused silica optics by using a CO_2 laser. *Opt. Express, 21*(23): 28272-28289.

Cormont, P., Gallais, L., Lamaignère, L., Rullier, J. L., Combis, P., & Hebert, D. (2010). Impact of two CO_2 laser heatings for damage repairing on fused silica surface. *Opt. Express, 18*(25): 26068-26076.

Crafer, R. C., Greening, D., & Brown M. (1998). Design, construction and operation of industrial CO_2 lasers (Engineering Lasers and Their Applications). *Kluwer Academic Publishers*.

Croswell, R. T., Reisman, A., Simpson, D. L., Temple, D., & Williams, C. K. (1999). Differential Thermal Analysis of Glass Mixtures Containing SiO_2, GeO_2, B_2O_3, and P_2O_5. *J. Electrochem. Soc., 142*(12): 4569-4579.

Daia, W., Xiang, X., Jiang, Y., Wang, H. J., Li, X. B., Yuan, X. D., Zheng, W. G., Lv, H. B., & Zu, X. T. (2011). Surface evolution and laser damage resistance of CO_2 laser irradiated area of fused silica. *Opt. Laser Eng., 49*(2): 273-280.

Danley, J. D., Robert, B. E. II, Miller, D. M., Tian, Z., Toepper, S. T., & Yeakel, K. D. (2015). Optical fibers having coatings removed therefrom and related methods, US20150277048 A1.

Danley, J. D., Wacaster, T. B., & Rosson, J. C. (2007). Method of making an optical fiber by laser cleaving, US7216512 B2.

Davis, D. D., Gaylord, T. K., Glytsis, E. N., & Mettler, S. C. (1999). Very-high-temperature stable CO_2 laser-induced long period fibre gratings. *Electron. Lett., 35*(9): 740-742.

DeMaria, A. J., & Hennessey, Jr., T. V. (2010). The CO_2 laser: The workhorse of the laser material processing industry. *SPIE Professional Magazine*.

Deprez, P., Melian, C. F., Breaban, F., & Coutouly, J.F. (2012). Glass marking with CO_2 Laser: Experimental study of the interaction laser-material. *Journal of Surface Engineered Materials and Advanced Technology, 2*(1): 32-39.

Dimmick, T. E., Kakarantzas, G., Birks, T. A., & Russell, P. S. J. (1999). Carbon dioxide laser fabrication of fused-fiber couplers and tapers. *Appl. Opt., 38*(33): 6845-6848.

Dobrovinskaya, E. R., Lytvynov, L. A., & Pishchik, V. (2009). Properties of sapphire, in Sapphire: Material, Manufacturing, Applications. *Springer*: 55–176.

Dong, L., Liu, W. F., & Reekie, L. (1996). Negative index gratings formed by 193nm laser. *Opt. Lett., 21*(24): 2032-2034.

Douay, M., Ramecourt, D., Taunay, T., Niay, P., Bernage, P., Dacosta, A., Mathiew, C., Bayon, J. F., & Poumellec, B. (1995). Microscopic investigations of Bragg grating photowritten in germanosilicate fibers. *Photosensitivity and Quadratic Nonlinearity in Glass Waveguides: Fundamentals and Applications,Vol. 22, OSA Technical Digest Series (Optical Society of America, Washington DC)*, 51-55.

Douay, M., Xie, W. X., Taunay, T., Bernage, P., Niay, P., Cordier, P., Poumellec, B., Dong, L., Bayon, J. F., Poignant, H., & Delevaque, E. (1997). Densification involved in the UV based photosensitivity of silica glasses and optical fibers. *J. Lightwave Technol., 15*(8): 1329-1342.

Duley, W. W. (1976). CO_2 lasers: Effects and applications. New York: Academic Press.

Duparré, M., Golub, M. A., Lüdge, B., Pavelyev, V. S., Soifer, V. A., Uspleniev, G. V., & Volotovskii, S. G. (1995). Investigation of computer-generated diffractive beam shapers for flattening of single- modal CO_2-laser beams. *Appl. Opt., 34*(14): 2489-2497.

Dutta, S., Jackson, H. E., & Boyd, J. T. (1980). Reduction of scattering from a glass thin-film optical waveguide by CO_2 laser annealing. *Appl. Phys. Lett., 37*(6): 512-514.

Dutta, S., Jackson, H. E., Boyd, J. T., Davis, R. L., & Hickernell, F. S. (1982). CO_2 laser annealing of Si_3N_4, Nb_2O_5 and Ta_2O_5 thin-film optical waveguides to achieve scattering loss reduction. *IEEE J. Quantum Elect., 18*(4): 800-805.

Dürr, F., Limberger, H. G., Salathé, R. P., Vasiliev, S. A., Medvedkov, O. I., Bozhkov, A. S., & Dianov, E. M. (2005). Annealing-induced stress changes in UV irradiated germanium-doped fibers. BGPP'2005, Bragg Gratings, Photosensitivity, and Poling in Glass Waveguides: OSA Topical Meeting.

Egashira. K., & Kobayashi, M. (1977). Optical fiber splicing with a low-power CO_2 laser. *Appl. Opt., 16*(6): 1636-1638.

Ermolaev G. V., & Yudin, P. V. (2014). Fundamental study of CO_2 and fiber laser cutting of steel plates with high speed visualization technique. *J. Laser Appl., 26*(4): 042004.

Evans, J. D. (1990). Selected papers on CO_2 lasers. *SPIE Milestone Series MS22, Bellingham: SPIE.*

Fairbanks, D. R. (1991). Thermal visco-elastic simulation model for tapering of laser-heated fused silica fiber. *Proc. SPIE 1580, Fiber Optic Components and Reliability*: 188–196.

Ferreira, L. A., Araujo, F. M., Santos, J. L., & Farahi, F. (2000). Simultaneous measurement of strain and temperature using interferometrically interrogated fiber Bragg grating sensors. *Opt. Eng., 39*(8): 2226–2234.

Fokine, M. (2002). Formation of thermally stable chemical composition gratings in optical. *J. Opt. Soc. Am. B, 19*(8): 1759-1765.

Fokine, M., & Margulis, W. (2000). Large increase in photosensitivity through massive hydroxyl formation. *Opt. Lett., 25*(5): 302–304.

Fonjallaz, P. Y., Limberger, H. G., Salathé, R. P., Cochet, F., & Leuenberger, B. (1995). Tension increase correlated to refractive index change in fibers containing UV written Bragg gratings. *Opt. Lett., 20*(11): 1346-1348.

Forrest, L., O'Key, M. A., Osborne, M. R., Musk, R. W., & Spicer, P. (1996). Laser machining of fibre ends. *Proceedings of IEEE Conference on Electrical Devices for Microwave and Optoelectronic Applications Workshop—EDMO, Leeds University, UK, Institute of Electrical and Electronics Engineers, New York*: 68–69.

Friebele, E. J., Sigel, Jr., G. H., & Gingerich, M. E. (1978). Radiation response of fiber optic waveguides in the 0.4 to 1.7 μ region. *IEEE Trans. Nucl. Sci., 25*(6): 1261–1266.

Fujita, H., Suzaki, Y., & Tachibana, A. (1976). Optical fiber splicing technique with a CO_2 laser. *Appl. Opt., 15*(2): 320-321.

Grellier, A. J. C., Zayer, N. K., & Pannell, C. N. (1997). Considerations in the use of CO_2 lasers for tapering fused silica fibre. *Proceedings in 12th International Conference on Optical Fiber Sensors, Vol. 16 of 1997 OSA Technical Digest Series, Optical Society of America, paper OWC19*: 217-220.

Grellier, A. J. C., Zayer, N. K., & Pannell, C. N. (1998). Heat transfer modelling in CO_2 laser processing of optical fibres. *Opt. Commun., 152*(4-6): 324–328.

Grobnic, D., Mihailov, S., Smelser, C., & Ding, H. (2004). Sapphire fiber Bragg grating sensor made using femtosecond laser radiation for ultrahigh temperature applications. *IEEE Photon. Technol. Lett., 16*(11): 2505–2507.

Grobnic, D., Smelser, C. W., Mihailov, S. J., & Walker, R. B. (2006). Long term thermal stability tests at 1000°C of silica fibre Bragg gratings made with ultrafast laser radiation. *Meas. Sci. Technol., 17*(5): 1009-1013.

Groothoff, N., & Canning, J. (2004). Enhanced type IIA gratings for high-temperature operation. *Opt. Lett., 29*(20): 2360-2362.

Harney, R. C. (1989). CO_2 lasers for military applications. *Proc. SPIE 1042, CO_2 Lasers and Applications*: 42-54.

Hill, K. O., Fujii, Y., Johnson, D. C., & Kawasaki, B. S. (1978). Photosensitivity in optical waveguides: Application to reflection filter fabrication. *Appl. Phys. Lett., 32*(10): 647.

Hill, P., Atkins, G. R., Canning, J., Cox, G., Sceats, M. G. (1995). Writing and visualisation of low threshold type II Bragg grating in stressed optical fibres. *Appl. Opt., 34*(33): 7689-7694.

Holmberg, P., & Fokine, M. (2013). Thermometric study of CO_2-laser heated optical fibers in excess of 1700°C using fiber Bragg gratings. *J. Opt. Soc. Am. B, 30*(7): 1835-1842.

Homsy, G., & Walker, K. (1979). Heat transfer in laser drawing of optical fibres. *Glass Technol., 20*(1): 20–26.

Hülsenberg, D., Harnisch, A., & Bismarck, A. (2008). Microstructuring of glasses. (Springer-Verlag Berlin Heidelberg, New York): 12-15.

Imen, K., Lee, C. H., Yang, Y. Y., & Allen, S. D. (1990). Laser fabricated fiber optical taps for interconnect and optical data processing device. *Proc. SPIE 1365, Components for Fiber Optic Applications V*: 60-64.

Inaudi, D., & Glisic, B. (2006). Fiber optic sensing for innovative oil and gas production and transport systems. *Optical Fiber Sensors, OSA Technical Digest (CD) (Optical Society of America)*, paper FB3.

Ion, J. C. (2005). Laser processing of engineering materials: Principles, procedure and industrial application. *Elsevier Butterworth-Heinemann*, 74-81,211-212, 470-471.

Jung, C. W. (2008). Understanding of CO_2 laser in dermatology. *Journal of Dermatology Korean Society for Laser Medicine and Surgery, 12*(1): 90-99.

Just, F., Spittel, R., Bierlich, J., Grimm, S., Jäger, M., & Bartelt, H. (2015). The influence of the fiber drawing process on intrinsic stress and the resulting birefringence optimization of PM fibers. *Opt. Mater., 42*: 345–350.

Kakarantzas, G., Birks, T. A., & Russell, P. S. (2002). Structural long-period gratings in photonic crystal fibers. *Opt. Lett. 27*(12): 1013-1015.

Kakarantzas, G., Dimmick, T. E., Birks, T. A., Roux, R. L., & Russell, P. S. J. (2001). Miniature all-fiber devices based on CO_2 laser microstructuring of tapered fibers. *Opt. Lett., 26*(15): 1137-1139.

Kakarantzas, G., Ortigosa-Blanch, A., Birks, T. A., Russell, P. S., Farr, L., Couny, F., & Mangan, B. J. (2003). Structural rocking filters in highly birefringent photonic crystal fiber. *Opt. Lett. 28*(3): 158-160.

Kashyap, R. (1999). Fiber Bragg gratings: Academic Press.

Kashyap, R., Armitage, J. R., Wyatt, R., Davey, S. T., & Williams, D. L. (1990). All fibre narrowband reflection gratings at 1500 nm. *Electron. Lett., 26*(11): 730.

Kewitsch, A. S., Rakuljic, G. A., Engin, D., Greenberg, S. J., Willems, P. A., & Tong, X. (2001). Methods of fabricating grating assisted coupler devices, US6169830 B1.

Khorram, A., Ghoreishi, M., Yazdi, M. R. S., & Moradi, M. (2011). Optimization of bead geometry in CO_2 laser welding of Ti_6Al_4V using response surface methodology. *Eng. 3*(7): 708-712.

Kim, B. H., Ahn, T. J., Kim, D. Y., Lee, B. H., Chung, Y., Paek, U. C., & Han, W. T. (2002). Effect of CO_2 laser irradiation on the refractive-index change in optical fibers. *Appl. Opt., 41*(19): 3809-3815.

Kim, B. H., Park, Y., Ahn, T. J., Kim, D. Y., Lee, B. H., Chung, Y., Paek, U. C., & Han, W. T. (2001). Residual stress relaxation in the core of optical fiber by CO_2 laser irradiation. *Opt. Lett., 26*(21):1657-1659.

Kim, C. S., Han, Y., Lee, B. H., Han, W. T., Paek, U. C., & Chung, Y. (2000). Induction of the refractive index change in B-doped optical fibers through relaxation of the mechanical stress. *Opt. Commun., 185*(4-6): 337-342.

Kinoshita K., & Kobayashi, M. (1982). Two-dimensionally arrayed optical-fiber splicing with a CO_2 laser. *Appl. Opt., 21*(19): 3419-3422.

Kritzinger, R., Schmieder, D., & Booysen, A. (2009). Azimuthally symmetric long-period fiber grating fabrication with a TEM_{01*}-mode CO_2 laser. *Meas. Sci. Technol., 20*: 034004.

Krohn, D. A. (1970). Determination of axial stress in clad glass fibers. *J. Am. Ceram. Soc., 53*(9): 505-507.

Krohn, D. A., & Cooper, A. R. (1969). Strengthening of glass fibers: I, Cladding. *J. Am. Ceram. Soc., 52*(12): 661-664.

Laffont, G., Cotillard, R., & Ferdinand, P. (2013a). Multiplexed regenerated fiber Bragg gratings for high temperature measurement. *Meas. Sci. Technol., 24*(9): 094010.

Laffont, G., Cotillard, R., & Ferdinand, P. (2013b). 9000 hours-long high temperature annealing of regenerated FBGs. *Proc. SPIE 8794*, 87941X.

Lamaire, P., Atkins, R. M., Mizrahi, V., & Reed, W. A. (1993). High pressure H_2 loading as a technique for achieving ultrahigh UV photosensitivity and thermal sensitivity in GeO_2 doped optical fibres. *Electron. Lett., 29*(13): 1191.

Lawrence, C. M., Nelson, D. V., Udd, E., & Bennett, T. (1999). A fiber optic sensor for transverse strain measurement. *Exp. Mech., 39*(3): 202–209.

Lee, H. W., Liu, Y., & Chiang, K. S. (2008). Writing of long-period gratings in conventional and photonic-crystal polarization-maintaining fibers by CO_2-Laser pulses. *IEEE Photonics Technol. Lett., 20*(2): 132-134.

Lee, S. K., & Jaluria, Y. (1997). Simulation of the transport processes in the neck-down region of a furnace drawn optical fibers. *Int. J. Heat Mass Transfer, 40*(4): 843–856.

Leviton, D. B., & Frey., B. J. (2008). Temperature-dependent absolute refractive index measurements of synthetic fused silica. *Proceedings of SPIE - The International Society for Optical Engineering 6273*.

Liao, C., Wang, D., Li, Y., Sun, T., & Grattan, K. T. V. (2009). Temporal thermal response of type II–IR fiber Bragg gratings. *Appl. Opt., 48*(16): 3001-3007.

Lim, K. S., Pua, C. H., Harun, S. W., & Ahmad, H. (2010). Temperature-sensitive dual-segment polarization maintaining fiber Sagnac loop mirror. *Opt. Laser Technol., 42*(2): 377–381.

Lim, K. S., Pua, C. H., Harun, S. W., & Ahmad, H. (2010). Temperature-sensitive dual-segment polarization maintaining fiber Sagnac loop mirror. *Opt. Laser Technol., 42*(2): 377–381.

Lim, K. S., Yang, H. Z., Chong, W. Y., Cheong, Y. K., Lim, C. H., Ali, N. M., & Ahmad, H. (2013). Axial contraction in etched optical fiber due to internal stress reduction. *Opt. Express, 21*(3): 2551-2562.

Liu, Y. G., Feng, X. H., Yuan, S. Z., Kai, G. Y., & Dong, X. Y. (2004). Simultaneous four-wavelength lasing oscillations in an erbium-doped fiber laser with two high birefringence fiber Bragg gratings. *Opt. Express, 12*(10): 2056–2061.

Liu, Y., & Chiang, K. S. (2008). CO_2-laser writing of long-period fiber gratings in optical fibers under tension. *Opt. Lett., 33*(17): 1933-1935.

Liu, Y., Chiang, K. S., Rao, Y. J., Ran, Z. L., & Zhu, T. (2007). Light coupling between two parallel CO_2-laser written long-period fiber gratings. *Opt. Express, 15*(26): 17645-17651.

Madić, M., Radovanović, M., Manić, M., & Trajanović, M. (2014). Optimization of CO_2 laser cutting process using taguchi and dual response surface methodology. *Tribol. Ind. 36*(1): 236-243.

Markillie, G. A. J., Baker, H. J., Villarreal, F. J., & Hall, D. R. (2002). Effect of vaporization and melt ejection on laser machining of silica glass micro-optical components. *Appl. Opt., 41*(27): 5660-5667.

Matsusaka, S., Ohta, M., Watanabe, T., Satoh, T., & Tabata, M. (2008). Fusion splicing of ribbon-shaped optical fibers with CO_2 laser beams. *Journal of the Japan Society for Precision Engineering, 74*(1): 57-61.

Mawatari, T., & Nelson, D. (2008). A multi-parameter Bragg grating fiber optic sensor and triaxial strain measurement. *Smart Mater. Struct., 17*(3): 035033.

McAtamney, C., Cronin, A., Sherlock, R., O'Connor, G. M., & Glynn, T. J. (2005). Reproducible method for fabricating fused biconical tapered couplers using a CO_2 laser based process. *Proceedings of the Third International WLT-Conference on Lasers in Manufacturing*.

Meltz, G., Morey W. W., & Glenn, W. H. (1989). Formation of Bragg gratings in optical fibres by transverse holographic method. *Opt. Lett., 14*(15):823.

Meltzand, G., & Morey, W. W. (1991). Bragg grating formation and germanosilicate fiber photosensitivity. *Proc. SPIE Int. Workshop Photoinduced Self-Org. Effects Opt. Fiber, 1516*: 185.

Messina, F., Cannas, M., Médjahdi, K., Boukenter, A., & Ouerdane, Y. (2005). UV-photoinduced defects in Ge-doped optical fibers. *Proceedings of WFOPC2005 - 4th IEEE/LEOS Workshop on Fibres and Optical Passive Components*: 313–317.

Mittelman, H., & Apfelberg, D. B. (1990). Carbon dioxide laser blepharoplasty-Advantages and disadvantages. *Ann. Plast. Surg., 24*(1): 1-6.

Moynihan, C. T., Easteal, A. J., Wilder, J., & Tucker, J. (1974). Dependence of the glass transition temperature on heating and cooling rate. *J. Phys. Chem., 78*(26): 2673–2677.

Myers, G.E. (1998). Analytical methods in conduction heat transfer. *Amch*, 2nd edition.

Myers, M. (1989). A model for unsteady analysis of preform drawing. *AIChE J., 35*: 592–602.

Ojovan, M. I. (2008). Viscosity and glass transition in amorphous oxides. *Adv. Condens. Matter Phys., 2008*: 817829.

Ossoff, R. H., Coleman, J. A., Courey, M. S., Duncavage, J. A., Werkhaven, J. A., & Reinisch, L. (1994). Clinical applications of lasers in otolaryngology- Head and neck surgery. *Lasers Surg. Med., 15*(3): 217-248.

Ourmazd, A., Birch, R. D., Varnham, M. P., Payne, D. N., & Tarbox, E. J. (1983). Enhancement of birefringence in polarization maintaining fiber by thermal annealing. *Electron. Lett., 19*(4): 143–144.

Ourmazd, A., Varnham, M. P., Birch, R. D., & Payne, D. N. (1983). Thermal properties of highly birefringent optical fibers & preforms. *Appl. Opt., 22*(15): 2374–2379.

Özcan, L. Ç., Tréanton, V., Guay, F., & Kashyap, R. (2007). Highly symmetric optical fiber tapers fabricated with a CO_2 laser. *IEEE Photonics Technol. Lett., 19*(9): 656-658.

Paek, U. C. (1974). Laser drawing of optical fibers. *Appl. Opt., 13*(6): 1383-1386.

Paek, U. C., & Weaver, A. L. (1975). Formation of a spherical lens at optical fiber ends with a CO_2 laser. *Appl. Opt., 14*(2): 294-298.

Paek, U. C., Chung, Y. J., Kim, C. S., Kim, J. H., Park, H. S., & Kwack, K. H., (2002). Device and method for forming anti-symmetric long period optical fiber gratings by microbending. US 6385370 B1.

Palmier, S., Gallais, L., Commandré, M., Cormont, P., Courchinoux, R., Lamaignère, L., Rullier, J. L., & Legros, P. (2009). Optimization of a laser mitigation process in damaged fused silica. *Appl. Surf. Sci., 255*(10): 5532-5536.

Patel, C. K. N. (1964). Continuous-wave laser action on vibrational-rotational transitions of CO_2. *Phys. Rev. A, 136*(5A): A1187–A1193.

Patole, S., Vasilev, C., El-Zubir, O., Wang, L., Johnson, M. P., Cadby, A. J., Leggett, G. J., & Hunter, C. N. (2015). Interference lithographic nanopatterning of plant and bacterial light-harvesting complexes on gold substrates. *Interface Focus, 5*(4).

Pavlath G. A., & Shaw, H. J. (1982). Birefringence and polarization effects in fiber gyroscopes. *Appl. Opt., 21*(10): 1752–1757.

Prajapati, B. D., Patel, R. J., & Khatri, B. C. (2013). Parametric investigation of CO_2 laser cutting of mild steel and hardox-400 material. *International Journal of Emerging Technology and Advanced Engineering, 3*(4): 204-208.

Presby, H. M., Benner, A. F., & Edwards, C. A. (1990). Laser micromachining of efficient fiber microlenses. *Appl. Opt., 29*(18): 2692– 2695.

R. Brückner (1970). Properties and structure of vitreous silica. I. *J. Non-Cryst. Solids, 5*(2): 123-175.

Rao, M. C. (2013). Applications of CO_2 laser in medicine. *International Journal of Advances in Pharmacy, Biology and Chemistry, 2*(3): 501-506.

Rao, Y. J., & Ran, Z. L. (2013). Optic fiber sensors fabricated by laser-micromachining. *Opt. Fiber Technol., 19*(6): 808–821.

Rao, Y. J., Duan, D. W., Fan, Y. E., Ke, T., & Xu, M. (2010). High-temperature annealing behaviors of CO_2 laser pulse-induced long-period fiber grating in a photonic crystal fiber. *J. Lightwave Technol., 28*(10): 1530-1535.

Riant, I., Borne, S., Sansonetti, P., & Poumellec, B. (1995). Evidence of densification in UV-written Bragg gratings in fibers. *Photosensitivity and Quadratic Nonlinearity in Waveguides: Fundamentals and Applications, Vol. 22, OSA Technical Digest Series (Optical Society of America, Washington DC)*: 51-55.

Ryu, H. S., Park, Y., Oh, S. T., Chung, Y., & Kim, D. Y. (2003). Effect of asymmetric stress relaxation on the polarization dependent transmission characteristics of a CO_2 laser-written long-period fiber grating. *Opt. Lett., 28*(3): 155-157.

Scherer, G. W., & Cooper, A. R. (1980). Thermal stresses in clad-glass fibers. *J. Am. Ceram. Soc., 63*(5-6): 346-347.

Shen, Y., He, J., Qiu, Y., Zhao, W., Chen, S., Sun, T., & Grattan, K. T. V. (2007). Thermal decay characteristics of strong fiber Bragg gratings showing high temperature sustainability. *J. Opt. Soc. Am. B, 24*(3): 430-438.

Siekieraa, A., Engelbrecht, R., Neumann, R., & Schmauss, B. (2010). Fiber Bragg gratings in polarization maintaining specialty fiber for Raman fiber lasers. *Phys. Procedia, 5*: 671–677.

Slavík, R. (2006). Extremely deep long-period fiber grating made with CO_2 laser. *IEEE Photonics Technol. Lett., 18*(16): 1705-1707.

Slavik, R., & Kulisohov, M. (2007). Active control of long-period fiber-grating-based filters made in erbium-doped optical fiber. *Opt. Lett., 32*(7): 757-759.

Spiegelberg, C., Geng, J., Hu, Y., Kaneda, Y., Jiang, S., & Peyghambarian, N. (2004). Low-noise narrow-linewidth fiber laser at 1550 nm (June 2003). *J. Lightw. Technol., 22*(1): 57–62.

Subramonian, S., Kasim, M. S., Ali, M. A. M., Abdullah, R. I. R., & Anand, T. J. S. (2015). Micro-drilling of silicon wafer by industrial CO_2 laser. *International Journal of Mechanical and Materials Engineering, 10*(2).

Szentesi, O. I., & McMahon, T. J. (1993). Method of laser polishing fiber optic connectors. US 5226101 A.

Taccaa, M., Ferrario, M., Boffi, P., & Martinelli, M. (2010). Drawing parameters optimization for birefringence reduction in optical fibers. *Opt. Commun., 283*(9): 1773–1776.

Temple, P. A., Lowdermilk, W. H., & Milam, D. (1982). Carbon dioxide laser polishing of fused silica surfaces for increased laser-damage resistance at 1064 nm. *Appl. Opt., 21*(18): 3249-3255.

Tian, W., & Chiu, W. K. S. (2004). Temperature prediction for CO_2 laser heating of moving glass rods. *Opt. Laser Technol., 36*(2): 131-137.

Townsend, J. E., Poole, S. B., & Payne, D. N. (1987). Solution-doping technique for fabrication of rare-earth-doped optical fibres. *Electron. Lett., 23*(7): 329–331.

Trpkovski, S., Kitcher, D. J., Baxter, G. W., Collins, S. F., & Wade, S. A. (2005). High temperature-resistant chemical composition gratings in Er^{3+}-doped optical fiber. *Opt. Lett., 30*(6): 607-609.

Turnbull, D., & Cohen, M. H. (1961). Free-volume model of the amorphous phase: Glass transition. *J. Chem. Phys.*, *34*(1): 120–125.

Vaidya, A., and Harrington, J. A. (1992). Sculpted optical silica fiber tips for use in Nd:YAG contact tip laser surgery: Part 1- Fabrication techniques. *Opt. Eng., 31*(7): 1404–1409.

Vergeest, H. J. (2001). Process for cutting an optical fiber. US 6246026 B1.

Wang, D. N., Wang, Y. P., & Jin, W. (2008a). Method of manufacturing CO_2 laser grooved long period fiber gratings. US 20080025669 A1.

Wang, T., Shao, L. Y., Canning, J., & Cook, K. (2013). Temperature and strain characterization of regenerated gratings. *Opt. Lett., 38*(3): 247-249.

Wang, Y. P., Jin, W., Ju, J., Xuan, H., Ho, H. L., Xiao, L., & Wang, D. N. (2008b). Long-period fiber-gratings in air-core photonic bandgap fibers. *Opt. Express, 16*(4): 2784-2790.

Wang, Y. P., Wang, D. N., Jin, W., Rao, Y. J., & Peng, G.D. (2006a). Asymmetric long period fiber gratings fabricated by use of CO_2 laser to carve periodic grooves on the optical fiber. *Appl. Phys. Lett., 89*(15): 151105.

Wang, Y. P., Xiao, L., Wang, D. N., & Jin, W. (2006b). Highly sensitive long-period fiber-grating strain sensor with low temperature sensitivity. *Opt. Lett., 31*(23): 3414-3416.

Wang, Y., Bian, X., & Jia, R. (2011). Effects of cooling rate on thermal expansion of $Cu_{49}Hf_{42}Al_9$ metallic glass. *Trans. Nonferrous Metals Soc. China, 21*(9): 2031–2036.

Ward, J. M., O'Shea, D. G., Shortt, B. J., Morrissey, M. J., Deasy, K., & Chormaic, S. G. N. (2006). Heat-and-pull rig for fiber taper fabrication. *Rev. Sci. Instrum., 77*(8): 083105.

Watanabe, Y., Kawazoe, H., Shibuya, K., & Muta, K. (1986). Structure and mechanism of formation of drawing- or radiation-induced defects in SiO2:GeO2 optical fiber. *Jpn. J. Appl. Phys., 25*(3): 425–431.

Werneck, M. M., Allil, R. C. S. B., Ribeiro, B. A., & Nazaré, F. V. B. (2013). A guide to fiber Bragg grating sensors, current trends in short- and long-period fiber gratings. Dr. Christian Cuadrado-Laborde (Ed.), InTech, DOI: 10.5772/54682.

Williamson, R. L., & Miles, M. J. (1996). Melt-drawn scanning near-field optical microscopy probe profiles. *J. Appl. Phys., 80*(9): 4804–4812.

Witteman, W. J. (1987). The CO_2 laser. *Springer-Verlag Berlin Heidelberg*,

Xie, W. X., Niay, P., Bernage, P., Douay, M., Bayon, J. F., Georges, T., Monerie, M., & Poumellec, B. (1993). Experimental evidence of two types of photorefractive effects occurring during photo inscriptions of Bragg gratings within germanosilicate fibers. *Opt. Commun., 104*(1-3): 185-195.

Xuan, H., Jin, W., & Zhang, M. (2009). CO_2 laser induced long period gratings in optical microfibers. *Opt. Express, 17*(24): 21882-21890.

Yablon, A. D. (2004). Optical and Mechanical Effects of Frozen-in Stresses and Strains in Optical Fibers. *IEEE J. Quantum Elect., 10*(2); 300-311.

Yang, F., Fang, Z., Pan, Z., Ye, Q., Cai, H., & Qu , R. (2012). Orthogonal polarization mode coupling for pure twisted polarization maintaining fiber Bragg gratings. *Opt. Exp., 20*(27): 28839–28845.

Yang, H. Z., Ali, M. M., Islam, M. R., Lim, K. S., Gunawardena, D. S., & Ahmad, H. (2015). Cladless few mode fiber grating sensor for simultaneous refractive index and temperature measurement. *Sensor Actuat. A Phys., 228*: 62–68.

Yang, H. Z., Chong, W. Y., Cheong, Y. K., Lim, K. S., Pua, C. H., Harun, S. W., & Ahmad, H. (2013). Thermal regeneration in etched-core fiber Bragg grating. *IEEE Sens. J., 13*(7): 2581–2585.

Yang, H. Z., Qiao, X. G., Das, S. & Paul., M. (2014). Thermal regenerated grating operation at temperature up to 1400 °C using new class of multimaterial glass based photosensitive fiber. *Opt. Lett., 39*(22): 6438-6441.

Yang, S. T., Matthews, M. J., Elhadj, S., Cooke, D., Guss, G. M., Draggoo, V. G., & Wegner, P. J. (2010). Comparing the use of mid-infrared versus far-infrared lasers for mitigating damage growth on fused silica. *Appl. Opt., 49*(14): 2606–2616.

Yang, S. T., Matthews, M. J., Elhadj, S., Draggoo, V. G., & Bisson, S. E. (2009). Thermal transport in CO_2 laser irradiated fused silica: in situ measurements and analysis. *J. Appl. Phys., 106*(10): 1031061–1031067.

Ye, C. C., Staines, S. E., James, S. W., & Tatam, R. P. (2002). A polarization-maintaining fiber Bragg grating interrogation system for multi-axis strain sensing. *Meas. Sci. Technol., 13*(9): 1446–1449.

Yeo, C. Y., Tam, S. C., Jana, S., & Lau, M. W. S. (1994). A technical review of the laser drilling of aerospace materials. *J. Mater. Process. Tech., 42*(1): 15-49.

Yokota, H., Sugai, E., Kashima, Y., & Sasaki, Y. (1997). Optical irradiation method for fiber coupler fabrications, *Opt. Rev., 4*(A104): 104–107.

Zhao, C. L., Yang, X., Lu, C., Ng, J. H., Guo, X, Chaudhuri, P. R., & Dong, X. (2004). Switchable multi-wavelength erbium-doped fiber lasers by using cascaded fiber Bragg gratings written in high birefringence fiber. *Opt. Commun., 230*(4–6): 313–317.

Zheng, W., Mizushima, T., Sugawara, H., Klimowych, W., & Duke, D. (2015). Optical fiber processing system using CO_2 laser. US20150192738 A1.

Zhou, Y., Gao, K., Huang, R., Qu, R., & Fang, Z. (2003). Temperature and stress tuning characteristics of long-period gratings imprinted in PANDA fiber. *IEEE Photonics Technol. Lett., 15*(12): 1728-1730.

LIST OF PUBLICATIONS AND PAPERS PRESENTED

Candidate's Journal Publications for Thesis

1. **Lai, M. H.**, Gunawardena, D. S., Lim, K. S., Yang, H. Z., & Ahmad, H. (2015). Observation of grating regeneration by direct CO_2 laser annealing. *Optics express, 23*(1): 452-463.
2. **Lai, M. H.,** Lim, K. S., Gunawardena, D. S., Yang, H. Z., Chong, W. Y., & Ahmad, H. (2015). Thermal stress modification in regenerated fiber Bragg grating via manipulation of glass transition temperature based on CO 2-laser annealing. *Opt. letters, 40*(5): 748-751.
3. **Lai, M. H.,** Lim, K. S., Islam, M. R., Gunawardena, D. S., Yang, H. Z., & Ahmad, H. (2015). Effect of CO_2 laser annealing on stress applying parts contributing toward birefringence modification in regenerated grating in polarization maintaining fiber. *Photonics Journal, IEEE, 7*(5): 1-9.
4. **Lai, M. H.,** Gunawardena, D. S., Lim, K. S., Machavaram, V. R., Lee, S. H., Chong, W. Y., Lee, Y. S., & Ahmad, H. (2016). Thermal activation of regenerated fiber Bragg grating in few mode fibers. *Optical Fiber Technology, 28*: 7-10.

Patents on Fabricated Device Included in Thesis

1. CO_2 Laser Radiation Heating Technique for Regenerated Fiber Bragg Grating Fabrication, Patent filed no. PI2014703770, Filing date: 12 December 2014. (National, Malaysia)

Candidate's work presented in Conferences/Colloquium/Seminar

1. **Lai**, **M. H. (**2015, February). Regeneration and thermal stress modification in fiber Bragg gratings using CO_2 laser annealing technique. In *Institute of Graduate Studies Proposal Defence Seminar* for the partial fulfilment of Ph.D Candidature.
2. **Lai**, **M. H.** (2014, September). Regenerated fiber Bragg grating (RFBG). In *Institute of Graduate Studies Postgraduate Seminar* for the partial fulfilment of Ph.D Candidature.
3. **Lai**, **M. H.,** Lim, K. S., & Ahmad, H. (2015, June). Observation of grating regeneration by direct CO_2 laser annealing. In *Annual Phyiscs Colloquium 2015*, University of Malaya, Malaysia.
4. Lim, K. S., **Lai**, **M. H.,** Gunawardena, D. S., & Ahmad, H. (2015, November). Fabrication of regenerated grating using carbon dioxide laser. In *Workshop on Specialty Optical Fibers and their Applications 2015*, Optical Society of America, Hong Kong.
5. **Lai, M. H.**, Gunawardena, D. S., Lim, K. S., & Ahmad, H. (2015, December). Cooling-rate induced fiber birefringence variation in regenerated high birefringent fiber. In *ICP 2015: 17th International Conference on Photonics*, Penang, Malaysia.
6. **Lai, M. H.**, Gunawardena, D. S., Lim, K. S., & Ahmad, H. (2016, February). A novel fabrication technique for high temperature resistant fiber sensor. *Poster presentation in the Winter College on Optics at ICTP*, Trieste, Italy.
7. **Lai, M. H.**, (2016, May) Regeneration and thermal stress modification in fiber Bragg gratings using CO_2 laser annealing technique. In *Institute of Graduate Studies Postgraduate Candidature Defence* for the partial fulfilment of Ph.D Candidature.
8. **Lai, M. H.**, Gunawardena, D. S, Lim, K. S., Lee, Y. S., & Ahmad, H. (2016, August). Thermal regeneration of fiber Bragg grating in two and four modes step-

index fibers. In *Photonics Conference Meeting 2016: Photonics and its Applications*, University of Malaya, Malaysia.

9. **Lai, M. H.,** (2016, Oct). Regeneration and thermal stress modification in fiber Bragg gratings using CO_2 laser annealing technique. In *Institute of Graduate Studies Postgraduate Research Findings Seminar* for the partial fulfilment of Ph.D Candidature.

Candidate's Related Publications during Candidature

1. Yang, H. Z., Qiao, X. G., Wang, Y. P., Ali, M. M., **Lai, M. H.**, Lim, K. S., & Ahmad, H. (2015). In-fiber gratings for simultaneous monitoring temperature and strain in ultrahigh temperature. *IEEE Photonics Technol. Lett., 27*(1): 58-61.
2. Gunawardena, D., Sharif, K. M., **Lai, M. H.**, Lim, K. S., Tamchek, N., Omar, N., Emami, S., Yasin, S. M., Zulkifli, M., Yusoff, Z., Yang, H. Z., Rashid, H. A., & Ahmad, H. (2015). Thermal activation of regenerated grating in hydrogenated gallosilicate fiber. *IEEE Sensors J., 16*(6): 1659 – 1664.
3. Gunawardena, D. S., **Lai, M. H.**, Lim, K. S., Malekmohammadi, A., & Ahmad, H. (2016). Fabrication of thermal enduring FBG sensor based on thermal induced reversible effect. *Sens. Actuators, A: Physical, 242*: 111-115.
4. Islam, M. R., Ali, M. M., **Lai, M. H.**, Lim, K. S., & Ahmad, H. (2014). Chronology of fabry-perot interferometer fiber-optic sensors and their applications: A review. *Sensors, 14*(4): 7451-7488.
5. Lim, K. S., Gunawardena, D. S., **Lai, M. H.**, Islam, M. R., Yang, H. Z., Qiao, X., Mohammadi, A. M., & Ahmad, H. (2015). Characterization of phasemask interference visibility and the evolution of grating visibility during grating formation. *Measurement, 64*: 163-167.

6. Gunawardena, D. S, Mat-Sharif, K. A., Tamchek, N., **Lai, M. H.**, Omar, N. YM., Emami, S. D, Muhamad-Yasin, S. Z., Zulkifli, M. I., Yusoff, Z., Abdul-Rashid, H. A., Lim, K. S., & Ahmad, H. (2015). Photosensitivity of gallium-doped silica core fiber to 193 nm ArF excimer laser. *Appl. Optics, 54*(17): 5508-5512.

7. Islam, M. R., Ali, M. M., **Lai, M. H.**, Lim, K. S., Gunawardena, D. S., Machavaram, V. R., & Ahmad, H. (2015). Wide-range in-fibre Fabry-Perot resonator for ultrasonic sensing. *IET Optoelectron., 9*(3): 136-140.

8. Gunawardena, D. S., **Lai, M. H.**, Lim, K. S., Ali, M. M., & Ahmad, H. (2015). Measurement of grating visibility of a fiber Bragg grating based on bent-spectral analysis *Appl. Optics, 54*(5): 1146-1151.

9. Ali, M. M., Lim, K. S., Becir, A., **Lai, M. H.**, & Ahmad, H. (2014). Optical Gaussian notch filter based on periodic microbent fiber Bragg grating. *IEEE Photonics J., 6*(1): 1-8.

10. Lee, Y. S., Lim, K. S., Islam, M., **Lai, M. H.**, & Ahmad, H. (2016). Dynamic LP_{01}-LP_{11} mode conversion by a tilted binary phase plate," *J. Lightwave Technol.* PP.

11. Gunawardena, D. S., **Lai, M. H.**, Lim, K. S., & Ahmad, H. (2016). Impact of CO_2 laser pretreatment on the thermal endurance of Bragg gratings. *JOSK, 20*(5): 575-578.

12. Gunawardena, D. S., **Lai, M. H.**, Lim, K. S., & Ahmad, H. (2017). Thermal decay analysis of fiber Bragg gratings at different temperature annealing rates using demarcation energy approximation. *Optical Fiber Technology, 34*: 16–19.